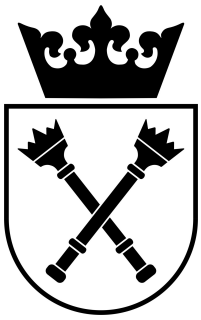

Astronomia neutrinowa - wyzwania XXI wieku

Rozprawa habilitacyjna

A. Odrzywołek

Zakład Teorii Względności i Astrofizyki
Instytut Fizyki UJ

14 maja 2011

Rozdział 1

Wstęp: astronomia neutrinowa wczoraj, dziś i jutro

Niezwykłe własności neutrin, w szczególności słabość ich oddziaływania z materią, pobudzały wyobraźnię teoretyków i eksperymentatorów. Ci pierwsi widzą w nich unikalne źródło informacji o egzotycznych obiektach astrofizycznych: supernowych, jądrach gwiazd, zderzających się gwiazdach neutronowych czy dyskach akrecyjnych. Dla tych drugich wyzwaniem jest chęć osiągnięcia celów uważanych powszechnie za iluzoryczne. Detekcja neutrin długo była uważana za synonim niemożliwości. Historia odkrywców swobodnego antyneutrina elektronowego (Reines & Cowan 1959; Reines 1996) jest bardzo dobrym przykładem niewyobrażalnego postępu w tej dziedzinie. Ich pierwszy, mało znany proposal, sugerował zastosowanie bomb jądrowych jako źródła impulsu neutrinowego. Umieszczony w pobliżu epicentrum eksplozji kilkutonowy detektor oparty na ciekłym scyntylatorze nazwano „*El Monstro*" (Reines 1952), gdyż jego rozmiary przekraczały granice zdrowego rozsądku ówczesnych badaczy. Można tylko domyślać się ich reakcji na propozycję zbudowania detektora LENA (Marrodán-Undagoitia et al. 2006; Oberauer et al. 2005), gdzie zasugerowano użycie 100 tysięcy ton ciekłego scyntylatora, cztery rzędy wielkości więcej niż w „*El Monstro*". Masy budowanych detektorów wodnych (LBNE, 300 kt, Scholberg 2010) czy lodowych (IceCube, Halzen & Klein 2010) już dziś są znacznie większe.

Neutrino udało się ostatecznie wykryć, przy użyciu reaktora jako źródła (Reines & Cowan 1959). Obserwacja neutrin produkowanych przez odległe obiekty astronomiczne wydawała się mimo to zadaniem niewykonalnym. Zakończony sukcesem eksperyment chlorowy (Davis et al. 1968) rozwiał w tej materii wszelkie wątpliwości. Neutrina emitowane przez Słońce zostały zarejestrowane w eksperymentach radiochemicznych. Zasadnicze dla zrozumienia energetyki reakcji termojądrowych neutrina *pp* zbadał eksperyment GALLEX (Hampel et al. 1999). Obecnie strumień neutrin słonecznych jest monitorowany także w czasie rzeczywistym (BOREXINO Collaboration et al. 2008; Arpesella et al. 2008; Fukuda et al. 2001; Ahmad et al. 2001).

Kolejnym, i jak dotąd ostatnim, kamieniem milowym na drodze rozwoju astronomii neutrinowej jest supernowa SN1987A (Arnett et al. 1989). Detekcja około 20 neutrin (Van Der Velde et al. 1988; Hirata et al. 1987; Galeotti et al. 1987; Alekseev et al. 1987) zainicjowała eksplozję badań nad supernowymi typu implozyjnego i konsekwencjami ich przyszłej detekcji (Burrows 1990; Keil et al. 2003; Kistler et al. 2008; Fogli et al. 2005a; Ando et al. 2005; Fogli et al. 2005b). Zaproponowano futurystyczne wizje neutrinowych obserwacji supernowych w Galaktyce (Suzuki 2001; Learned 2004). Od tego czasu minęło ponad 20 lat (Nakahata, M. and Sobel, H. 2007; Immler et al. 2007). Niestety, supernowa w Galaktyce nie wybuchła w czasach współczesnych, pomimo że 400 lat upłynęło od ostatnich obserwacji (Odrzywolek 2006), wykonanych jeszcze gołym okiem (Kepler 1606).

Czynnik	Słońce	SN 1987A	Pre-supernowa	SN Ia	Reliktowe
$\langle \mathcal{E}_\nu \rangle$	0-20 MeV	10-40 MeV	0.5-4 MeV	2-6 MeV	10^{-4} eV
Typ	ν_e	ν_x	$\bar{\nu}_e$, ν_e	ν_e	ν_x
F_ν $[\mathrm{cm}^{-2}\mathrm{s}^{-1}]$	6×10^{10} (pp)	10^{14}	$10^2 \ldots 10^{10}$	10^{10}	10^{12}
Skala czasowa	∞	$\sim$10 sekund	dni	1 s	∞
Odległość	1 AU	50 kpc	0.1-20 kpc	?-20 kpc	0
Prawdopodobieństwo	1		1-10/100 lat	1-2/1000 lat	1
Tło			Słońce, geo $\bar{\nu}_e$	Słońce	

Tablica 1.1: Czynniki warunkujące możliwości astronomii neutrinowej. Strumienie pochodzące od pre-supermnowych i SN Ia podano dla odległości d=1 kpc.

Nazywanie dziedziny, która ma na swoim koncie dwa (Słońce i SN1987A) zaobserwowane pozaziemskie źródła astronomią neutrinową może wydawać się przesadą. Komentując taką terminologię we wstępie swojej książki Bahcall (1989), podkreśla jej motywujące do dalszej pracy teoretycznej i eksperymentalnej znaczenie. Przypadek SN1987A unaocznił wszystkim konieczność przygotowania się na sporadyczne, ale bezcenne z naukowego punktu widzenia zdarzenia w kosmosie. Źle ustawione zegary komputerów zbierających dane pomiarowe detektora Kamiokande II obrosły już w legendę. Rolą autora tej rozprawy, jako astrofizyka-teoretyka, jest dostarczenie eksperymentatorom informacji, które pozwolą wydobyć maksimum informacji w przypadku zaistnienia wykrywalnego zdarzenia w kosmosie. Zachodzi tu swoiste sprzężenie zwrotne. Z jednej strony propozycje nowych, większych i bardziej czułych detektorów pozwalają na rozważania dotyczące obserwacji bardziej odległych czy nowych źródeł. Z drugiej strony, wizja detekcji neutrin z obiektów innych niż Słońce i supernowa szczególnie motywuje eksperymentatorów. W wielu przypadkach proponowane przez teoretyków modyfikacje są niewielkie, np. dodanie soli $GdCl_3$ do wody (Beacom & Vagins 2004). Prace takie często pozwalają rozstrzygnąć dylemat polegający na konieczności wyboru jednego proposalu z kilku, w sytuacji gdy inne argumenty się równoważą, np. detektor wodny *vs* ciekły argon *vs* ciekły scyntylator dla eksperymentu neutrinowego z długą bazą (Scholberg 2010).

Czy astronomia neutrinowa kiedykolwiek wyjdzie poza Słońce i SN1987A oraz jej Galaktyczne następczynie? W kosmosie właściwie wszystkie ciała niebieskie są źródłami neutrin. Dobrym przykładem jest Ziemia, której neutrina (*geoneutrina*) zostały nie tak dawno zarejestrowane (Bellini et al. 2010; Araki et al. 2005). Obserwacje źródeł znajdujących się na odległościach astronomicznych będą wymagały pokonania ogromnych trudności technicznych i poniesienia znacznych kosztów. Pytanie o sens czy możliwość takiej astronomii wymaga uwzględnienia wielu, częściowo redundantnych czynników, które zebrałem w Tabeli 1.1. Są nimi średnia energia neutrin $\langle \mathcal{E}_\nu \rangle$ (a właściwie całe widmo energetyczne), typ neutrina, ilość cząstek która przechodzi przez detektor w jednostce czasu F_ν, czas trwania emisji, odległość od obiektu, prawdopodobieństwo zajścia zjawiska i wreszcie nieredukowalne tło. Do tej listy można dodać fizyczne i techniczne parametry eksperymentu jak przekrój czynny użytych reakcji, masa „tarczy", efektywność identyfikacji zdarzeń oraz skuteczność eliminacji radiogenicznego i kosmogenicznego szumu.

Każda z wymienionych informacji jest istotna. Na przykład neutrina reliktowe (Tabela 1.1) spełniają prawie wszystkie kryteria wykrywalności, są stale obecne, mają gigantyczny strumień, ale ich niska energia wyklucza użycie znanych technik. Neutrina elektronowe emitowane przez supernowe typu Ia są z kolei niewykrywalne z Ziemi poza Galaktyką ze względu na nieusuwalne tło pochodzące

od Słońca. Przekroczenie tej bariery wymaga nowych technologii (np. detekcji kierunkowej) lub podjęcia radykalnych kroków, jak zbudowanie detektora poza Ziemią w większej odległości od Słońca (Chiu 1964).

Autor rozprawy we współpracy z kolegami astrofizykami i fizykami neutrin (M. Kutschera, T. Plewa i M. Misiaszek) rozważa detekcję neutrin z dwóch nowych obiektów. Są to: (1) gwiazdy pre-supernowe na etapie chłodzonym neutrinowo, oraz (2) supernowe typu Ia. Przyszłość zweryfikuje nasze sugestie możliwości neutrinowych obserwacji tych obiektów. XXI wiek niemal na pewno przyniesie znaczące powiększenie liczby zjawisk zbadanych przez astronomię neutrinową. Będą kontynuowane już działające eksperymenty oraz budowane nowe obserwatoria neutrin słonecznych. Wcześniej lub później, dojdzie do wybuchu supernowej typu implozyjnego (*core-collapse*) w Galaktyce. Czy krótka lista dwóch[1] źródeł podana przez J. Bahcalla (Bahcall 1989) zostanie uzupełniona o neutrina z pre-supernowej lub supernowej termojądrowej? Zależy to przede wszystkim od dwóch czynników: (a) odległości zdarzenia od Układu Słonecznego oraz (b) masy i pozostałych parametrów działających w tym momencie detektorów neutrin. Najważniejszym wnioskiem z przedstawionych prac jest jednak pokazanie możliwości takiej detekcji przy użyciu będących w zasięgu środków technicznych, z małym, ale wyraźnie większym od zera prawdopodobieństwem.

Futurologiczne rozważania obarczone są bardzo dużym ryzykiem, a przyszłość nieprzewidywalna. Pomimo tego przedstawię własną wizję rozwoju astronomii neutrinowej w XXI wieku. Wielka fizyka doświadczalne po zakończeniu eksperymentu LHC będzie musiała ulec zmianie. Obserwacje neutrinowe są diametralnie różne od fizyki akceleratorowej, ale także pozwalają na badanie fizyki elementarnej, równocześnie oferując całe spektrum dodatkowych zastosowań oraz możliwość rozwoju nowych technologii. Już obecnie obserwuje się geoneutrina (Dye 2006). Awaria elektrowni w Fukushimie rozpaliła na nowo dyskusję o bezpieczeństwie energetyki atomowej. Niedawne propozycje (Bowden 2008; Lhuillier 2009; Learned 2005; Guillian 2006) obligatoryjnego monitorowania reaktorów jądrowych za pomocą detektorów neutrin mogą zostać urzeczywistnione. Badania nad ciemną materią wymuszają budowę laboratoriów osadzonych głęboko powierzchnią Ziemi, gdzie powstaną również nowe detektory neutrin (Zalewska et al. 2010). Wszystko to przyczynia się do znacznego obniżenia kosztów i powstawania coraz większych, doskonalszych obserwatoriów neutrinowych. Eksperymentatorzy będą rozwiązywać problemy techniczne oraz uzyskiwać coraz lepsze limity na parametry modelu Słońca, neutrin, geoneutrin, oraz reliktowych antyneutrin pochodzących od supernowych. W tej atmosferze dojdzie (wcześniej lub później) do wybuchu supernowej typu implozyjnego w Galaktyce. Dalszy rozwój wypadków będzie zależny od uzyskanych przy tej okazji wyników. W pierwszym wariancie, istniejące teorie (dotyczące supernowych i neutrin) zostaną potwierdzone eksperymentalnie, i nastąpi odprężenie. W drugim, zarejestrowane neutrina obalą wcześniejsze poglądy, i rozpocznie się wyścig mający na celu zarejestrowanie kolejnych supernowych w czasie rzędu dekady. Będzie to wymagało zbudowania detektorów sięgających innych galaktyk. W tej nowej sytuacji będzie konieczne ponowne rozważenie obserwacji neutrinowych słabszych źródeł, np: nowych, młodych białych karłów, dysków akrecyjnych, sumarycznej emisji dysku Galaktycznego itp. Neutrinowy monitoring pre-supernowych, w tym Betelgeuse, stanie się rzeczywistością. Moment wybuchu trzeciej Galaktycznej supernowej będzie mógł zostać ogłoszony co najmniej kilka godzin wcześniej.

[1] A dokładnie trzech, gdyż Bahcall rozważa też możliwość obserwacji neutrin pochodzących od wszystkich gwiazd w Galaktyce. Poświęca temu zagadnieniu jedynie dwie strony, oceniając negatywnie szanse detekcji.

Rozdział 2

Wybrane publikacje

2.1 Detekcja neutrin z pre-supernowej

Oparte na pierwszej z serii prac o pre-supernowych: A. Odrzywolek, M. Misiaszek, M. Kutschera, *Detection possibility of the pair-annihilation neutrinos from the neutrino-cooled pre-supernova star*, Astroparticle Physics, 21, 303–313, 2004

Artykuł Odrzywolek et al. (2004a) jest pierwszym i najważniejszym z serii prac (Odrzywołek & Heger 2010; Kutschera et al. 2009; Odrzywolek et al. 2007, 2004b) dotyczących możliwości obserwacji sygnału neutrinowego **przed** kolapsem grawitacyjnym i wybuchem supernowej. Cel ten jest nowym, realnym zadaniem współczesnej astronomii neutrinowej. W wariancie pesymistycznym (brak nowych detektorów neutrin, odległa gwiazda) otrzymamy górne limity na strumień neutrin przed kolapsem uzyskane w analizie off-line, tj. po zdarzeniu. Wariant optymistyczny (liczne nowoczesne detektory neutrin o dużej masie, bliska gwiazda) pozwoliłby na uzyskanie sygnału wczesnego ostrzegania kilka godzin a nawet dni przed kolapsem (w przypadku supernowej Betelgeuse).

W mojej opinii detekcja neutrin z pre-supernowej jest najważniejszym **nowym** celem dla astronomii neutrinowej w XXI wieku, i jedynym rzeczywiście realistycznym. Można ją rozpatrywać jako osobne zjawisko (Odrzywolek et al. 2004a) lub część ciągłego procesu ewolucji gwiazdy (Odrzywołek & Heger 2010). Logiczne rozdzielenie strumienia neutrin na emitowane *przed* ($t < 0$) i *po* ($t > 0$) starcie kolapsu ma liczne uzasadnienia. Po pierwsze, powszechnie stosowana terminologia określa etap dla $t < 0$ ewolucją gwiazdy, natomiast dla $t > 0$ wybuchem supernowej. Po drugie, używane metody obliczeniowe są inne (model hydrostatyczny przed, hydrodynamiczny po kolapsie). Po trzecie, skale czasowe różnią się istotnie, od lat, dni i godzin przed kolapsem, do milisekund i sekund po nim. Po czwarte, konsekwencje obserwacji są różnej wagi: detekcja neutrin przed kolapsem stanowi sygnał wczesnego ostrzegania dla m. in. detektorów fal grawitacyjnych; detekcja po kolapsie to w najlepszym wypadku powtórzenie sukcesu SN1987A.

Tablica 2.1: Porównanie emisji neutrin z SN1987A i pre-supernowej.

	$\langle \mathcal{E}_\nu \rangle$	typ	L_ν	t	d
SN1987A	10-40 MeV	ν_x	10^{51} erg/s	∼10 s	50 kpc
Pre-SN	∼2-4 MeV	$\bar{\nu}_e$, ν_e	$10^{40} - 10^{46}$ erg/s	dni, tygodnie	0.1-20 kpc

Uzyskane na przestrzeni kilku lat wyniki można streścić następująco: detekcja $\bar{\nu}_e$ przed kolapsem jest możliwa, co zostało ostatecznie zademonstrowane na przykładzie Betelgeuse (Odrzywolek 2007; Scholberg 2011). W praktyce konieczne jest zastosowanie technik koincydencyjnych, aby jednoznacznie wykryć zajście reakcji:

$$\bar{\nu}_e + p \rightarrow n + e^+ \quad . \tag{2.1}$$

Dodanie do H_2O substancji wychwytującej neutrony z emisją wysokoenergetycznych fotonów pozwala na odróżnienie antyneutrin[1] od innych reakcji tła. Takim agentem jest gadolin, który zastępuje używany przez Reinesa i Cowana kadm. Dysponując detektorem wodnym klasy Super-Kamiokande, usprawnionym poprzez dodanie soli gadolinowej (Beacom & Vagins 2004), proces spalania Si będzie widoczny ponad tło na poziomie 3σ 8 dni (!) przed wybuchem supernowej. Jest to sytuacja wyjątkowa (Scholberg 2011), ze względu na niewielki dystans do Betelgezy (130 parseków), a także wysoce nieprawdopodobna (Misiaszek & Odrzywolek 2011). Przykład ten pokazuje jednak dobitnie, że twierdzenie o niemożliwości detekcji neutrin z pre-supernowej jest fałszywe. Pytanie, na które próbuję od kilku lat odpowiedzieć nie brzmi więc „czy" ale „jak" należy przygotować się na Galaktyczną (pre-)supernową. Detekcja $\bar{\nu}_e$ powstających w procesach termicznych na etapie spalania Si w jądrze jest idealnym zadaniem dla dużego wodnego detektora z $GdCl_3$. Zasięg takiego detektora w Galaktyce rośnie mniej więcej liniowo z jego rozmiarem, gdyż masywne gwiazdy gromadzą się w płaskim dysku Galaktyki, a każdy kiloparsek przybliża nas do jej eksponencjalnie gęstniejącego jądra. Detektor klasy 0.5 Mt miałby zasięg kilku kiloparseków. W tym kontekście warto podać, że rozpoczęto budowę detektora „dalekiego" (ang. *far detector*) dla eksperymentu neutrinowego z długą bazą (Long Baseline Neutrino Experiment, LBNE) o masie 0.3 Mt H_2O. Być może właśnie ten detektor zarejestruje po raz pierwszy antyneutrina z pre-supernowej. W momencie gdy uda się przezwyciężyć trudności techniczne związane z chemicznymi własnościami $GdCl_3$ (spadek przezroczystości wody) otrzymamy obserwatorium neutrinowe na miarę XXI wieku. Aby objąć zasięgiem całą Galaktykę, potrzebne są jeszcze większe urządzenia, jak proponowany Titan-D (5 Mt, Suzuki 2001; Kistler et al. 2008), czy podwodny oceaniczny balon o masie 10 Mt (Learned 2004).

Ograniczone możliwości techniczne detekcji antyneutrin elektronowych w wielkiej skali (nie rozważa się np. detektorów z ciekłym scyntylatorem o masie powyżej 100 kt), oraz nieoczekiwane problemy z roztworem wodnym[2] $GdCl_3$ motywowały mnie do dalszych prac nad emisją neutrinową pre-supernowej. Dzięki szczegółowym modelom ewolucji masywnych gwiazd uzyskanym dzięki współpracy z A. Hegerem (Odrzywołek & Heger 2010) udało się wykonać dodatkową analizę, uwzględniającą jądrowe procesy beta. Okazuje się, że w zbadanych modelach gwiazd termiczna emisja neutrin powiązana ze spalaniem Si w jądrze gwiazdy nie jest ostatnim etapem ewolucji. Po wyczerpaniu się paliwa w centrum, następuje kurczenie się połączone z termiczną emisją neutrin. Rosnąca degeneracja powoduje masowe zachodzenie procesu wychwytu elektronu przez jądra atomowe, i związaną z nią emisję neutrin elektronowych. Kurczenie zostaje przerwane dzięki zapłonowi Si w sferycznej powłoce otaczającej jądro. W neutrinach i antyneutrinach obserwujemy ostry pik jasności, oraz wzrost energii emitowanych cząstek. Na tym etapie dominujące są neutrina elektronowe, a sygnał na krótko (kilkanaście minut) stukrotnie przekracza ten pochodzący od spalania Si w jądrze. Emisja ν_e pochodząca od spalania Si w sferycznej powłoce wokół jądra jest możliwa do zaobserwowania w detektorach

[1] Podobne możliwości posiadają detektory scyntylacyjne. Niedawno zaproponowano metodę pozwalającą ma rozróżnienie pozytonu i elektronu. W przypadku reakcji (2.1) (Franco et al. 2011) dodatkowo poprawia to identyfikację $\bar{\nu}_e$.

[2] Nie są to problemy nierozwiązywalne, ale odsuwają w czasie wprowadzenie technik koincydencyjnych opartych o wychwyt neutronu. Sól gadolinowa powoduje gwałtowną korozję stalowych zbiorników używanych od czasu Kamiokande, ale np. zbiornik akrylowy rozwiązuje ten problem. Istotne jest dodanie gadolinu, który posiada najwyższy znany przekrój czynny na pochłanianie neutronów. Nie musi on występować w postaci soli, istnieje cała gama rozpuszczalnych związków chemicznych. Zbadanie ich wszystkich wymaga sporo czasu.

wodnych Czerenkowa, scyntylacyjnych a także opartych o ciekły argon. Zachodzi ona kilka godzin przed rozpoczęciem wybuchu supernowej (Smirnov 2009; Odrzywołek & Heger 2010).

Po zakończeniu spalania Si w powłoce wokół jądra zaczyna się ostateczny etap kurczenia przed kolapsem. Emisja neutrinowa staje się bardzo silna, i w sposób ciągły przechodzi w pik neutronizacyjny supernowej. Formalnie ciągle jest to emisja pochodząca od pre-supernowej, ale jej oddzielenie wymaga precyzyjnego ustalenia momentu utraty stabilności przez jądro gwiazdy i zdefiniowania co rozumiemy przez $t = 0$ przy eksplozji supernowej.

Podsumowując: detekcja neutrin z pre-supernowej jest możliwa na trzech etapach: (1) spalanie Si w jądrze, (2) spalanie Si w *shell*-u, (3) faza kontrakcji prowadząca bezpośrednio do kolapsu. Detekcja (1) jest najtrudniejsza, dotyczy tylko $\bar{\nu}_e$, ale jest najbardziej interesująca, ze względu na spory czas (rzędu dni) dzielący ją od wybuchu supernowej. Proces (2) jest znacznie łatwiejszy do obserwacji, emituje głównie ν_e, ale czas dzielący go od kolapsu to godziny. Można się spodziewać, że sygnał taki zostanie ujawniony *post factum*. Emisja (3) będzie możliwa do oddzielenia od sygnału pochodzącego od supernowej dopiero w trakcie analizy danych, po ustaleniu czasu $t = 0$.

2.2 Detekcja neutrin z supernowej typu Ia

Streszczenie wyników badań przedstawionych szczegółowo w: A. Odrzywolek and T. Plewa, *Probing thermonuclear supernova explosions with neutrinos*, Astronomy and Astrophysics, 529:A156, 2011.

Obserwacje supernowych typu Ia (termojądrowych) są niezwykle istotne z kosmologicznego punktu widzenia (Sandage & Tammann 1993; Riess et al. 1998; Wood-Vasey et al. 2007; Kowalski et al. 2008; Ellis et al. 2008; Riess et al. 2009; Kessler et al. 2009; Hicken et al. 2009). Niezależnie od sukcesów fenomenologicznego opisu krzywej blasku (Phillips 2005), brak powszechnie akceptowanego modelu wybuchu będzie kładł się cieniem na hipotezie ciemnej energii i budził uzasadnione wątpliwości kosmologów. Dwie konkurujące klasy modeli zdobyły największe uznanie astronomów i astrofizyków: deflagracja czyli spalanie termojądrowe białego karła (Nomoto et al. 1976), oraz jego opóźniona detonacja (Khokhlov 1991; Woosley & Weaver 1994; Plewa 2007; Odrzywolek 2008). Ustalenie, który z modeli faktycznie opisuje eksplozje supernowych Ia w podgrupie tzw. *Branch-normals* („świec standardowych") jest niezbędne dla wykluczenia hipotetycznej ewolucji w czasie kosmologicznym, mogącej naśladować efekt istnienia stałej kosmologicznej. Niestety, nie jest to zadanie proste, gdyż **oba** modele produkują skutki identyczne z punktu widzenia obserwacji w widmie elektromagnetycznym oraz nukleosyntezy. Nie budzącym wątpliwości testem byłaby detekcja neutrin, która okazuje się być diametralnie różna w tych dwóch modelach (Odrzywołek & Plewa 2011).

Odrzywołek & Plewa (2011) prezentują analizę emisji neutrinowej dla dwóch konkurujących modeli wybuchu supernowej Ia. Obliczenia modelowe w 2D (dwa wymiary przstrzenne, symetria cylindryczna) wykonał T. Plewa (Plewa 2007; Kasen & Plewa 2007). Dwa badane modele nie różnią się praktycznie od siebie już kilkanaście sekund po zakończeniu spalania termojądrowego. Emisja neutrinowa natomiast, dokładnie odzwierciedla szybkość i typ spalania. Wystarczy przeanalizować Rys. 1d i Rys. 3d załączonego artykułu, aby przekonać się, że detekcja nawet jednego neutrina może rozstrzygnąć o mechanizmie wybuchu. Otóż model, w którym dochodzi do detonacji produkuje niemal rząd wielkości mniej neutrin elektronowych. Znając odległość do supernowej, można obliczyć spodziewaną odpowiedź detektora. Brak pozytywnej detekcji w sytuacji gdy model zakładający „czystą" deflagrację powinien wyprodukować sygnał w postaci kilku zdarzeń będzie argumentem za tym, że większość energii była wyprodukowana podczas detonacji. Dodatkową informację niesie energia ν_e: deflagracja zachodzi w warunkach silnej degeneracji gazu elektronowego, dzięki czemu energie neutrin są nieco wyższe (Tabela 1 w omawianej pracy).

Do detekcji na poziomie jednego zdarzenia potrzebne jest przynajmniej megatonowe wodne obserwatorium neutrinowe, lub detektor oparty o ciekły argon (Rubbia 2009). Ten ostatni, zakładając że uda się obniżyć próg na detekcję poniżej 5 MeV, może okazać się szczególnie skuteczny, dzięki detekcji ν_e w reakcji absoprcji:

$$\nu_e + {}^{40}\mathrm{Ar} \rightarrow {}^{40}\mathrm{K}^* + e^-.$$

Budowa detektora tego typu o masie rzędu 100 kt jest planowana w Europie (Katsanevas 2006) oraz USA. W przypadku bardzo bliskiej[3] eksplozji, będzie można analizować szybkość spalania, opóźnienie ewentualnej detonacji i stopień degeneracji materii.

[3]Sytuacja jest tu nieco bardziej skomplikowana niż dla pre-supernowych, gdzie jest jasne, że najbliższa kandydatka to Betelgeza. Po pierwsze nie wiadomo co dokładnie wybucha jako supernowa Ia, po drugie hipotetyczny *progenitor* na bardzo małą jasność i może zostać łatwo przeoczony.

2.3 Widmo energetyczne neutrin produkowanych z udziałem jąder atomowych

Na podstawie artykułu: A. Odrzywolek, *Nuclear statistical equilibrium neutrino spectrum*, Phys. Rev. C, 80 (4) 045801, October 2009.

Niezależnie od prac, które mają na celu zbadanie konkretnych aktualnych modeli *znanych* obiektów astrofizycznych i procesów, potrzebne są badania, które dają ogólne spojrzenie na emisję neutrin. Może ona zachodzić poprzez reakcje z udziałem jąder atomowych, w tym protonów i neutronów (Rozdział 2.4 dyskutuje drugą kategorię: reakcji termicznych). Dwa podejścia (modelowe i ogólne) dyskutuje Hoyle (1946) oraz Odrzywolek (2010). Współcześnie nasza wiedza na temat kosmosu dramatycznie przekracza ilość informacji, którą posiadał ponad 50 lat temu F. Hoyle. Niemniej jednak konkretne obliczenia teoretyczne oraz symulacje, nawet te najbardziej zaawansowane, zawsze będą budziły różnorakie wątpliwości. Dlatego istotne jest posiadanie wyników ogólnych, z którymi to modele nie powinny być sprzeczne. W obszarze, gdzie wynik ogólny dopuszcza interesujące rozwiązanie, *mogą* kryć się zjawiska jeszcze nieodkryte, przeoczone lub mylnie sklasyfikowane.

Przykładami naturalnej emisji neutrinowej pochodzącej w całości z reakcji jądrowych są neutrina słoneczne i tzw. geoneutrina ($\bar{\nu}_e$). Podobnie, większość neutrin emitowanych przez supernową typu Ia pochodzi z reakcji beta. W ogólnym przypadku jedyną metodą pozwalającą na obliczenie widma energetycznego neutrin lub antyneutrin elektronowych jest model opisujący całą historię badanej „gwiazdy" od momentu narodzin, a jeszcze lepiej całą historię Wszechświata od Wielkiego Wybuchu. W takiej sytuacji nie jest możliwe wyciąganie ogólnych wniosków, gdyż nawet śladowa ilość wyprodukowanego na wcześniejszym etapie izotopu może okazać się katalizatorem reakcji jądrowych miliony lat później. W praktyce jednak, najbardziej interesujące z punktu widzenia astronomii neutrinowej (a także z naukowego punktu widzenia) są zjawiska i obiekty najbardziej ekstremalne. Wysokie temperatury i gęstości panujące w gwiazdach, supernowych i dyskach akrecyjnych pozwalają na zastosowanie do emisji neutrinowej skutecznych metod fizyki statystycznej. Dotyczy to także widma energetycznego neutrin.

Zastosowanie metod fizyki statystycznej do opisu reakcji jądrowych, określane jest we współczesnej astrofizyce jako **NSE** (Nuclear Statistical Equilibrium). Nie jest to pełna równowaga w sensie termodynamicznym, a stan materii jest zdeterminowany przez temperaturę, gęstość oraz stosunek liczby protonów do neutronów. Ta ostatnia wielkość zwykle opisywana jest równoważną (ze względu na zachowanie ładunku elektrycznego) liczbą Y_e stanowiącą stosunek liczby leptonów do barionów. Jest to parametr kluczowy. W zbadanym przez astrofizyków zajmujących się teorią ewolucji masywnych gwiazd przedziale $0.4 < Y_e < 0.5$ stan[4] NSE wykazuje gwałtowną zmienność. Cecha ta powoduje, że NSE jest użytecznym narzędziem, pozwalającym na zaskakująco dokładne przewidywania ilościowe w teorii nukleosyntezy oraz emisji neutrinowej. Analiza taka, w przypadku uwzględnienia energii neutrin (antyneutrin) elektronowych, odbywa się w przestrzeni czterowymiarowej: $T, \rho, Y_e, \mathcal{E}_\nu$. Szczegółowe wyniki podano w załączonym artykule (Odrzywolek 2009).

Dla astronomii neutrinowej istotne są warunki, w których strumień neutrin jest maksymalnie duży. Ponieważ neutrina są leptonami, ich emisja powoduje nieuniknione zmiany Y_e. Każdorazowo, zamiana neutronu w proton lub odwrotnie jest związana z emisją antyneutrina lub neutrina elektronowego. Dlatego emitowany duży strumień neutrin musi doprowadzić do jednej z trzech sytuacji: (1) $Y_e = 0$, (2) $Y_e = 1$ lub (3) $Y_e = const, R_{\nu_e} = R_{\bar{\nu}_e}$, gdzie przez R_ν oznaczyłem szybkość emisji neutrin danego typu na jednostkę objętości. Stan (3), w którym strumienie neutrin i antyneutrin się zrównują

[4]Rozumiany jako znajomość abundancji *wszystkich* rozważanych izotopów w zadanych warunkach, Odrzywołek 2011.

jest określany jako *kinetyczna równowaga* β. Zachodzi ona dla *wszystkich* zbadanych w omawianym artykule temperatur i gęstości. Krytyczna wartość Y_e zmienia się natomiast w zaskakująco szerokim zakresie. W „standardowych" sytuacjach (pre-supernowe, supernowe) Y_e spada, a neutrina dominują. Dla zderzeń gwiazd neutronowych startujemy od wartości $Y_e = 0$, jak w historycznych modelach kosmologicznych z „neutronem" pierwotnym. Dla niskich gęstości i wysokich temperatur (rzędu 1 MeV) krytyczne Y_e staje się bliskie jedności, co skutkuje intensywną emisją $\bar{\nu}_e$. Zjawisko to może zachodzić wewnątrz dysków akrecyjnych znajdujących się w aktywnych jądrach galaktyk.

Stan równowagi beta jest tematem dociekań przyszłych astronomów neutrinowych i astrofizyków (Arcones, A. et al. 2010). Ilość neutrin czy antyneutrin emitowana w tej sytuacji jest limitowana wyłącznie poprzez zasadę zachowania energii. W szczególności nie jest ograniczona przez dane na temat nukleosyntezy. Emisja intensywnego strumienia $\bar{\nu}_e$ o energii kilku MeV, pochodzącego z reakcji:

$$n + e^+ \rightarrow p + \bar{\nu}_e,$$

jest możliwa, ale nie zaobserwowano i nie zaproponowano jak dotąd adekwatnego zjawiska. Proces taki byłby łatwy do zarejestrowania we wszystkich typowych detektorach neutrin o niskim ($E_{th} \ll 10$ MeV) progu energetycznym. Pozwolę sobie na spekulację, że źródłem energii dla takiego zjawiska może być termojądrowa synteza wodoru, a same antyneutrina jej katalizatorem (Kishimoto & Fuller 2007). Nie jest wykluczone, że tzw. antyneutrina LSD (zarejestrowane w detektorze pod Mont Blanc, Aglietta et al. 1987) zarejestrowane około 5 godzin przez kolapsem jądra SN1987A zostały wyprodukowane w podobnym procesie.

Opisane metody zostały użyte do wyznaczenia jądrowego składnika emisji ν_e i $\bar{\nu}_e$ supernowej typu Ia (Odrzywołek & Plewa 2011) oraz pre-supernowej na etapie spalania Si w *shell*-u (Odrzywołek & Heger 2010).

2.4 Termiczne procesy neutrinowe

Oparte na pracy: A. Odrzywołek, *Plasmaneutrino spectrum*, European Physical Journal C, 52 425–434, October 2007.

Drugą klasę procesów prowadzących do emisji neutrin stanowią tzw. *procesy termiczne*. Nazwa pochodzi od wysokich ($T > 10^8$ K) temperatur, w których procesy te stają się dominujące. W niskich temperaturach procesy te także działają, są natomiast całkowicie zdominowane przez procesy jądrowe, jak w przypadku neutrin słonecznych czy emisji ν_e z supernowej Ia w modelu czystej deflagracji (Odrzywołek & Plewa 2011). Dla gwiazd chłodzonych neutrinowo, czyli masywnych gwiazd ($M > 8M_\odot$, Smartt 2009) na etapie spalania C i późniejszych, procesy termiczne decydują o szybkości ewolucji (Odrzywołek & Heger 2010). Najważniejsze są: *anihilacja par* e^+e^- (Odrzywolek et al. 2004a,b; Misiaszek et al. 2006), *fotoprodukcja* oraz *rozpad plazmonu* Odrzywołek (2007). Procesy te są znane i badane teoretycznie od lat, ale głównie w kontekście energii utraconej przez gwiazdę. Z tego powodu bardzo rzadko analizowano wielkości inne niż utrata energii w postaci neutrin. Dla astronomii neutrinowej istotny jest cały szereg dodatkowych parametrów opisujących emisję neutrinową: ilość cząstek, ich energia, rozkład na zapachy oraz widmo energetyczne. Wymagało to powtórzenia klasycznych obliczeń (Itoh et al. 1996; Beaudet et al. 1967; Schinder et al. 1987) od zera, bez licznych upraszczajacych założeń.

Zjawisko rozpadu plazmonu jest dominującym źródłem neutrin w rejonach o dużej gęstości i niezbyt wysokich temperaturach. Decyduje o ewolucji zdegenerowanych jąder gwiazd mało masywnych, w tym o powstawaniu białych karłów. Neutrina emitowane w tym procesie stale przenikają nasze detektory, emitowane bez przerwy przez miliony czerwonych olbrzymów i gorących białych karłów w Galaktyce. Wyniki pracy (Odrzywołek 2007) pokazały, że widmo energetyczne tych neutrin jest skoncentrowane w zakresie keV. Wygodnie jest rozpatrywać proces jak złożenie dwóch: rozpadu plazmonu podłużnego oraz poprzecznego (masywnego „ubranego" fotonu). Rozpad plazmonu podłużnego w pierwszym przybliżeniu produkuje widmo w postaci piku skoncentrowanego wokół $\omega_p/2$, czyli połowy częstości plazmowej („masy" kwaziczą̨ski). Widmo pochodzące od rozpadu masywnego fotonu ma postać piku z ogonem postaci $\exp\left(-\mathcal{E}_\nu/kT\right)$, gdzie $\mathcal{E}_\nu$ - energia neutrina, k - stała Boltzmana, T - temperatura.

Uzyskane wyniki pokazują, że detekcja powszechnie występujących neutrin pochodzących od rozpadu plazmonu nie jest możliwa przy użyciu znanych nam technik, ze względu na zbyt niskie energie, i występujące w tym zakresie radiogeniczne tło. Obliczenia, w których widmo energetyczne neutrin jest obliczane *explicite*, pozwoliło natomiast na usprawnienie znanych wcześniej metod i uzyskanie dokładniejszych wyników dotyczących chłodzenia neutrinowego gwiazd. W szczególności ustalony został prawidłowy sposób aproksymacji relacji dyspersji dla plazmonu poprzecznego.

Opisane metody zostały użyte do obliczeń składnika termicznego pre-supernowych Odrzywołek & Heger (2010); Kutschera et al. (2009); Odrzywolek et al. (2007, 2004b) oraz supernowych typu Ia (Odrzywołek & Plewa 2011). Detekcję neutrin m. in. z rozpadu plazmonu w eksperymencie Borexino rozważał Kulakowski (2009). Wstępne zainteresowanie implementacją omawianych obliczeń dotyczących rozpadu plazmonu w symulacjach supernowych typu core-collapse wyraziła grupa powiązana z MPA Garching.

2.5 Opóźniony kolaps protogwiazdy neutronowej

W nawiazaniu do pracy: A. Odrzywolek and M. Kutschera, *Kaon condensate with trapped neutrinos and high-density symmetry energy behavior*, Acta Phys. Pol. B, 40 195, January 2009.

Artykuł prezentuje model gęstej materii jądrowej z kondenstatem Bosego-Einsteina kaonów. Rozważana jest sytuacja tuż po kolapsie grawitacyjnym żelaznego rdzenia pre-supernowej, kiedy to uformowana zostaje protogwiazda neutronowa. W odróżnieniu od „dojrzałych" gwiazd neutronowych jest ona bardzo gorąca (kT $\sim$ 100 MeV) i zawiera uwięzione neutrina. Te ostatnie tworzą zdegenerowany gaz fermionowy. Obydwa czynniki: temperatura i zawartość leptonów (elektronów, mionów i neutrin) mają wpływ na równanie stanu, a zatem na maksymalną masę protogwiazdy neutronowej. Początkowa zawartość liczby leptonowej $Y_L \simeq 0.4 \ldots 0.45$ jest niesiona przed kolapsem wyłącznie przez elektrony, które są w „normalnej" materii jedynymi leptonami. Postępujący kolaps powoduje wzrost temperatury i gęstości co ostatecznie powoduje złapanie neutrin. Od tego momentu można założyć, że lokalnie liczby leptonowe są zachowane. Ewolucja postępuje kwazistatycznie na skali czasowej rzędu $\sim$ 100 sekund, w zawartość liczb leptonowych systematycznie spada, by ostatecznie osiągnąć wartości bliskie zeru (dokładnie zero w modelu materii czysto neutronowej). Zjawisko deleptonizacji protogwiazdy neutronowej zostało potwierdzone poprzez obserwację neutrin z SN1987A.

Niestety, do dziś nie udało się znaleźć nawet śladu gwiazdy neutronowej, która powinna znajdować się w pozostałości po supernowej SN1987A. Fakt ten jest zastanawiający, gdyż z jednej strony nie ma wątpliwości, że gwiazdy neutronowe istnieją (np. pulsary) oraz że powstają w wybuchach supernowych typu implozyjnego. Hipotetycznym rozwiązaniem tej zagadki jest równanie stanu, które na skutek emisji neutrin (obniżenia Y_L) staje się coraz bardziej „miękkie" ostatecznie prowadząc do opóźnionego kolapsu, w wyniku czego powstaje czarna dziura. Kondenstat kaonów prowadzi do takiego efektu. Astronomia neutrinowa jest w stanie potwierdzić ten scenariusz w przypadku wybuchu supernowej w Galaktyce. Wymaga to zarejestrowania statystycznie istotnego sygnału dla czasów znacznie powyżej 1 sekundy. Opóźnione powstanie czarnej dziury objawia się niemal natychmiastowym ucięciem emisji neutrinowej. Nowa generacja detektorów będzie w stanie zaobserwować to zjawisko.

Bibliografia

Aglietta, M., Badino, G., Bologna, G., et al. 1987, EPL (Europhysics Letters), 3, 1315

Ahmad, Q. R., Allen, R. C., Andersen, T. C., et al. 2001, Physical Review Letters, 87, 071301

Alekseev, E. N., Alekseeva, L. N., Volchenko, V. I., & Krivosheina, I. V. 1987, JETP Lett., 45, 589

Ando, S., Beacom, J. F., & Yüksel, H. 2005, Physical Review Letters, 95, 171101

Araki, T., Enomoto, S., Furuno, K., et al. 2005, Nature, 436, 499

Arcones, A., Martínez-Pinedo, G., Roberts, L. F., & Woosley, S. E. 2010, A&A, 522, A25

Arnett, W. D., Bahcall, J. N., Kirshner, R. P., & Woosley, S. E. 1989, ARA&A, 27, 629

Arpesella, C., Back, H. O., Balata, M., et al. 2008, Physical Review Letters, 101, 091302

Bahcall, J. N. 1989, Neutrino Astrophysics (Cambridge: Cambridge University Press)

Beacom, J. F. & Vagins, M. R. 2004, Phys. Rev. Lett., 93, 171101

Beaudet, G., Petrosian, V., & Salpeter, E. E. 1967, *Astrophys. J.*, 150, 979

Bellini, G., Benziger, J., Bonetti, S., et al. 2010, Physics Letters B, 687, 299

BOREXINO Collaboration, Arpesella, C., Bellini, G., et al. 2008, Physics Letters B, 658, 101

Bowden, N. S. 2008, Journal of Physics: Conference Series, 136, 022008

Burrows, A. 1990, Annual Review of Nuclear and Particle Science, 40, 181

Chiu, H.-Y. 1964, Cosmic neutrinos and their detection, NASA-TM-X-51721

Davis, R., Harmer, D. S., & Hoffman, K. C. 1968, Phys. Rev. Lett., 20, 1205

Dye, S. E. 2006, Neutrino Geophysics : Proceedings of Neutrino Sciences 2005 (Springer Verlag)

Ellis, R. S., Sullivan, M., Nugent, P. E., et al. 2008, *Astrophys. J.*, 674, 51

Fogli, G. L., Lisi, E., Mirizzi, A., & Montanino, D. 2005a, Journal of Cosmology and Astro-Particle Physics, 4, 2

Fogli, G. L., Lisi, E., Mirizzi, A., & Montanino, D. 2005b, Journal of Cosmology and Astro-Particle Physics, 4, 2

Franco, D., Consolati, G., & Trezzi, D. 2011, Phys. Rev. C, 83, 015504

Fukuda, S. et al. 2001, Phys. Rev. Lett., 86, 5651

Galeotti, P. et al. 1987, Helv. Phys. Acta, 60, 619

Guillian, E. H. 2006, Earth, Moon and Planets, 99, 309

Halzen, F. & Klein, S. R. 2010, Review of Scientific Instruments, 81, 081101

Hampel, W. et al. 1999, Phys. Lett., B447, 127

Hicken, M., Wood-Vasey, W. M., Blondin, S., et al. 2009, The Astrophysical Journal, 700, 1097

Hirata, K. et al. 1987, Phys. Rev. Lett., 58, 1490

Hoyle, F. 1946, MNRAS, 106, 343

Immler, S., Weiler, K., & McCray, R. 2007, in American Institute of Physics Conference Series, Vol. 937, Supernova 1987A: 20 Years After: Supernovae and Gamma-Ray Bursters, ed. S. Immler, K. Weiler, & R. McCray

Itoh, N., Hayashi, H., Nishikawa, A., & Kohyama, Y. 1996, *Astrophys. J. Suppl.*, 102, 411

Kasen, D. & Plewa, T. 2007, *Astrophys. J.*, 662, 459

Katsanevas, S. 2006, Acta Physica Polonica B, 37, 2115

Keil, M. T., Raffelt, G. G., & Janka, H.-T. 2003, *Astrophys. J.*, 590, 971

Kepler, J. 1606, De Stella nova in pede Serpentarii (Praga)

Kessler, R., Becker, A. C., Cinabro, D., et al. 2009, *Astrophys. J. Suppl.*, 185, 32

Khokhlov, A. M. 1991, A&A, 245, 114

Kishimoto, C. T. & Fuller, G. M. 2007, *Astrophys. J.*, 656, 1104

Kistler, M. D., Yuksel, H., Ando, S., Beacom, J. F., & Suzuki, Y. 2008, Core-Collapse Astrophysics with a Five-Megaton Neutrino Detector, http://arxiv.org/abs/0810.1959K

Kowalski, M., Rubin, D., Aldering, G., et al. 2008, The Astrophysical Journal, 686, 749

Kulakowski, T. 2009, Master's thesis, Jagiellonian University, Poland

Kutschera, M., Odrzywołek, A., & Misiaszek, M. 2009, Acta Physica Polonica B, 40, 3063

Learned, J. G. 2004, White paper on Gigaton Array, `www.phys.hawaii.edu/~jgl/post/gigaton_array.pdf`

Learned, J. G. 2005, Nuclear Physics B - Proceedings Supplements, 143, 152

Lhuillier, D. 2009, Nuclear Physics B - Proceedings Supplements, 188, 112 , proceedings of the Neutrino Oscillation Workshop

Marrodán-Undagoitia, T., von Feilitzsch, F., Goeger-Neff, M., et al. 2006, Progress in Particle and Nuclear Physics, 57, 283 , international Workshop of Nuclear Physics 27th course - Neutrinos in Cosmology, in Astro, Particle and Nuclear Physics

Misiaszek, M. & Odrzywolek, A. 2011, Comments on Betelgeuse explosion in 2012, http://bryza.if.uj.edu.pl/zdfk/?p=521

Misiaszek, M., Odrzywolek, A., & Kutschera, M. 2006, Phys. Rev. D, 74, 043006

Nakahata, M. and Sobel, H. 2007, Twenty Years after SN1987A. What did we learn, what will the next Supernova teach us?, http://sn1987a-20th.physics.uci.edu/

Nomoto, K., Sugimoto, D., & Neo, S. 1976, Ap&SS, 39, L37

Oberauer, L., von Feilitzsch, F., & Potzel, W. 2005, Nuclear Physics B - Proceedings Supplements, 138, 108 , proceedings of the Eighth International Workshop on Topics in Astroparticle and Undeground Physics

Odrzywolek, A. 2006, Prace Komisji Astrofizyki PAU, 10, 73

Odrzywołek, A. 2007, European Physical Journal C, 52, 425

Odrzywolek, A. 2007, Silicon burning neutrinos, http://sn1987a-20th.physics.uci.edu/1630-Odrzywolek.pdf

Odrzywolek, A. 2008, Foton, 102, 4

Odrzywolek, A. 2009, Phys. Rev. C, 80, 045801

Odrzywolek, A. 2010, Prace Komisji Astrofizyki PAU, 13

Odrzywołek, A. 2011, Atomic Data and Nuclear Data Tables, accepted for publication

Odrzywołek, A. & Heger, A. 2010, Acta Physica Polonica B, 41, 1001

Odrzywolek, A., Misiaszek, M., & Kutschera, M. 2004a, Astroparticle Physics, 21, 303

Odrzywolek, A., Misiaszek, M., & Kutschera, M. 2004b, Acta Phys. Pol. B, 35, 1981

Odrzywolek, A., Misiaszek, M., & Kutschera, M. 2007, in American Institute of Physics Conference Series, Vol. 944, Next Generation Nucleon Decay and Neutrino Deterctors NNN06, ed. J. R. Wilkes, 109–118

Odrzywołek, A. & Plewa, T. 2011, Astronomy and Astrophysics, 529, A156

Phillips, M. M. 2005, in Astronomical Society of the Pacific Conference Series, Vol. 342, 1604-2004: Supernovae as Cosmological Lighthouses, ed. M. Turatto, S. Benetti, L. Zampieri, & W. Shea, 211

Plewa, T. 2007, *Astrophys. J.*, 657, 942

Reines, F. 1952, http://www.lsc-international.org/conf/pfiles/lsc1957_246.pdf

Reines, F. 1996, Rev. Mod. Phys., 68, 317

Reines, F. & Cowan, C. L. 1959, Phys. Rev., 113, 273

Riess, A. G., Filippenko, A. V., Challis, P., et al. 1998, AJ, 116, 1009

Riess, A. G., Macri, L., Casertano, S., et al. 2009, *Astrophys. J.*, 699, 539

Rubbia, A. 2009, Journal of Physics: Conference Series, 171, 012020

Sandage, A. & Tammann, G. A. 1993, *Astrophys. J.*, 415, 1

Schinder, P. J., Schramm, D. N., Wiita, P. J., Margolis, S. H., & Tubbs, D. L. 1987, *Astrophys. J.*, 313, 531

Scholberg, K. 2010, Journal of Physics: Conference Series, 203, 012079

Scholberg, K. 2011, Is an early warning of a supernova possible from observation of Si-burning neutrino events?, http://lbne2-docdb.fnal.gov/0033/003336/001/si-burning.pdf

Smartt, S. J. 2009, Annual Review of Astronomy and Astrophysics, 47, 63

Smirnov, A. 2009, Workshop Towards Neutrino Technologies, http://cdsagenda5.ictp.trieste.it/full_display.php?ida=a

Suzuki, Y. 2001, Multi-Megaton Water Cherenkov Detector for a Proton Decay Search – TITAND, http://arxiv.org/abs/hep-ex/0110005

Van Der Velde, J. C. et al. 1988, Nucl. Instrum. Meth., A264, 28

Wood-Vasey, W. M., Miknaitis, G., Stubbs, C. W., et al. 2007, *Astrophys. J.*, 666, 694

Woosley, S. E. & Weaver, T. A. 1994, in Supernovae, ed. S. A. Bludman, R. Mochkovitch, & J. Zinn-Justin, 63, given at Les Houches Summer School, Session 54: Supernovae, Les Houches, France, 31 Jul - 1 Sep 1990

Zalewska, A., Pytel, W., Chorowski, M., et al. 2010, Acta Physica Polonica B, 41, 1803

Rozdział 3

Oryginalne prace załączone do rozprawy

Available online at www.sciencedirect.com
SCIENCE DIRECT®
Astroparticle Physics 21 (2004) 303–313
Astroparticle Physics
www.elsevier.com/locate/astropart

Detection possibility of the pair-annihilation neutrinos from the neutrino-cooled pre-supernova star

A. Odrzywolek [a], M. Misiaszek [a,*], M. Kutschera [a,b]

[a] M. Smoluchowski Institute of Physics, Jagiellonian University, Reymonta 4, 30-059 Krakow, Poland
[b] H. Niewodniczanski Institute of Nuclear Physics, Radzikowskiego 152, 31-342 Krakow, Poland

Received 1 November 2003; received in revised form 11 February 2004; accepted 18 February 2004
Available online 4 March 2004

Abstract

The signal produced in neutrino observatories by the pair-annihilation neutrinos emitted from a 20 $M_\odot$ pre-supernova star at the silicon burning phase is estimated. The spectrum of the neutrinos with an average energy ~2 MeV is calculated with the use of the Monte Carlo method. A few relevant reactions for neutrinos and anti-neutrinos in modern detectors are considered. The most promising results are from $\bar{\nu}_e + p \rightarrow n + e^+$ reaction. During the Si-burning phase we expect 1.27 neutrons/day/kton of water to be produced by neutrinos from a star located at a distance of 1 kpc. Small admixture of effective neutron-absorbers as e.g. NaCl or $GdCl_3$ makes these neutrons easily visible because of Cherenkov light produced by electrons which were hit by ~8 MeV photon cascade emitted by Cl or Gd nuclei. The estimated rate of neutron production for SNO and Super-Kamiokande is, respectively, 2.2 and 41 events per day for a star at 1 kpc. For future detectors UNO and Hyper-Kamiokande we expect 5.6 and 6.9 events per day even for a star 10 kpc away. This would make it possible to foresee a massive star death a few days before its core collapse. Importance of such a detection for theoretical astrophysics is discussed.

PACS: 95.85.Ry; 97.60.−s; 97.60.Bw; 29.40.Ke
Keywords: Massive stars; Neutrino detection; Pre-supernova evolution

1. Introduction

The detection of solar neutrinos by the R. Davis's chlorine detector and supernova 1987A neutrinos by the Kamiokande water Cherenkov observatory are milestones of modern science, *Nobel Prize* honored in 2002. Currently built and operating neutrino detectors are larger, much more efficient and are able to detect all neutrino species in a wide range of energy. There are already proposed new experiments with next-generation megaton-scale detectors, like Hyper-Kamiokande [1] and UNO [2].

Solar neutrinos were detected with sub-kiloton detectors, because of relatively small distance to the Sun and continuous emission. Supernova

* Corresponding author. Tel.: +48-18-33-10-255; fax: +48-12-633-6377.
E-mail addresses: odrzywolek@th.if.uj.edu.pl (A. Odrzywolek), misiaszek@zefir.if.uj.edu.pl (M. Misiaszek), marek.kutschera@ifj.edu.pl (M. Kutschera).

0927-6505/$ - see front matter © 2004 Elsevier B.V. All rights reserved.
doi:10.1016/j.astropartphys.2004.02.002

neutrinos carry enormous energy of 10^{53} ergs released in gravitational collapse of the stellar core. This makes their detection possible from quite large distances, but such events are rare. We consider here the feasibility of detection of another giant astrophysical sources of neutrinos, namely massive ($M > 8M_{\odot}$) stars at late stages of their evolution. Such stars, during C, Ne, O and Si burning phases, emit neutrinos copiously and are referred to as neutrino-cooled stars ([3], Section 10) or pre-supernova stars [4]. The structure of such evolutionary advanced stars is different from main sequence stars like the Sun. The most important differences relevant to the neutrino detection possibility are summarized in Table 1.

The solar neutrino luminosity is 7.8×10^{31} erg/s [5]. The maximum neutrino luminosity during Si burning exceeds 3×10^{45} erg/s [6,7]—a value larger by a factor of 3.85×10^{13}. The neutrino energy flux at Earth from such a star and from the Sun are equal for a star $\sqrt{3.85\times10^{13}} = 6.2\times10^{6}$ AU, i.e. 30 pc away. This indicates that neutrino-cooled stars could be detected at astronomical distances. Actually, because of a different spectrum (cf. Fig. 2) and the presence of anti-neutrinos (cf. Table 3), we are able to detect them from kiloparsec distances.

Massive (neutrino-cooled) stars are believed to end as *core-collapse* supernovae. SN 1987A confirmed this theory. This close connection may be used to estimate chance of neutrino-cooled stage observation. If some of massive stars die other way, rate of neutrino-cooled events may be higher than of SNe, but it is reasonable to use estimates made for supernovae. At least three different methods exist there: historical records & remnants counts [8], extragalactic observations [9] and population synthesis (i.e. simulated stellar evolution of the Galaxy) methods [10]. Only first method gives *local rate* directly: time between events less than 5 kpc away is estimated to be 175 years [11]. Two other methods give rate for entire Galaxy. Extragalactic counts give 40...200 years [9] of average time interval between supernova explosions. Population Synthesis give 10 years [10]. To compare *local rates* we may use Galaxy model of e.g Bahcall and Soneira [12]. For the solar neighbourhood we found 0.5%, 10% and 50% of disc stars closer than 1, 5 and 10 kpc respectively. Assuming that the Sun is not in privileged position close to e.g. giant star forming region, we get time between supernovae closer than 5 kpc from 100 (population synthesis) to 400...2000 (extragalactic counts) years. Apparent disagreement between these two methods is usually explained by a large number of unobserved events. Clouds of interstellar gas and dust obscuring optical detection are obviously transparent for neutrinos, so we may conclude that neutrino-cooled events closer than 5 kpc may be observed even more frequent than one per century. Close candidates for such a detection apparently do exist, with Betelgeuse (β Ori) being the most popular example [13]. In Section 5 we combine rates discussed above with our results to estimate a chance of successful detection.

As an example we consider a 20 $M_{\odot}$ star model with properties reported in Table 1 of Ref. [6], with *explicite* given total neutrino luminosities of various stages of nuclear burning. As our scope here is to study the feasibility of neutrino detection, not to find state-of-art details of emission, [1] we assume

Table 1
Differences between the Sun (main sequence star) and the neutrino-cooled 20 $M_{\odot}$ star ([6], Table 1)

	The Sun	Neutrino-cooled phase of 20 $M_{\odot}$ star
Lifetime (years)	10^{10}	300
Photon luminosity	$L_{\odot}$	10^{5} $L_{\odot}$
Maximum *v* luminosity	0.02 $L_{\odot}$	10^{12} $L_{\odot}$
Average neutrino energy (MeV)	0.3	0.7–2
Total *v* energy released (erg)	10^{49}	10^{51}

Approximate values (orders of magnitude) are given. The total energy carried by neutrinos for a 20 $M_{\odot}$ neutrino-cooled star corresponds only to late stages of nuclear burning (without supernova neutrinos).

[1] Detailed picture of late stages of nuclear burning is still a subject of active research as there are unanswered questions about e.g. hydrodynamical nature of nuclear burning [14]. Neutrinos itself are still enigmatic objects and e.g. the role of spin-flip interactions and the influence of right-handed neutrinos [15] is investigated.

Table 2
Properties of a 20 $M_\odot$ star according to Ref. [6]

Burning phase	T_c (MeV)	ρ_c (g/cc)	μ_e (MeV)	L_ν (erg/s)	Duration (τ)	Total energy emitted (erg)
C	0.07	2.7×10^5	0.0	7.4×10^{39}	300 years	7×10^{49}
Ne	0.146	4.0×10^6	0.20	1.2×10^{43}	140 days	1.4×10^{50}
O	0.181	6.0×10^6	0.24	7.4×10^{43}	180 days	1.2×10^{51}
Si	0.319	4.9×10^7	0.84	3.1×10^{45}	2 days	5.4×10^{50}

We have calculated the total energy radiated in neutrinos as a product τL_ν. Actually, the neutrino emission is expected to be a function of time.

that the entire neutrino flux is resulting from e^+e^- annihilation. The values from Table 2 of the temperature, density and the electron chemical potential at the stellar center are assumed to approximate conditions in the stellar core. For simplicity we treat neutrino propagation without oscillation, however the effect of neutrino oscillations may change significantly the number of observed events in a given experiment [16]. To calculate the relevant neutrino cross-sections the standard Weinberg-Salam theory [17] is used.

In Section 2 we calculate the neutrino spectrum with the use of Monte Carlo method, in Section 3 we briefly present neutrino-induced reactions and outline of selected detectors. Section 4 contains the expected neutrino signal from a star located at a distance of 1 kpc. In Section 5 astrophysical implications of the pre-supernova neutrino detection are discussed.

2. The spectrum of pair-annihilation neutrinos

Neutrinos produced by thermal processes are the most important part of the neutrino flux balancing the nuclear energy generation in the central region of massive ($M > 8M_\odot$) stars at late phases of nuclear burning, i.e. from carbon burning up to silicon burning. For simplicity, we have assumed that the entire neutrino flux is produced by pair annihilation. [2] Actually, so-called photoneutrinos and neutrinos from plasmon decay (cf. [19], Fig. 1) may contribute to the total neutrino flux [18], depending on physical conditions. This assumption is valid up to the silicon burning. After this phase the amount of neutrinos produced by weak nuclear reactions (β decays, electron capture) increases, and finally dominates the neutrino flux [4].

Pair annihilation neutrinos are produced in the reaction ([20, p. 171])

$$e^+ + e^- \rightarrow \nu_x + \bar{\nu}_x. \tag{1}$$

A high temperature ($T > 10^9$ K) is required to produce enough e^+e^- pairs. Usually, in the local thermodynamical equilibrium, these pairs annihilate back into photons, but sometimes the reaction (1) occurs. Neutrinos produced by the reaction (1) escape freely from the central region of a star. In reaction Eq. (1) the fluxes of neutrinos and antineutrino are the same.

We calculate the spectrum of neutrinos produced in reaction (1) with the Monte Carlo method of Ref. [21]. Both, electrons and positrons are described by Fermi–Dirac (FD) distributions. Conditions in the central region of the 20 $M_\odot$ star which define FD distribution parameters are summarized in Table 2.

In the simulation we pick up electron and positron four-momenta from FD distributions, transform to the center-of-mass frame, distribute neutrino momentum directions randomly, and convert neutrinos energy back to the rest frame. Every single event is binned and counted as $|M|^2$, where our annihilation matrix is proportional to:

$$\begin{aligned}|M|^2 \propto\ & (C_A - C_V)^2 (p_{e^-} \cdot q_{\nu_x})(p_{e^+} \cdot q_{\bar{\nu}_x}) \\ & + (C_A + C_V)^2 (p_{e^+} \cdot q_{\nu_x})(p_{e^-} \cdot q_{\bar{\nu}_x}) \\ & + m_e^2 (C_V^2 - C_A^2) q_{\nu_x} \cdot q_{\bar{\nu}_x}.\end{aligned} \tag{2}$$

Here p and q are four-momenta, m_e is the electron mass and:

[2] Inspection of Fig. 3, 4, 8, 9, 12, and 13 from Itoh et al. [18] together with the values of electron fraction, $Y_e = 0.5$, central temperature, T_c, and density, ρ_c, from Table 2 shows that the annihilation neutrinos are dominant.

$$C_{\mathrm{V}} = \frac{1}{2} \pm 2\sin^2\theta_{\mathrm{W}}, \quad C_{\mathrm{A}} = \frac{1}{2}, \tag{3}$$

where θ_{W} is the Weinberg angle and $\sin^2\theta_{\mathrm{W}} = 0.2224$. The '+' sign refers to electron neutrinos, while the '−' sign is for μ and τ neutrinos. The relative number of events from two simulation runs (one for the '+' sign, the other one for the '−' sign) has been used to determine the $\nu_{\mu,\tau}/\nu_{\mathrm{e}}$ ratio.

The resulting anti-neutrino spectrum is presented in Fig. 1. We have used this spectrum together with the neutrino luminosity from Table 2 and the flavor fractions given in Table 3 to find the detector response.

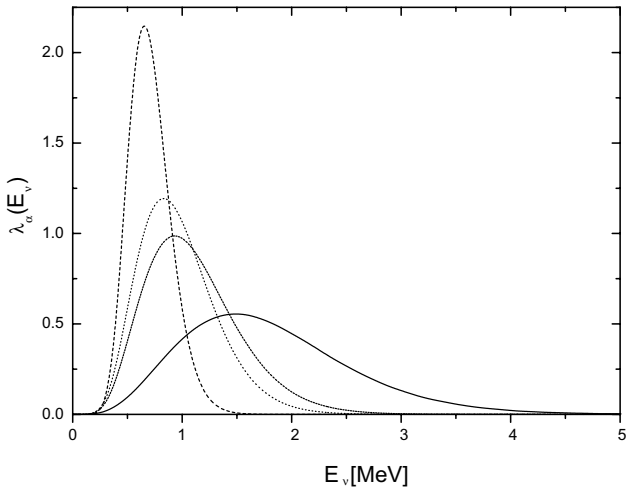

Fig. 1. Normalized spectrum of pair-annihilation anti-neutrinos emitted by 20 $M_\odot$ star during carbon (dashed line), neon (dotted line), oxygen (short-dashed line) and silicon (solid line) burning stage. The spectrum shape for all flavors of neutrinos and anti-neutrinos is very similar. However, relative fluxes of given neutrino flavors (cf. Table 3) are different. There is equal amount of neutrinos and anti-neutrinos. The average anti-neutrino energy is 1.80, 1.11, 0.97, and 0.71 MeV for Si, O, Ne, and C burning stage, respectively. As we expect, for $T \to 0$ the spectrum shape approaches the $E_{\bar{\nu}} = m_{\mathrm{e}} = 0.51$ MeV annihilation line.

Table 3
Fraction of given neutrino flavor emitted by pair-annihilation, used in formula (9)

Burning phase	ν_{e} ($\bar{\nu}_{\mathrm{e}}$) fraction (%)	$\nu_{\mu,\tau}/\nu_{\mathrm{e}}$ ratio	Average ν_x energy (MeV)
C	42.5	1:11.4	0.71
Ne	39.8	1:7.8	0.99
O	38.9	1:6.9	1.13
Si	36.3	1:5.4	1.85

One can notice increasing with temperature fraction of muon and tau neutrinos.

3. Neutrino reactions and cross-sections in modern neutrino detectors

3.1. Brief description of selected experiments

Super-Kamiokande [22] and SNO [23] are the largest present supernova neutrino detectors. Super-Kamiokande contains about 32,000 tons of water in the inner volume. The SNO detector consists of 1000 tons of ultra-pure heavy water and about 1700 tons of light water. Both the light and heavy water form active detector volumes for supernova neutrino detections, providing proton and deuteron targets for neutrino interactions.

Because of low, due to large distance, neutrino flux from candidate stars undergoing advanced stages of nuclear burning, very large detectors are needed in order to detect the signal. Fortunately, there are proposals of two next generation water Cherenkov detectors for proton decay searches, UNO [2] and Hyper-Kamiokande [1], with 440,000 and 540,000 tons of water in fiducial volumes, respectively. We consider here also two detectors employing liquid scintillator (LS) that will be capable of detecting supernova neutrinos. These are KamLAND [24], already operating, and Borexino [25], to be operating soon. The low energy threshold for recoil electrons and the scintillation light are their most important advantages over water Cherenkov detectors.

3.1.1. Water Cherenkov detectors

Water Cherenkov detectors have good efficiency of detection of recoil electrons with energy above a rather high threshold (about 5 MeV). Recoil electrons are produced mainly in NC/CC interactions between neutrinos and electrons. However, almost all interesting events will be produced in CC interactions between electron anti-neutrinos and protons (inverse β decay). The neutrino/anti-neutrino spectrum is closely related to the electron/positron spectrum. Pair-annihilation neutrinos from considered last stages of pre-

supernova star cannot be detected because of their low energy. We want, however, to point out that despite this high energy threshold problem, we may detect the signal from capture of neutrons produced in inverse β decay, if some neutron absorbent material will be added to the pure water. The salt phase of the SNO experiment proves that this is feasible. SNO detects ^{36}Cl de-excition via an 8.6 MeV total energy gamma-ray cascade which is distinguishable from CC (single energetic particle Cherenkov) events by angular isotropy measures.

The remaining flavors, ν_μ, ν_τ, $\bar{\nu}_\mu$ and $\bar{\nu}_\tau$, interact only by neutral-currents, i.e. only elastically scatter off electrons.

3.1.2. Liquid scintillator detectors

The primary goal of the Kamioka Liquid Scintillator Anti-Neutrino Detector (KamLAND) experiment is a search for the oscillation of $\bar{\nu}_e$'s emitted from distant power reactors [24]. The inverse β decay reaction is utilized to detect $\bar{\nu}_e$'s with energies above 1.8 MeV in 1000 tons of liquid scintillator (LS). The detection of the e^+ and the 2.2 MeV gamma-ray from neutron capture on proton in delayed coincidence is a powerful tool for reducing background.

The Borexino experiment main physics goal is the detection of the 0.86 MeV ν_e's from electron-capture decay of ^{7}Be in the Sun [25]. The central volume of the detector contains 300 tons of liquid scintillator. Neutrinos from the last stages of nuclear burning will interact in the LS via electron scattering and the inverse β-decay.

3.2. Reactions and cross-sections

3.2.1. The $\bar{\nu}_e + p \to e^+ + n$ reaction

Neutrino–proton scattering (often referred to as quasi-elastic neutrino–proton scattering) is historically called inverse β decay. The structure of nucleon in neutrino–proton scattering at MeV energies is not important, because the momentum transfer between the two nucleons is small. We may approximate the vector and axial-vector form factors with two constants: $F_{\mathrm{V}}(0) = g_{\mathrm{V}} = 1$ and $F_{\mathrm{A}}(0) = g_{\mathrm{A}} = 1.27$. The value of $g_{\mathrm{A}}/g_{\mathrm{V}}$ is determined from the measured lifetime of the neutron.

Electron antineutrino quasi-elastic scattering on proton turns a proton into a neutron and produces positron of $E_{\mathrm{e}^+} = E_\nu - \Delta$ energy (at zeroth order in $1/M$), where $\Delta = M_{\mathrm{n}} - M_{\mathrm{p}}$ is the mass difference between the proton and neutron. The momentum of produced positron is $p_{\mathrm{e}^+} = \sqrt{E_{\mathrm{e}^+}^2 - m_{\mathrm{e}}^2}$.

The standard expression for the total cross-section is,

$$\begin{aligned}\sigma_{\mathrm{tot}} &= \sigma_0 (g_{\mathrm{V}}^2 + 3g_{\mathrm{A}}^2) E_{\mathrm{e}^+} \mathrm{p}_{\mathrm{e}^+} \\ &= 0.0952 \left(\frac{E_{\mathrm{e}^+} \mathrm{p}_{\mathrm{e}^+}}{1\ \mathrm{MeV}^2} \right) \times 10^{-42}\ \mathrm{cm}^2. \end{aligned} \tag{4}$$

The constant σ_0 includes the energy-independent inner radiative corrections [26]:

$$\sigma_0 = \frac{G_F^2 \cos^2 \theta_{\mathrm{C}}}{\pi} (1 + \Delta_{\mathrm{inner}}^R), \tag{5}$$

where $\Delta_{\mathrm{inner}}^R \simeq 0.024$, and the Cabbibo angle $\cos\theta_{\mathrm{C}} = 0.974$.

The inverse neutron β-decay, $\bar{\nu}_{\mathrm{e}} + \mathrm{p} \to \mathrm{e}^+ + \mathrm{n}$, is the reaction giving the largest yield for the detection of pre-supernova neutrinos. The large cross-section, low energy threshold, delayed coincidence between positron's annihilation and neutron capture signals, abundance of target protons makes this reaction the most promising.

We calculate the signal, which is the number of produced neutrons from this reaction in all the considered experiments.

3.2.2. Neutrino–electron scattering

Neutrino–electron scattering produces recoil electrons with kinetic energy from zero up to the kinematic maximum. The laboratory differential cross-section for the $\nu_x \mathrm{e}^-$ scattering is of the form:

$$\frac{\mathrm{d}\sigma}{\mathrm{d}T'_{\mathrm{e}}} = \frac{2G_F^2 m_{\mathrm{e}}}{\pi} \left[c_L^2 + c_R^2 \left(\frac{E_\nu - T'_{\mathrm{e}}}{E_\nu} \right)^2 - c_L c_R \frac{m_e}{E_\nu} \frac{T'_{\mathrm{e}}}{E_\nu} \right], \tag{6}$$

where $T'_{\mathrm{e}} = E'_{\mathrm{e}} - m_{\mathrm{e}}$ is the recoil electron kinetic energy.

In our rate calculation we approximate by integrating Eq. (6) over all electron recoil energies. The total cross-section is

Table 4
Coefficients that appear in neutrino–electron scattering cross-section [27]

Reaction	c_L	c_R	$c_L^2+\frac{1}{3}c_R^2$	$\frac{1}{2}c_Lc_R$
$\nu_e e^-$	$1/2+\sin^2\theta_W$	$\sin^2\theta_W$	0.5525	0.0845
$\bar{\nu}_e e^-$	$\sin^2\theta_W$	$1/2+\sin^2\theta_W$	0.2317	0.0845
$\nu_{\mu,\tau} e^-$	$-1/2+\sin^2\theta_W$	$\sin^2\theta_W$	0.0901	−0.0311
$\bar{\nu}_{\mu,\tau} e^-$	$\sin^2\theta_W$	$-1/2+\sin^2\theta_W$	0.0775	−0.0311

$$\sigma=\int_0^{T'_{\max}}\frac{\mathrm{d}\sigma}{\mathrm{d}T'_e}\mathrm{d}T'_e=\frac{2G_F^2m_eE_\nu}{\pi}\left[c_L^2+\frac{1}{3}c_R^2-\frac{1}{2}c_Lc_R\frac{m_e}{E_\nu}\right], \quad (7)$$

where c_L, c_R coefficients depend on the neutrino species considered (Table 4). Total scattering cross-section is calculated without radiative corrections.

The elastically-scattered electrons will have kinetic energies of a few MeV. These relativistic electrons will be difficult to detect in any Cherenkov detector, because of high energy threshold. However, the next-generation liquid-scintillator Borexino detector will have low target threshold of approximately 0.25 MeV, mainly due to progress in radiopurity research [28]. It is possible that KamLAND experiment will improve radiopurity to detect low energy recoil electrons in future, so we calculate signal from elastic processes in both detectors.

3.2.3. Interactions with heavy water

The Sudbury Neutrino Observatory (SNO) employs inelastic neutrino–deuteron scattering to study the solar neutrino flux. The total ^{8}B solar neutrino flux is determined from observation of the following reactions:

$$\nu_e+d\to p+p+e^-(CC),$$
$$\nu_x+d\to p+n+\nu_x(NC),$$
$$\nu_x+e^-\to\nu_x+e^-(ES),$$

where $x=e$, μ or τ. The pre-supernova anti-neutrinos of all flavors can interact with deuterons and electrons through the following additional reactions:

$$\bar{\nu}_e+d\to n+n+e^+(\text{inverse }\beta),$$
$$\bar{\nu}_x+d\to p+n+\bar{\nu}_x(NC),$$
$$\bar{\nu}_x+e^-\to\bar{\nu}_x+e^-(ES).$$

By observing the charged-current interactions (CC and inverse β-decay) only electron neutrino (anti-neutrino) flux is measured. The NC reaction of any flavour neutrino on deuteron breaks up the deteron and produces a proton and a neutron. The NC cross-section is the same for all neutrino flavours, thus one can determine the total flux of all active neutrino and anti-neutrino flavors above an energy threshold of 2.2 MeV. The cross-sections for ν–d reactions are of primary importance in the analysis of SNO data, it is motivation for theoretical calculations employing nuclear physics and effective field theory. We use in our paper the cross-section values for the deuteron break-up interactions from the tables provided by Kubodera and Nozawa [29]. In all cases of anti-neutrino reactions with light or heavy water only the neutron is detected in the final state. The ES reaction produces low energy recoil electron mainly below energy threshold, so we do not consider further this reaction.

3.2.4. Averaged cross-section

The spectrum-averaged cross-section is

$$\bar{\sigma}_\alpha=\int_0^\infty\sigma(E)\lambda_\alpha(E)\,\mathrm{d}E, \quad (8)$$

where $\lambda_\alpha(E)$ is the *normalized* spectrum for neutrinos produced by the pair-annihilation in pre-supernova star at C, Ne, O and Si burning phase ($\alpha=$ C, Ne, O and Si). The integration over the spectrum of incoming neutrino energies, E, was performed numerically and the results are shown in Table 5. We use the total cross-sections $\sigma(E)$ for

Table 5
Spectrum-averaged cross-sections for interactions of pre-supernova neutrinos in the light and heavy-water Cherenkov detectors and liquid scintillator detectors

Reaction	E_{th} (MeV)	$\bar{\sigma}_{Si}$ (cm^2)	$\bar{\sigma}_{O}$ (cm^2)	$\bar{\sigma}_{Ne}$ (cm^2)	$\bar{\sigma}_{C}$ (cm^2)
$\bar{\nu}_e + p \to e^+ + n$	1.8	6.80×10^{-44}	3.74×10^{-45}	9.07×10^{-46}	4.88×10^{-49}
$\bar{\nu}_e + d \to e^+ + n + n$	4.0	1.22×10^{-46}	4.38×10^{-50}	4.64×10^{-52}	–
$\nu_x + d \to \nu_x + p + n$	2.2	1.68×10^{-45}	1.64×10^{-47}	1.63×10^{-48}	4.76×10^{-54}
$\bar{\nu}_x + d \to \bar{\nu}_x + p + n$	2.2	1.41×10^{-45}	1.20×10^{-47}	1.19×10^{-48}	3.27×10^{-54}
$\nu_e + e^- \to \nu_e + e^-$	0.0	1.76×10^{-44}	1.04×10^{-44}	9.07×10^{-45}	6.40×10^{-45}
$\bar{\nu}_e + e^- \to \bar{\nu}_e + e^-$	0.0	6.79×10^{-45}	4.05×10^{-45}	3.49×10^{-45}	2.45×10^{-45}
$\nu_{\mu,\tau} + e^- \to \nu_{\mu,\tau} + e^-$	0.0	3.07×10^{-45}	1.95×10^{-45}	1.72×10^{-45}	1.26×10^{-45}
$\bar{\nu}_{\mu,\tau} + e^- \to \bar{\nu}_{\mu,\tau} + e^-$	0.0	2.63×10^{-45}	1.68×10^{-45}	1.49×10^{-45}	1.10×10^{-45}

E_{th} is the neutrino energy threshold for a given reaction; ν_x stands for ν_e, ν_μ and ν_τ; $\bar{\nu}_x$ stands for $\bar{\nu}_e$, $\bar{\nu}_\mu$ and $\bar{\nu}_\tau$.

the most important interactions in considered detectors as described in previous sections.

4. The event rate and the background signal in selected detectors

The number of incoming particles interacting (per day) with the target is equal to the product of the spectrum averaged cross-section $\bar{\sigma}_\alpha$, the number N of target atoms or electrons, the total intensity of the flux per day ϕ_α, and the fraction f of total flux that is interacting with a given target. The reaction rate r per day is written as

$$r\ (\mathrm{day}^{-1}) = f \cdot \bar{\sigma}_\alpha\ (\mathrm{cm}^2) \cdot N \cdot \phi_\alpha\ (\mathrm{cm}^{-2}\,\mathrm{day}^{-1}). \tag{9}$$

For anti-neutrinos from silicon burning stage in 1 kton water Cherenkov detector we have: $\bar{\sigma}_{Si} = 6.8 \times 10^{-44}$ (cm^2), $N = 6.69 \times 10^{31}$, $\phi_{Si} = 7.6 \times 10^{11}$ (cm^{-2} day^{-1}) and, from Table 3, $f = 0.363$.

The number of target particles is easy to calculate if the mass and the chemical composition of material in the fiducial volume are known. We obtain the total flux per day from the pre-supernova star 1 kpc away by dividing the luminosity L_ν (Table 2) by the average neutrino energy (Table 3) and the surface area of a $R = 1$ kpc radius sphere. The spectrum of the total neutrino flux from the silicon burning stage is compared with that for solar neutrinos in Fig. 2. The fraction of total flux that interact, f, depends on the burning stage and the type of interactions in the detector. All these expected properties are shown in Table 6. Here the most important is the final result of our calculation which is the event rate per day.

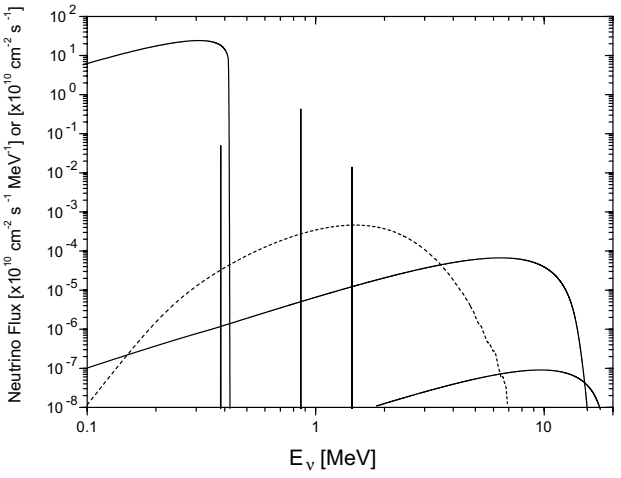

Fig. 2. The standard solar neutrino spectrum (BP2000, [5]) for pp fusion reactions in the Sun (solid lines) and the spectrum of pair-annihilation neutrinos emitted by a 20 $M_\odot$ star during silicon burning stage (dashed line). Star is located at a distance of 1 kpc.

The Eq. (9) gives for the silicon burning neutrinos 1.27 neutrons/day/kiloton of water for a star 1 kpc away. Event rates for large detectors are summarized in Table 6. Super-Kamiokande is the best currently working detector for such an observation, with 41 events per day, but needs a modification for making neutron detection possible. The same modification would be required in the light water volume of the SNO detector, allowing it to detect 2.2 events/day.

To make detection of pre-supernova anti-neutrinos feasible we propose to supplement the

Table 6
Event rate per day in selected neutrino detectors from silicon burning stage in neutrino-cooled star at distance of 1 kpc

Detector	Mass (kton)	Reactions	Number of targets	Flux at 1 kpc ($cm^{-2}\,day^{-1}$)	Event rate (day^{-1})
Borexino	0.3 (C_9H_{12})	$\bar{\nu}_e + p \to e^+ + n$	1.80×10^{31}	2.8×10^{11}	0.34
		$\nu_e + e^- \to \nu_e + e^-$	9.92×10^{31}	2.8×10^{11}	0.49
		$\bar{\nu}_e + e^- \to \bar{\nu}_e + e^-$	9.92×10^{31}	2.8×10^{11}	0.19
		$\nu_{\mu,\tau} + e^- \to \nu_{\mu,\tau} + e^-$	9.92×10^{31}	1.0×10^{11}	0.03
		$\bar{\nu}_{\mu,\tau} + e^- \to \bar{\nu}_{\mu,\tau} + e^-$	9.92×10^{31}	1.0×10^{11}	0.026
KamLAND	0.2 (C_9H_{12})	$\bar{\nu}_e + p \to e^+ + n$	8.55×10^{31}	2.8×10^{11}	1.6
	0.8 ($C_{12}H_{26}$)	$\nu_e + e^- \to \nu_e + e^-$	3.43×10^{32}	2.8×10^{11}	1.7
		$\bar{\nu}_e + e^- \to \bar{\nu}_e + e^-$	3.43×10^{32}	2.8×10^{11}	0.65
		$\nu_{\mu,\tau} + e^- \to \nu_{\mu,\tau} + e^-$	3.43×10^{32}	1.0×10^{11}	0.11
		$\bar{\nu}_{\mu,\tau} + e^- \to \bar{\nu}_{\mu,\tau} + e^-$	3.43×10^{32}	1.0×10^{11}	0.09
SNO	1.7 (H_2O)	$\bar{\nu}_e + p \to e^+ + n$	1.14×10^{32}	2.8×10^{11}	2.2
	1 (D_2O)	$\bar{\nu}_e + d \to e^+ + n + n$	6.00×10^{31}	2.8×10^{11}	0.004
		$\nu_x + d \to \nu_x + p + n$	6.00×10^{31}	3.8×10^{11}	0.038
		$\bar{\nu}_x + d \to \bar{\nu}_x + p + n$	6.00×10^{31}	3.8×10^{11}	0.032
Super-K	32 (H_2O)	$\bar{\nu}_e + p \to e^+ + n$	2.14×10^{33}	2.8×10^{11}	41
UNO	440 (H_2O)	$\bar{\nu}_e + p \to e^+ + n$	2.94×10^{34}	2.8×10^{11}	560
Hyper-K	540 (H_2O)	$\bar{\nu}_e + p \to e^+ + n$	3.61×10^{34}	2.8×10^{11}	687

existing and future water Cherenkov detectors with some addition of NaCl or $GdCl_3$ (see the proposition made by Beacom and Vagins *GADZOOKS*! [30]) to the water. Neutrons produced in inverse β decay are captured by Gd or Cl nuclei producing high energy (above 8 MeV) gamma cascades. The addition of neutron absorbers is very important, because in a pure light water neutrons are captured by protons and produce not detectable 2.2 MeV gamma cascades, e.g. energy threshold in SK is about 5 MeV. This modification has been proved to work in the salt phase of solar neutrino detection in the SNO detector. The addition of NaCl to the kiloton of heavy water increased the neutron capture efficiency and the associated Cherenkov light [31]. Neutron capture efficiency is different in every experiment and has to be calibrated with neutron source, as e.g. ^{252}Cf in SNO.

Background neutron events are disturbing pre-supernova neutrino detection, and thus should be carefully studied in every detector before the addition of the neutron absorber. The average rate of background neutron production from activity in the D_2O region is 0.72 neutrons per day in the SNO detector [31]. These background events are produced mainly by deuteron photodisintegration (not relevant for a light water detectors) and due to the external-source neutrons. The background of neutrons in spallation products from energetic muons can be suppressed by a veto following the muon [24]. Long-lived muon induced isotopes, which decay by the production of a neutron and a beta (e.g. ^8He, ^9Li and ^{11}Li), can simulate the $\bar{\nu}_e$ coincidence signature. Thus, the study of muon induced spallation products in the neutron absorber nuclei is important. Other major sources of the neutron background are : (α, n) interactions, fission of radioactive impurities, interactions of atmospheric and fission anti-neutrinos (both natural and from reactors) with protons. The neutrino flux from nuclear power plants depends strongly on location of nearby ones, and this factor has to be included in projects of future pre-supernova detectors.

5. Importance of pre-supernova neutrinos detection

Our results for 20 $M_\odot$ pre-supernova star show that neutrinos (particularly $\bar{\nu}_e$) from last stages of nuclear burning in such a star are possible to de-

tect. Future detectors (UNO, Hyper-Kamiokande) will be able to cover significant fraction of the Galaxy. However, when we take into account relatively low, from typical experiment lifetime point of view, local *core-collapse* SN rate, of 1 per $\sim$100 years or less (Table 1 of [32,33] for overview, see however [34]), only projects of long standing, namely nucleon decay and neutrino observatories, have chance to be operating during such an event. At present it is difficult to reliably estimate probability of successful neutrino-cooled star detection because of: (1) uncertainties of local supernova rate, (2) unexplored yet variety of massive stars and their models, and (3) unknown details of detection technique, especially neutron background level. Making optimistic assumption of 10 events/day detectable and clearly distinguishable from background, we get (using Galaxy model [12] and Si burning event rate for 20 $M_\odot$ star from Table 6) 1.7% Galaxy coverage (i.e. up to 2 kpc from earth) for Super Kamiokande. Next generation detectors UNO and Hyper Kamiokande cover significant fraction 30% (7.5 kpc) and 37% (8.2 kpc) of Galaxy disk stars, respectively. The highest Galaxy supernova rate estimate of 1 per 10 years [10] gives (under above assumptions) successful detection probability of 3% (SK), 60% (UNO) and 75% (HyperK) during 20 years of uninterrupted observation.

Benefits given by the detection of the pre-supernova neutrino signal can be divided into two sets: (1) those related to possible prediction of subsequent supernova event and (2) insight into processes related to deep interior of massive stars prior to its death.

5.1. Supernova prediction?

Supernova event is an unpredictable phenomenon. Astronomers await nearby supernova for 400 years. Therefore, many of them speculate on the likely next Galaxy event. The list of candidates includes Betelgeuse, Mira Ceti, Antares, Ras Algheti, γ^2 Vel, Sher25 and Eta Carinae. Unfortunately, the surface of these stars is unaffected by (possibly) dramatic nuclear and hydrodynamical processes deep inside. This is effect of $\tau \sim 10000$ years timescale of hydrogen envelope [35]. No electromagnetic observation at any wavelength and resolution can help. Only neutrinos carry informations on the current state of the stellar core. That is why only neutrinos could warn us before the supernova event. The case of SN1987A [6] unexpectedly revealed this fact. The silicon-burning neutrinos, although carry only about 1% energy compared to the main supernova neutrino burst, are possible to detect, as we showed in previous sections (cf. Table 6). The information about an incoming supernova is transmitted around 2 days [3] earlier. The early warning would provide an additional time which may be crucial for preparation of all available observational techniques, including gravitational radiation detectors, and would allow us to be ready for the main neutrino burst from collapse and proto-neutron star cooling.

In a very favorable case of a close star, much less than 1 kpc away [4] with operating megaton-scale neutrino observatory modified by addition of appropriate neutron absorber, we could expect detection of oxygen and neon-burning neutrinos a few months before the explosion. The detection, however, would be more difficult than silicon-burning neutrinos, mainly due to lower luminosities L_ν (Table 2), lower average energies E_ν (Fig. 1) and smaller cross-sections (Table 5).

Let us note, that the above speculations are no longer valid if the neutrino detection is *offline*. Realtime (*on-line*) data analysis is strongly preferred from this point of view.

5.2. Astrophysical importance of Si burning neutrinos

The aim of our work is to show the feasibility of pair-annihilation neutrinos detection. We did not discuss the calculations of the neutrino luminosities, but actually the silicon burning is very complicated and "potentially numerically unstable

[3] For a 20 $M_\odot$ star. This time strongly depends on the stellar mass (cf. [35], Table 1), and is in the range 0.7–18 days.

[4] A 20 $M_\odot$ pre-SN star at Betelgeuse distance (Betelgeuse is actually a 15 $M_\odot$ red giant at a distance of 185 pc) which just entered the oxygen burning stage would produce in HyperK 45 neutrons/day during 6 months before its explosion.

stage'' ([35], Section IV A-4) of stellar modeling, mainly due to similar timescales of nuclear burning and convection. The behaviour of spherically symmetric models employing the mixing-length convection appears to be completely different from 2D hydrodynamic models ([3], Epilogue). Thus any observational data, even few detected events may be very important to constrain theoretical models. In a favorable situation of a close star with new-generation observatories we should be able to constrain the time-dependence of the neutrino flux and of the spectrum.

The Si-burning neutrino emission precedes a subsequent explosion event independently of the actual stellar death scenario. The SN1987A confirmed standard supernova mechanism [36]. However, it is believed that at least some of the massive stars die in other ways. The most recent research is concentrated on GRB-SN connection [37], their relation to failed supernovae [38] and the core rotation [33]. It is not yet understood why some massive stars become supernovae, hypernovae or even GRBs. The detection of pre-supernova Si-burning neutrinos together with the following observations of optical, neutrino and gravitational signals from the supernova and the identification of the progenitor would establish the relation of pre-supernova conditions and the explosion dynamics. Let's note, that in case of the supernova shrouded in interstellar clouds, Si burning neutrinos carry exclusive information on the progenitor.

5.3. Discussion

This article shows that detection of pre-supernova star neutrinos is a feasible new goal for neutrino astronomy. Our simplified analysis may be extended to stars of different masses. The constant neutrino flux can be replaced with more realistic time-dependent flux generated by stellar evolution codes. The simple spectrum of pair-annihilation neutrinos can be augmented with detailed plasma and weak-nuclear-neutrinos spectra. These refinements could change the results somewhat, not affecting our predictions as to the detection feasibility considerably. Clearly, the most important circumstance is the distance to the next Galactic supernova. It is also, however, the most indeterminable one. Therefore, if we want to get results, we have to maximize our observation range. Detectors like Hyper-Kamiokande, UNO, or even better should be operating at the ''time zero''.

Acknowledgements

We thank K. Grotowski and M. Wojcik for helpful discussions and advice. This work was partially supported by the research grant from the Institute of Physics of Jagiellonian University, and through KBN grants 2 P03B 110 24 and PBZ-KBN-054/P03/02.

References

[1] M. Koshiba, Phys. Rep. 220 (1992) 229;
K. Nakamura, Neutrino Oscillations and Their Origin, Universal Academy Press, Tokyo, 2000, p. 359.
[2] C.K. Jung, in: International Workshop on Next Generation Nucleon Decay and Neutrino Detector (NNN 99), Stony Brook, New York, 23–25 September 1999. hep-ex/0005046.
[3] D. Arnett, Supernovae and Nucleosynthesis, Princeton University Press, 1996.
[4] A. Heger, S.E. Woosley, G. Martinez-Pinedo, K. Langanke, Astrophys. J. 560 (2001) 307–325.
[5] John N. Bahcall, M.H. Pinsonneault, Sarbani Basu, Astrophys. J. 555 (2001) 990–1012.
[6] W.D. Arnett, J.N. Bahcall, R.P. Kirshner, S.E. Woosley, Ann. Rev. Astron. Astrophys. 27 (1989) 629.
[7] T.A. Weaver, G.B. Zimmerman, S.E. Woosley, Astrophys. J. 225 (1978) 1021.
[8] S. Van den Bergh, G.A. Tammann, Ann. Rev. Astron. Astrophys. 29 (1991) 368.
[9] E. Cappellaro, M. Turrato, Astrophys. Space Sci. Libr. 264 (2000) 321.
[10] J.N. Bahcall, T. Piran, Astrophys. J. Lett. 267 (1983) L77.
[11] R.G. Strom, Astron. Astrophys. 288 (1994) L1.
[12] J.N. Bahcall, R.M. Soneira, Astrophys. J. Lett. 238 (1980) L17.
[13] http://antwrp.gsfc.nasa.gov/apod/ap990605.html.
[14] S.M. Asida, D. Arnett, Astrophys. J. 545 (2000) 435.
[15] S. Ciechanowicz, M. Misiaszek, W. Sobków, hep-ph/0305107, Eur. Phys. J., in press.
[16] I. Gil-Botella, A. Rubbia, J. Cosmol. Astropart. Phys. JCAP 10 (2003) 009.
[17] W. Greiner, B. Muller, Gauge Theory of Weak Interactions, 2nd ed., Springer-Verlag, Heidelberg, Berlin, New York, 2000.
[18] N. Itoh, et al., Astrophys. J. Suppl. Ser. 102 (1996) 411.
[19] B. Aufderheide, Astrophys. J. 411 (1993) 813.

[20] R. Kippenhahn, A. Weigert, Stellar Structure and Evolution, Springer-Verlag, 1994.
[21] X. Shi, G.M. Fuller, Astrophys. J. 503 (1998) 307.
[22] M. Malek, et al., Phys. Rev. Lett. 90 (2003) 061101.
[23] Q.R. Ahmad, et al., Phys. Rev. Lett. 89 (2002) 011301.
[24] K. Eguchi, et al., Phys. Rev. Lett. 90 (2003) 021802.
[25] G. Alimonta, et al., Astropart. Phys. 16 (2002) 205–234.
[26] P. Vogel, J.F. Beacom, Phys. Rev. D 60 (1999) 053003.
[27] M. Fukugita, T. Yanagida, Physics of Neutrinos and Applications to Astrophysics, Springer-Verlag, Heidelberg, Berlin, New York, 2003.
[28] G. Zuzel, et al., Nucl. Instrum. Meth. A 498 (2003) 240–255.
[29] K. Kubodera, S. Nozawa, Int. J. Mod. Phys. E 3 (1994) 101–148.
[30] J.F. Beacom, M.R. Vagins, Phys. Rev. Lett., hep-ph/0309300, submitted for publication.
[31] The SNO Collaboration, Phys. Rev. Lett., nucl-ex/0309004, submitted for publication.
[32] J.F. Beacom, R.N. Boyd, A. Mezzacappa, Phys. Rev. D 63 (2001) 073011.
[33] A. Odrzywolek, M. Kutschera, M. Misiaszek, K. Grotowski, Acta Phys. Polo. B 34 (5) (2003) 2791.
[34] A. Di Paola, et al., Astron. Astrophys. 393 (2002) L21.
[35] S.E. Woosley, A. Heger, T.A. Weaver, Rev. Mod. Phys. 74 (2002) 1015.
[36] H.A. Bethe, Rev. Mod. Phys. 62 (1990) 801.
[37] A. MacFayden, S.E. Woosley, Astrophys. J. 524 (1999) 262.
[38] Andrew Gould, Samir Salim, Astrophys. J. 572 (2002) 944.

A&A 529, A156 (2011)
DOI: 10.1051/0004-6361/201015133

Astronomy & Astrophysics

Probing thermonuclear supernova explosions with neutrinos⋆

A. Odrzywolek[1] and T. Plewa[2]

[1] Marian Smoluchowski Institute of Physics, Jagiellonian University, Reymonta 4, 30-059 Cracow, Poland
e-mail: andrzej.odrzywolek@uj.edu.pl
[2] Department of Scientific Computing, Florida State University, Tallahassee, FL 32306, USA

Received 2 June 2010 / Accepted 8 March 2011

ABSTRACT

Aims. We present neutrino light curves and energy spectra for two representative type Ia supernova explosion models: a pure deflagration and a delayed detonation.
Methods. We calculate the neutrino flux from β processes using nuclear statistical equilibrium abundances convoluted with approximate neutrino spectra of the individual nuclei and the thermal neutrino spectrum (pair+plasma).
Results. Although the two considered thermonuclear supernova explosion scenarios are expected to produce almost identical electromagnetic output, their neutrino signatures appear vastly different, which allows an unambiguous identification of the explosion mechanism: a pure deflagration produces a single peak in the neutrino light curve, while the addition of the second maximum characterizes a delayed-detonation. We identified the following main contributors to the neutrino signal: (1) weak electron neutrino emission from electron captures (in particular on the protons ^{55}Co and ^{56}Ni) and numerous β-active nuclei produced by the thermonuclear flame and/or detonation front, (2) electron antineutrinos from positron captures on neutrons, and (3) the thermal emission from pair annihilation. We estimate that a pure deflagration supernova explosion at a distance of 1 kpc would trigger about 14 events in the future 50 kt liquid scintillator detector and some 19 events in a 0.5 Mt water Cherenkov-type detector.
Conclusions. While in contrast to core-collapse supernovae neutrinos carry only a very small fraction of the energy produced in the thermonuclear supernova explosion, the SN Ia neutrino signal provides information that allows us to unambiguously distinguish between different possible explosion scenarios. These studies will become feasible with the next generation of proposed neutrino observatories.

Key words. hydrodynamics – neutrinos – nuclear reactions, nucleosynthesis, abundances – supernovae: general

1. Introduction

The origins of type Ia supernovae (SN Ia) remain one of the major unsolved problems of stellar evolution (Höflich & Stein 2002; Kuhlen et al. 2006; Piro 2008; Zingale et al. 2009). The commonly accepted theoretical framework considers an explosion scenario in which a massive white dwarf slowly gains mass in the process of accretion from a non-degenerate companion (Whelan & Iben 1973; Yoon & Langer 2003; Han & Podsiadlowski 2004; Meng & Yang 2010). Alternatively, the degenerate matter might be ignited in the process of a violent merger of binary white dwarfs (Iben & Tutukov 1984; Webbink 1984; Han 1998). The latter channel might be a dominant source of thermonuclear events in early type galaxies (Gilfanov & Bogdán 2010; Wang et al. 2010), while there is no consensus as to which evolutionary process dominates in other environments (Scannapieco & Bildsten 2005; Raskin et al. 2009; Ruiter et al. 2009; Schawinski 2009).

Our progress toward understanding these events is hampered by the relatively low luminosity of their progenitors, and to date the evidence is largely circumstantial and exclusively indirect (Ruiz-Lapuente et al. 2004; Badenes et al. 2007; Schawinski 2009; Gilfanov & Bogdán 2010). This stays in contrast with numerous identifications of core-collapse progenitors (Smartt 2009; Leonard 2009, and references therein). Furthermore, the nature of the explosion process is very uncertain, though it is commonly accepted that the energy source of the explosion is a thermonuclear burn (Hoyle & Fowler 1960). For a single-degenerate channel, the nuclear fuel is expected to burn first subsonically (Nomoto et al. 1976) with a likely transition to detonation at a later time (Khokhlov 1991; Woosley & Weaver 1994). It is much less clear what the ultimate fate of the merger is (Hachisu et al. 1986; Saio & Nomoto 1985; Yoon et al. 2007; Pakmor et al. 2010), and perhaps additional routes to an explosion are admissible (Podsiadlowski et al. 2008; Podsiadlowski 2010, and references therein). These questions along with the role that SN Ia play in studies of the early universe (Sandage & Tammann 1993; Riess et al. 1998; Phillips 2005; Wood-Vasey et al. 2007; Ellis et al. 2008; Riess et al. 2009; Kessler et al. 2009) motivate our search for additional sources of information about thermonuclear supernovae, and in particular about the explosion process.

Neutrinos are a proven source of information about astrophysical objects and phenomena, such as the Earth (Smirnov 2009; Araki et al. 2005; Dye 2006), and engineering systems such as nuclear power plants (Bowden 2008; Lhuillier 2009; Learned 2005; Guillian 2006). The Sun is one of the best-studied astrophysical neutrino sources thanks to its proximity and constancy of the ν_e flux (Bahcall 1989). Solar neutrino studies were first conducted using radiochemical detectors (Cleveland et al. 1998; Hampel et al. 1999) and more recently also in real-time (BOREXINO Collaboration et al. 2008; Arpesella et al. 2008; Fukuda et al. 2001; Ahmad et al. 2001). For contemporary non-solar neutrino experiments, the solar neutrino signal caused by the dominant reactions (pp, ^{8}B) constitutes somewhat undesirable background. However, supernova SN 1987A

⋆ Figures 9 to 20 are available in electronic form at
http://www.aanda.org

(Arnett et al. 1989) has been clearly observed in neutrinos in many detectors (Van Der Velde et al. 1988; Hirata et al. 1987; Galeotti et al. 1987; Alekseev et al. 1987) despite its nearly extragalactic distance (~50 kpc). The event has been the main trigger for intensive theoretical studies and modeling in the recent years (Immler et al. 2007; Nakahata & Sobel 2007) while a possibility of neutrino detection and obtaining neutrino energy spectra from core-collapse supernovae (Burrows 1990; Keil et al. 2003) attracted constant attention of theorists (Kistler et al. 2008; Fogli et al. 2005a; Ando et al. 2005; Fogli et al. 2005b) and stimulated experimental developments (Suzuki 2001; Learned 2004). Neutrino detection is a mature field of research nowadays. For instance, a stellar core-collapse at a distance <4 kpc will produce a signal strong enough to saturate the Super-Kamiokande detector (Nakahata 2007). Therefore, it is natural to consider the detectability of neutrinos from previously ignored sources, including thermonuclear supernova events.

As originally suggested by Nomoto et al. (1993), the neutrino signal produced by the thermonuclear deflagrations offers direct insight into the explosion process. Clearly, such observations would be extremely helpful in directing future SN Ia research and may possibly allow for distinguishing between various stellar evolution and explosion scenarios. A striking differences between neutrino emission from deflagrations and delayed detonations has been noted by Nomoto et al. (1993). More recently, in a series of articles Kunugise & Iwamoto (Iwamoto & Kunugise 2006; Kunugise & Iwamoto 2007) studied the ν_e light curve and spectra from the standard W7 explosion model (Nomoto et al. 1984) and discussed the detectability of this type of event by the Super-Kamiokande detector. We aim to extend those early studies to recent multi-dimensional thermonuclear supernova explosion models. We obtain supernova neutrino light curves and energy spectra for pure deflagration and delayed detonation explosion models. We show that the predicted neutrino signatures are markedly different in those two cases and can be used to identify the explosion mechanism.

2. Neutrino emission from thermonuclear supernovae

Neutrino emission from a type Ia supernova is considered negligible in most of the thermonuclear explosion models because the weak interaction rates are too slow compared to the hydrodynamic timescale (see Arnett 1996, Sect. 9.1) and the matter is essentially completely transparent to neutrinos. However, it is conceivable that if the amount of the energy emitted via neutrinos is significant compared to the energy produced in the thermonuclear burning, the neutrino cooling may play an important role in the explosion dynamics. In either case, neutrinos may provide important insights into the SN Ia explosion mechanism.

Neutrino emission from the existing SN Ia explosion models can be computed by post-processing snapshots of the hydrodynamical simulations. For the thermal neutrino emission this is a straightforward procedure because the neutrino spectrum only depends on the temperature and the (electron) density of the plasma. For weak nuclear processes, we have to know the isotopic composition of the plasma. Given the current computational resources, it is not feasible to include large nuclear reaction networks in multidimensional explosion model. The situation, however, is not completely hopeless because the hottest regions associated with thermonuclear flames and detonations, which is also where the neutrino emission is expected to be relatively high, are in the nuclear statistical equilibrium (NSE) (see Clayton 1984, Sect. 7.2). Under NSE conditions, isotopic abundances are determined solely by the thermodynamic properties of the plasma. Therefore, in the most important regions of the exploding star, we are again able to post-process models and compute required abundances. Once the isotopic composition is known, computing a neutrino emission is relatively straightforward (Kunugise & Iwamoto 2007).

In NSE, the isotopic composition of the matter is fully determined by the density, temperature, and electron density of the plasma (Clifford & Tayler 1965a,b). The NSE conditions are characterized by

1. a very high temperature to break-up the most strongly bound nuclei;
2. an evolutionary timescale long enough to allow for re-arranging of nucleons into equilibrium nuclei via strong/electromagnetic interactions.

These conditions can be found in the iron cores of pre-supernova stars, during core-collapse, and last but not least, during thermonuclear burn in type Ia supernovae. More recently, protoneutron star evolution and accretion-induced collapse recently has been analyzed from this point of view by Arcones et al. (2010).

For completeness we will discuss shortly the major properties of the considered neutrino emission processes. Model neutrino spectra are computed with help of the PSNS code (Odrzywolek 2005–2010).

2.1. Sources of neutrinos

2.1.1. Thermal processes

Three "classic" neutrino processes,

$$e^- + e^+ \rightarrow \nu_{e,\mu,\tau} + \bar{\nu}_{e,\mu,\tau} \quad (1a)$$

$$\gamma^*_{L,T} \rightarrow \nu_{e,\mu,\tau} + \bar{\nu}_{e,\mu,\tau} \quad (1b)$$

$$\gamma + e^- \rightarrow e^- + \nu_{e,\mu,\tau} + \bar{\nu}_{e,\mu,\tau} \quad (1c)$$

are the major source of the so-called thermal neutrinos (Munakata et al. 1985; Schinder et al. 1987; Esposito et al. 2003): annihilation of the e^+e^- pairs into neutrinos (Eq. (1a), Misiaszek et al. 2006); plasmon decay (Eq. (1b), Braaten 1991; Braaten & Segel 1993), and photoemission (Eq. (1c), Dutta et al. 2004). Emissivity and spectra of these neutrinos are uniquely determined by the plasma temperature and electron density. All flavors of the neutrinos are produced in these processes: $\nu_e, \bar{\nu}_e, \nu_\mu, \bar{\nu}_\mu, \nu_\tau, \bar{\nu}_\tau$. Following the standard theory of electroweak interactions, the fluxes for all flavors are quite similar, yet some differences exist between the electron and μ/τ flavors. Additionally, because of the parity violation, neutrino and antineutrino energies are not equal under the degenerate conditions considered here (Odrzywołek 2007; Misiaszek et al. 2006).

Pair annihilation neutrino fluxes and spectra were calculated according to Misiaszek et al. (2006). This approach is superior to both the Itoh et al. (1996a) method, which is typically used in stellar evolution calculations (because the neutrino flavors are not summed up) and the Bruenn (1985); Burrows & Thompson (2002) method that is used for core-collapse supernova modeling (because the electron rest mass is not neglected).

The plasma neutrino flux and spectrum were calculated according to Odrzywołek (2007). Procedures were tested against the Itoh et al. (1992), Kohyama et al. (1994), and Itoh et al. (1996b) tables (calculated using slightly different dispersion relations for plasmons) with reasonable agreement, and also

against the recent calculations of Kantor & Gusakov (2007). In the latter case, the results agree up to the machine precision.

The photoneutrino process and thermal processes of a lesser importance (e.g. neutrino bremsstrahlung, cf. Yakovlev et al. 2001) were omitted in our calculations, because of the lack of relevant results on the neutrino spectrum. This may lead to a negligible underestimate of the thermal neutrino flux.

2.1.2. Weak nuclear processes

Weak processes, namely electron/positron captures on both nucleons and nuclei and $\beta^{\pm}$ decays are extremely important in the astrophysical environments. They are essential ingredients of, e.g., massive star evolution (especially pre-supernova phase, Kutschera et al. 2009), core-collapse supernovae, and thermonuclear explosions: X-ray flashes, novae and SN Ia. Weak nuclear neutrino processes usually work in the cycles such as:

$$\begin{array}{ccc} \mathrm{e}^- + (A,Z) & \longrightarrow & (A,Z-1) + \nu_\mathrm{e} \\ \uparrow & & \downarrow \\ \bar{\nu}_\mathrm{e} + \mathrm{e}^- + (A,Z) & \longleftarrow & (A,Z-1) \end{array} \tag{2a}$$

$$\begin{array}{ccc} \mathrm{e}^+ + (A,Z-1) & \longrightarrow & (A,Z) + \bar{\nu}_\mathrm{e} \\ \uparrow & & \downarrow \\ \nu_\mathrm{e} + \mathrm{e}^+ + (A,Z-1) & \longleftarrow & (A,Z), \end{array} \tag{2b}$$

and the total number of emitted neutrinos per nucleus is usually not equal to 1, in contrast to terrestrial beta decays and electron captures.

One of the most important motivations for including the weak nuclear rates was a search for nuclei producing $\bar{\nu}_\mathrm{e}$ or ν_e, which leads to a very strong signal in the detectors (in analogy to Solar ^{8}B neutrinos). These nuclei must meet three conditions: (1) they have to be abundant in NSE, (2) they need posses very high β or a very high capture rate, and (3) they need to emit energetic ν_e or $\bar{\nu}_\mathrm{e}$ with energies above, say, 10–15 MeV. Unfortunately, an inspection of Figs. 6, 7 and Table 2 reveals no such nuclei in our study. A strong degeneracy during the initial stage of the deflagration enhances transitions with relatively high-energy neutrinos (we thank G. Fuller for pointing out this important aspect to us). For some nuclides, e.g. ^{57}Zn, ^{54}Cr, and ^{28}P, the average neutrino energy $\langle \mathcal{E}_{\nu_\mathrm{e}} \rangle$ reaches 15 MeV. The NSE abundance and therefore the neutrino flux from these nuclides is negligible (cf. Fig. 6). The nucleus producing the highest elastic scattering event rate is ^{55}Co, but equally important are electron captures on protons. The case of ^{54}Co, with a quite high average neutrino energy (≈9 MeV) is very interesting and deserves a more detailed analysis.

Some of the nuclei also produce relatively energetic antineutrinos, e.g. $\langle \mathcal{E}_{\nu_\mathrm{e}} \rangle \approx 6$ MeV for ^{56}V and ^{58}V during the deflagration and detonation stages. The corresponding flux, however, is low compared to thermal (pair) and $\mathrm{e}^+(n,p)\bar{\nu}_\mathrm{e}$ electron antineutrinos fluxes. We conclude that the β processes involving nuclei provide only a negligible contribution to the $\bar{\nu}_\mathrm{e}$ flux.

While the energy loss rate as well as the decrease of the electron fraction because of weak processes were extensively studied in the past (Fuller et al. 1980, 1982a,b; Oda et al. 1994; Aufderheide et al. 1994a,b; Caurier et al. 1999; Langanke & Martínez-Pinedo 2000; Nabi & Klapdor-Kleingrothaus 1999; Seitenzahl et al. 2009; Juodagalvis et al. 2010, and references therein), relatively little is known about the combined energy spectrum of these neutrinos (Langanke et al. 2001; Odrzywolek 2009). Typically, the spectrum is integrated in advance and the results are tabulated. This approach saves both computer memory and computing time. To restore information about the spectrum, a simple parameterization (e.g. the Fermi-Dirac distribution) is assumed (see, e.g. Pons et al. 2001). We employ a similar method here. However, some fine details of the nuclear structure reflected in the neutrino spectrum are lost when using this approach. In certain conditions, this may lead to a serious underestimate of the neutrino signal, especially in the high-energy ($\mathcal{E}_\nu > 10$ MeV) tail. With this in mind, our results provide a lower detection threshold for the neutrino signal. Furthermore, some newest results suggest an upward revision of the crucial ^{55}Co electron capture rate by up to two orders of magnitude (Nabi & Sajjad 2008). These findings apparently are in conflict with the nucleosynthesis results though, in particular with the observed degree of neutronization of the ejecta (Nomoto et al. 1997; Isern et al. 1993; Thielemann 1984; Iwamoto et al. 1999).

Our calculations of the weak nuclear neutrino emission proceed as follows. In contrast to the thermal neutrino emission, the contribution from weak nuclear processes to the neutrino signal cannot be calculated solely based on the thermodynamic properties of matter. These calculations in general require detailed knowledge of the isotopic composition. Typically, the composition is a result of the long and complicated history of the astrophysical object. Because the electron fraction has not been calculated consistently in the adopted explosion models, we assume $Y_\mathrm{e} = 0.5$. This value corresponds to the initial electron fraction of the progenitor with 50/50 carbon/oxygen composition mix used in the explosion calculations[1]. In more realistic models, the electron neutrino emission would result in decreasing Y_e. For example, the NSE abundance of the ^{55}Co nucleus, which significantly contributes to the ν_e flux, decreases rapidly for $Y_\mathrm{e} < 0.5$.

The remaining required information about the matter density, ρ, and the temperature, T, is obtained from the actual explosion model. We consider only regions where the NSE state can be established on a timescale shorter than the explosion timescale. The NSE timescale can be approximated as (Khokhlov 1989, 1991)

$$\tau_\mathrm{NSE} \sim \rho^{0.2} \mathrm{e}^{179.7/T_9 - 40.5} \text{ s}. \tag{3}$$

For the reference NSE threshold temperature, $T_\mathrm{NSE} = 5 \times 10^9$ K ($T_9 = 5$, $kT \approx 0.432$ MeV) , adopted after Kunugise & Iwamoto (2007) and the characteristic density of $\rho = 10^9$ g cm^{-3}, the NSE timescale is, $\tau_\mathrm{NSE} \approx 0.66$ s, and is shorter than than the explosion timescale, $\tau_\mathrm{exp} \approx 1$ s.

To estimate the sensitivity of the results to the assumed NSE threshold temperature, we performed several additional calculations with the threshold temperature $T_9 = 6$ ($kT \approx 0.517$ MeV, $\tau_\mathrm{NSE} \sim 10^{-3}$ s). This resulted in a reduction of the total neutrino flux by a few percent. The remaining non-NSE zones were omitted from the weak neutrino emission calculations[2]. Their contribution remains unknown at present, but it is unlikely to be important.

For zones with $T > T_\mathrm{NSE}$, the NSE abundances were calculated using an 800 isotope network up to ^{97}Br (Odrzywolek 2009). From the NSE abundances, we selected nuclei (188 nuclides) for which weak rates have been tabulated by

[1] In more realistic progenitor models, Y_e should be slightly below 0.5 because of core burning before the explosion (Piro & Bildsten 2008) and/or variation in the initial chemical composition of the progenitor star on the main-sequence (Timmes et al. 2003).

[2] Those regions produce neutrinos from decaying beta-unstable nuclides, e.g. ^{56}Ni. This process does not depend on temperature.

Fuller et al. (1980, 1982a,b). Model energy spectra for neutrinos from electron captures on protons and for antineutrinos from positron captures on neutrons and neutron decay were calculated using

$$\frac{\mathrm{d}R_\nu}{\mathrm{d}\mathcal{E}_\nu} = \left(\frac{\ln 2}{m_\mathrm{e}^5}\right) r_\mathrm{eff}\Theta\left(\pm\mathcal{E}_\nu \mp Q_\mathrm{eff} - m_\mathrm{e}\right) \times \frac{\mathcal{E}_\nu^2(\pm\mathcal{E}_\nu \mp Q_\mathrm{eff})\sqrt{(\mathcal{E}_\nu - Q_\mathrm{eff})^2 - m_\mathrm{e}^2}}{1 + \mathrm{e}^{(\mathcal{E}_\nu - Q_\mathrm{eff} \mp \mu)/kT}}, \quad (4)$$

where R_ν is the particle production rate per unit volume and time, $\mathcal{E}_\nu$ is the neutrino energy, r_eff and Q_eff describe adopted parameterization (see Langanke et al. 2001, for details), Θ is the unit step function, upper and lower sign correspond to captures and decays, respectively, and the other symbols have their usual meanings. To account for positron captures (ϵ^+) and β^+ decays, one simply needs to change the sign of μ (the electron chemical potential including rest mass) in Eq. (4). The neutrino spectra were calculated using Eq. (4) with the effective Q-values and effective rates (Langanke et al. 2001; Kunugise & Iwamoto 2007) with additional switching between capture and decay (Odrzywolek 2009). The above procedure reproduces neutrino fluxes and average neutrino energies of the original tabulated values at the FFN grid points. Between grid points, we used a bilinear interpolation of the effective rates and Q-values (Fuller et al. 1985). The electron chemical potential required in Eq. (4) was computed separately with a precision better than 1×10^{-12}.

2.2. Representative SN Ia explosion models

For the neutrino explosion diagnostic analysis, we selected two representative explosion models from our database (Plewa 2007): a pure deflagration, n7d1r10t15c, and a delayed detonation, Y12. Both models were obtained for a standard carbon/oxygen Chandrasekhar mass white dwarf. A slightly modified flame capturing method of Khokhlov (1995) was used to follow a deflagration, and we used a 13-isotope alpha-network to directly compute the energetics of the detonation wave. Both models are relatively energetic with explosion energies between ≈0.97 B (1 Bethe ≡ 1 B = 1×10^{51} erg) for the pure deflagration and ≈1.36 B for the delayed-detonation.

2.3. Detailed analysis of the neutrino emission

For the selected explosion models, we computed the neutrino emission resulting from pair annihilation, plasmon decay and weak nuclear processes. The results are presented in the form of emissivity maps and total fluxes. Additionally, we provide time-dependent neutrino energy spectra in numerical form (see Figs. 9–20). Following practice known from core-collapse supernova studies, we show individual neutrino emission light curves for electron neutrinos (ν_e), electron antineutrinos ($\bar{\nu}_\mathrm{e}$) and the average of the remaining four muon and tau neutrinos (ν_μ). The latter are produced exclusively in thermal processes, as long as we neglect neutrino oscillations. The electron neutrino (ν_e) flux is dominated either by electron captures on protons and iron group nuclei[3] (when the burning is the most intense) or by pair annihilation (otherwise).

Electron antineutrinos ($\bar{\nu}_\mathrm{e}$) are produced mainly in the pair process and through positron captures on neutrons. Heavy nuclei (β^- decays and e^+ captures) do not significantly contribute to the total $\bar{\nu}_\mathrm{e}$ flux. Muon and tau neutrinos are produced in much smaller quantities only in the thermal processes, and one may expect that actually more μ/τ neutrinos are produced owing to flavor conversion between source and detector (see Fig. 3 in Kunugise & Iwamoto 2007). Plasmon decay is almost negligible because of the low densities, and the low energy of the emitted neutrinos (~few keV, Odrzywołek 2007) makes their detection essentially impossible.

2.3.1. Pure deflagration model

Pure deflagrations produce neutrino emission with a single maximum (because an explosion involves only one stage), and nuclear burning takes ≈1 s. We calculate the total neutrino flux (Fig. 1d) as the sum of thermal and weak components. The evolution is slower compared to a detonation (see below), and in this case therefore neutrino cooling processes are given more time compared to a detonation. Moreover, a larger volume is involved in neutrino cooling in deflagration compared to a "failed" case, Y12 (cf. Fig. 2 versus Fig. 4). Overall the neutrino luminosity is much higher compared to Y12 model and reaches 1.92×10^{50} erg/s, almost one order of magnitude larger compared to the first-peak luminosity of the Y12 model (1.1×10^{49} erg/s). The total energy radiated in neutrinos is 0.04 B, five times more than for Y12 (0.008 B), but still small compared to the overall explosion energy of ≈1 B.

The temporal evolution of the neutrino emission in the deflagration model is shown in Fig. 1a (ν_e), Fig. 1b ($\bar{\nu}_\mathrm{e}$), Fig. 1c (ν_μ), with the total neutrino luminosity shown in Fig. 1d. Overall, the emission varies smoothly in time and we notice only very small emission fluctuations. Even though the flame is geometrically very convoluted (Fig. 2), the neutrino emission is produced in regions of nearly identical density and temperature. We found that most (99%) of the NSE neutrino flux is produced for $T_\mathrm{NSE} < T_9 < 10$ and $8.9 < \log_{10}\rho < 9.3$. At the peak neutrino emission, only 3% of the total white dwarf mass is emitting neutrinos.

We note that the model neutrino emission obtained in our axisymmetric deflagration is very similar to that of the spherically symmetric model W7 (Nomoto et al. 1984, 1993; Kunugise & Iwamoto 2007). This suggests that the neutrino emission from pure deflagrations may have a generic form. To verify this impression, we computed the neutrino light curves for two other deflagration models presented by (Plewa 2007), n11d2r10t15a and n11d2r20t20b. In both cases the neutrino emission displayed very similar characteristics to W7 and the deflagration model analyzed in detail here. The generic form of the emission also implies that *neutrinos may provide no information helpful for separating between various scenarios of pure deflagrations*.

2.3.2. Delayed-detonation model

In contrast to the pure deflagrations, the delayed-detonation class of models produces multi-peak neutrino emission. The two distinct neutrino emission maxima caused by the initial deflagration stage and delayed detonation can be clearly discerned (Fig. 3). The deflagration peak is completely dominated by the ν_e emission from the electron captures. The detonation peak, while still dominated by the weak nuclear processes, includes a significant fraction of the thermal emission. Actually, pair annihilation dominates after end of rapid detonation stage and form an exponentially decaying tail. This is the result of the efficient neutrino

[3] Especially ^{55}Co and ^{56}Ni.

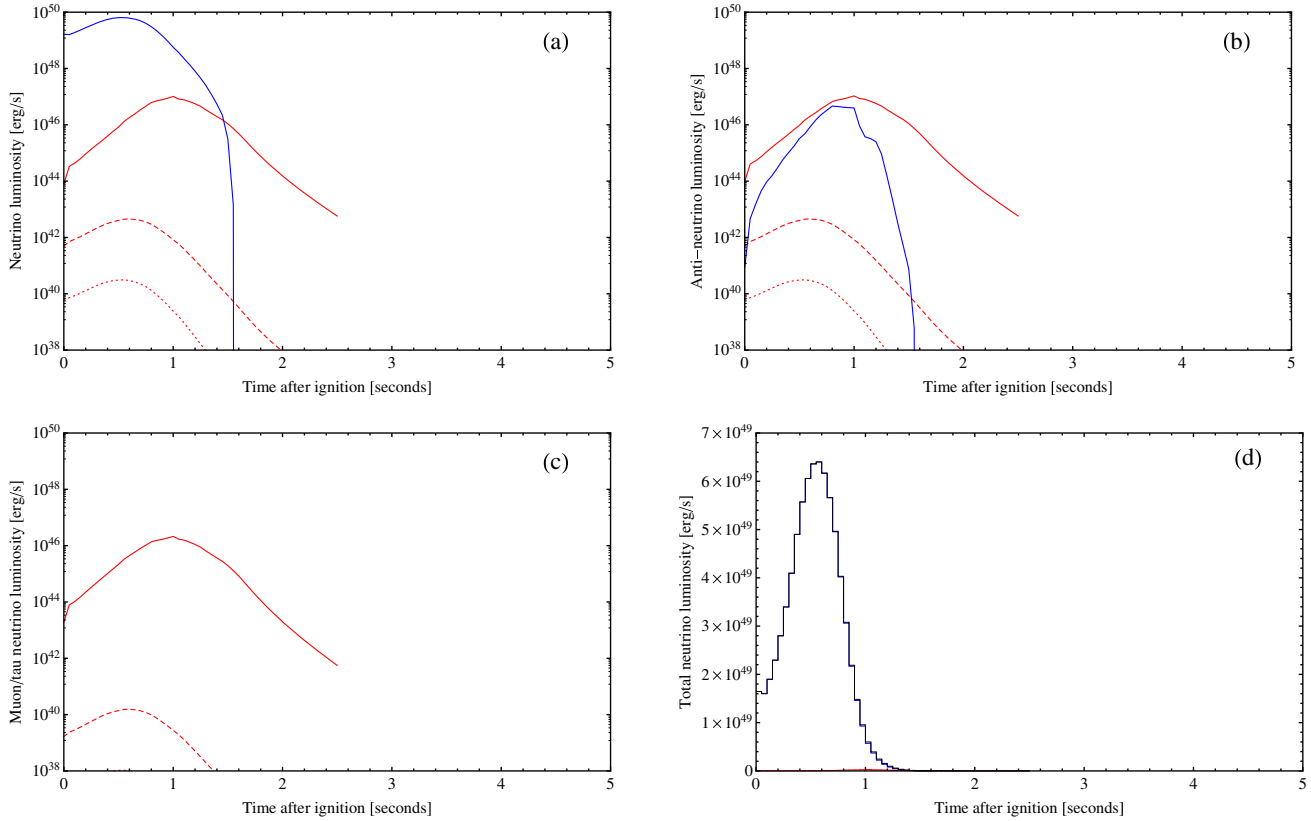

Fig. 1. Model neutrino luminosities of the pure deflagration n7d1r10t15c. **a)** Electron neutrinos, L_{ν_e}; **b)** electron anti-neutrinos, $L_{\bar{\nu}_e}$; **c)** μ and τ neutrinos, $L_{\bar{\nu}_x}$; **d)** total flux. In each panel we show the contribution of weak (solid blue, Eq. (2)), pair annihilation (solid red, Eq. (1a)), transverse (dashed red) and longitudinal (red dotted) plasmon decay (Eq. (1b)).

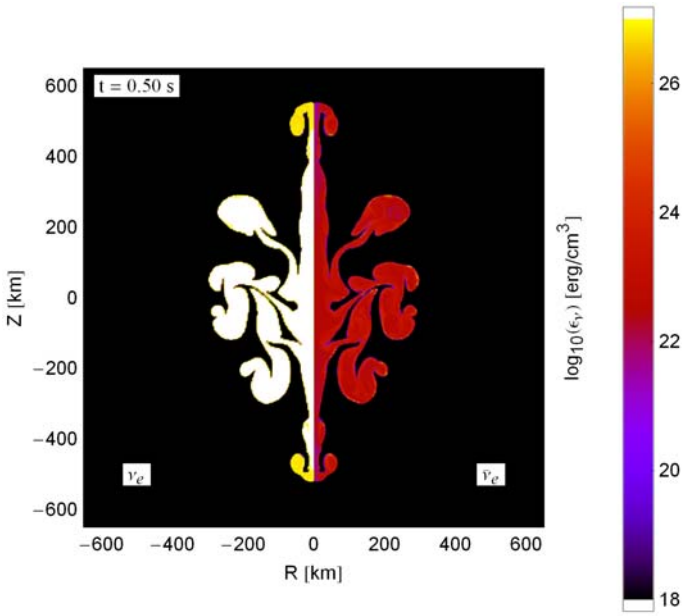

Fig. 2. Maps of the neutrino emissivity in the pure deflagration model at $t = 0.5$ s, i.e. near the peak of the neutrino emission; left segment, $R < 0$ km ν_e; right segment, $R > 0$ km $\bar{\nu}_e$.

cooling in the large volume of the former white dwarf that is overrun by the detonation wave (cf. Fig. 5).

The electron flavor neutrino and antineutrino emission maps (Figs. 4 and 5) reflect the explosion physics. Roughly speaking, neutrino emission is a by-product of the thermonuclear flame or the detonation wave. During the deflagration stage, almost all ν_e are emitted in the electron capture processes in the region incinerated by the thermonuclear flame. Hot plumes expanding into the higher density gas are prominent sources of electron neutrinos, because the electron capture rates are increasing rapidly with the temperature (because of the thermal population of the excited states with large matrix elements) and density (because of the Fermi-energy crossing capture threshold for excited nuclei). The total mass involved in neutrino emission is much smaller than for pure deflagration model, 0.2% of the total white dwarf mass.

Antineutrinos ($\bar{\nu}_e$) are emitted from the much larger volume heated by the thermonuclear burning. The electron antineutrino emission from the thermal processes (pair annihilation) during the deflagration stage is initially suppressed owing to the high degeneracy of the electron gas. The main source of $\bar{\nu}_e$'s is pair annihilation, Eq. (1a), and the reaction

$$e^+ + n \rightarrow p + \bar{\nu}_e.$$

After $t \approx 1$ s, pair annihilation completely dominates the $\bar{\nu}_e$ flux (Fig. 3b, red solid curve).

The deflagration stage ends with a bubble breakout and the neutrino emission from nuclear processes ends. Thermal neutrinos are still emitted from the area heated during nuclear burning, but the neutrino flux decreases by several orders of magnitude (see Figs. 3a–c). At $t = 3.7$ s, the material accelerated by the expanding bubble starts converging at the location opposite to the bubble breakout point, and eventually triggers a detonation. Interestingly, the thermal neutrino emission starts to rise just before to the detonation ignition (Fig. 3c). This is because of the neutrino cooling of the colliding matter, which heats up enough

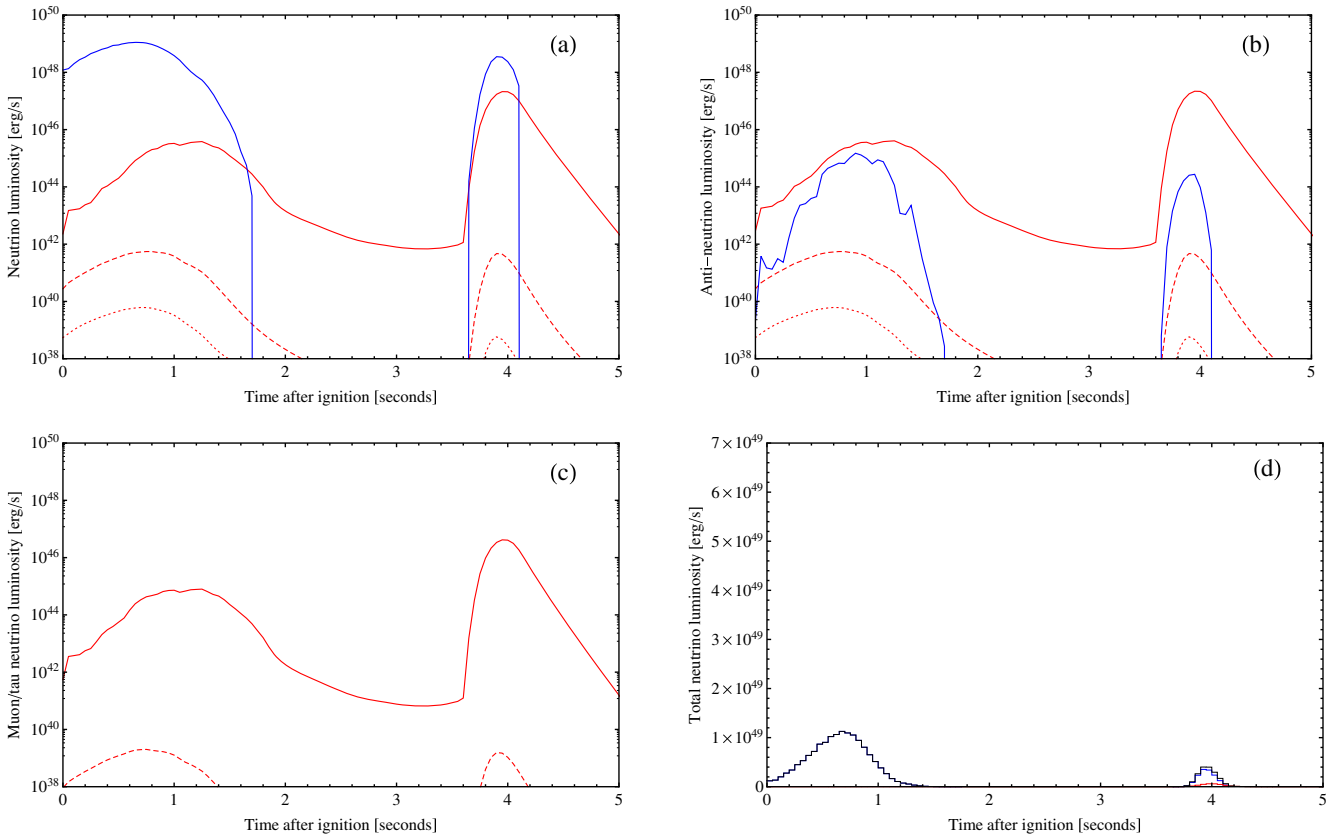

Fig. 3. Model neutrino luminosities of the delayed detonation Y12. **a)** Electron neutrinos, L_{ν_e}; **b)** electron antineutrinos, $L_{\bar{\nu}_e}$; **c)** μ and τ neutrinos, $L_{\bar{\nu}_x}$; **d)** total flux. The color and line-style coding is identical to that in Fig. 1.

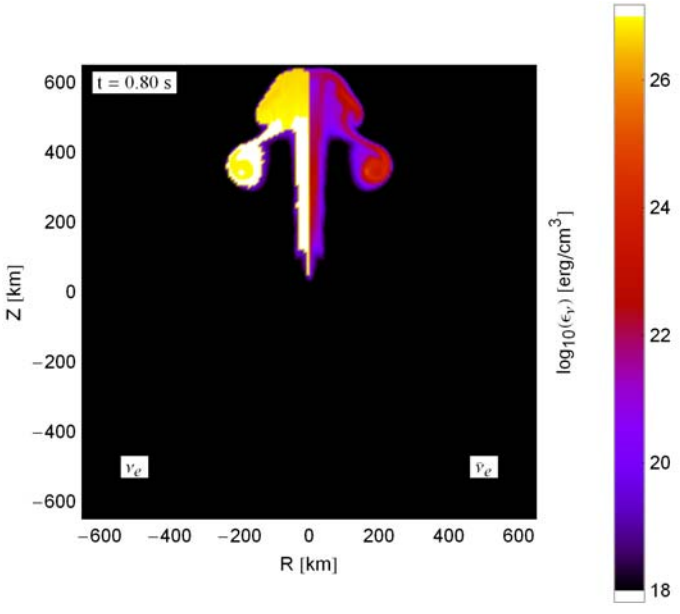

Fig. 4. Maps of the neutrino emissivity in the delayed-detonation model at $t = 0.8$ s, i.e. near the peak of the neutrino emission produced by the initial failed deflagration stage; left segment, $R < 0$ km ν_e; right segment, $R > 0$ km $\bar{\nu}_e$.

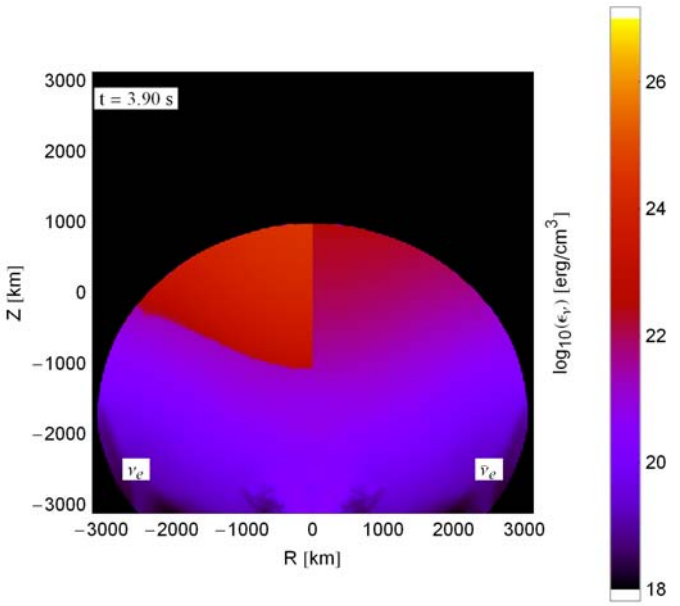

Fig. 5. Maps of the neutrino emissivity in the delayed-detonation model at $t = 3.9$ s, i.e. near the peak of the neutrino emission produced by the detonation stage; left segment, $R < 0$ km ν_e; right segment, $R > 0$ km $\bar{\nu}_e$.

to produce e^+e^- pairs. Once the detonation[4] is formed, the wave quickly moves into the white dwarf core. The nuclear burning involves electron captures, and weak nuclear neutrinos are the dominant component of the neutrino emission (left segment in Fig. 5).

[4] The detonation is a reactive wave in which a thin hydrodynamic shock activates a thermonuclear burn and is followed by an extended post-shock region in which the thermonuclear fuel is processed and the energy is released (Fickett & Davis 1979).

Table 1. Integrated properties of the model neutrino signals.

Model	n7d1r10t15c	Y12 (def)	Y12 (det)	Y12 (total)
$E_\nu^{\rm total}$ [erg]	3.85×10^{49}	7.3×10^{48}	8.7×10^{47}	8.2×10^{48}
$E_\nu^{\rm total}/E_{\rm nucl}^{\rm total}$	0.03	0.05	0.0005	0.004
$E_{\nu_{\rm e}}^{\rm total}$ [erg]	3.85×10^{49}	7.3×10^{48}	7.7×10^{47}	8.05×10^{48}
$E_{\bar\nu_{\rm e}}^{\rm total}$ [erg]	7.0×10^{46}	8.9×10^{45}	5.9×10^{46}	6.8×10^{46}
$E_{\nu_x}^{\rm total}$ [erg]	6.4×10^{46}	2.2×10^{45}	4.4×10^{46}	4.6×10^{46}
$\langle\mathcal{E}_{\nu_{\rm e}}\rangle^{\rm total}$ [MeV]	3.8	3.7	2.35	3.5
$\langle\mathcal{E}_{\bar\nu_{\rm e}}\rangle^{\rm total}$ [MeV]	2.9	3.0	1.9	2.0
$\langle\mathcal{E}_{\nu_x}\rangle^{\rm total}$ [MeV]	2.5	2.8	2.0	2.0
double L_ν peaks	no	peak 1	peak 2	yes
signal duration [s]	1.0	1.0	0.4	separation ~3 s.

In contrast to the pure deflagration, during the detonation phase a large fraction of the white dwarf (≈30% in mass) is participating in producing the neutrino emission. We found that in this case ≈50% of the emission is produced by matter with $T_{\rm NSE} < T_9 < 7.2$ and $7.85 < \log_{10}\rho < 8.25$. Thermal neutrinos are also emitted from a much larger volume (of the deflagration-expanded white dwarf) swept by the detonation (see right panel in Fig. 5), and they are the main contributor to the $\bar\nu_{\rm e}$ flux. Only residual pair neutrino emission from the deflagration stage can still be seen at this time. Once the detonation ends, however, the ejecta quickly expand and cool down adiabatically, and the supernova becomes an exponentially fading source of thermal neutrinos[5].

2.3.3. Comparison of neutrino emission signatures

One of the most exciting possibilities opened by the neutrino channel is a potential for distinguishing between various explosion scenarios. While the overall number of scenarios is quite large, most of them fit into either the pure deflagration or the delayed-detonation category. Therefore, the two models analyzed in previous sections provide a small but representative sample. We have at least three observables available for the explosion diagnostics: the total energy radiated by neutrinos (directly related to the observed number and energy of events), the time variation of the neutrino signal (sensitive to the burning speed and burning type), and the energy of detected neutrinos (probing the degeneracy of the burning matter). The analyzed models differ quite significantly in these three respects (see Table 1). The most striking difference is the total emitted neutrino energy, which almost entirely comes from the electron flavor neutrino. The delayed-detonation model produces five times less energy in neutrinos despite a comparable explosion energy. Therefore, if we look at a nearby explosion that is unobscured by interstellar matter, we can easily identify the explosion scenario provided the total (kinetic+radiative) explosion energy can be determined. Neutrino energies are also a little bit smaller in the delayed-detonation model (Table 1). Unfortunately, only $\nu_{\rm e}$ provides a clear signature. Other neutrino flavors, including relatively easy to detect $\bar\nu_{\rm e}$, are emitted in comparable quantities. The total energy radiated in $\bar\nu_{\rm e}$ is $\approx7.0\times10^{46}$ erg for n7d1r10t15c, comparable to $\approx6.2\times10^{46}$ erg for Y12. The average $\bar\nu_{\rm e}$ energy in the Y12 model (3.5 MeV) is only 0.3 MeV lower than a pure deflagration (3.8 MeV).

The characteristic double-peaked neutrino luminosity curve (Fig. 3) is a "smoking gun" of the delayed-detonation supernova, although the second maximum is fairly weak. However, owing to the ≈4 s delay between the maxima, and compared to ≈2.5 s long deflagration, a detection of a neutrino events a few seconds apart would offer evidence for an explosion caused by a delayed detonation.

3. Discussion

3.1. Prospects for neutrino detection from a galactic type Ia supernova

In the context of SN Ia neutrino emission, possibly the most important question is whether the supernova neutrino signal can be measured using the available neutrino-detection technologies. To answer this question one requires the following information: (1) estimated galactic supernova rates and expected supernova distances, (2) the integrated supernova neutrino ($\nu_{\rm e}$) and antineutrino ($\bar\nu_{\rm e}$) spectra; (3) characteristics of suitable neutrino detector. In the following discussion we will consider a supernova located at the distance of 1 kpc[6]. The results for a widely adopted 10 kpc distance (roughly a distance to the Galactic Center with the corresponding volume including ≈50% stars in the Milky Way, Bahcall & Soneira 1980) can be obtained by dividing the current numbers by a factor of 100.

The selection of the interesting nuclei and processes of interest is potentially quite complicated because of large number of the nuclei involved in NSE neutrino emission, each with unique (often poorly known) spectral properties, and contribution from additional thermal processes. To aid the selection process, we constructed a diagram showing the temporal evolution of neutrino emission from individual nuclides and/or processes integrated over the stellar volume as a function of the neutrino energy[7]. Specifically, we plot $(\langle\mathcal{E}_\nu\rangle(t), F_\nu(t))$ on the F_ν-$\langle\mathcal{E}_\nu\rangle$ plane. This diagram might be referred to as the ν-HR diagram, with the mean neutrino energy considered an analogue of the effective stellar temperature and the neutrino flux now playing a role of the stellar bolometric luminosity. For a given supernova distance and detector, one can also show isocontours of detection rates. Because the knowledge of the mean neutrino energy and integrated flux is not sufficient to reproduce the energy spectrum, in calculating detection rates we are forced to assume a single

[5] See http://ribes.if.uj.edu.pl/snIa/ for step-by-step neutrino emissivity maps, animations, digitized neutrino spectra, and additional data.

[6] Before SN 1987A, it was not unusual to adopt a 1 kpc distance to the "future core-collapse supernova"; see, e.g., Burrows (1984).

[7] Similar diagrams can be used to discuss other phenomena, e.g., the evolution of pre-supernovae (Odrzywolek 2007).

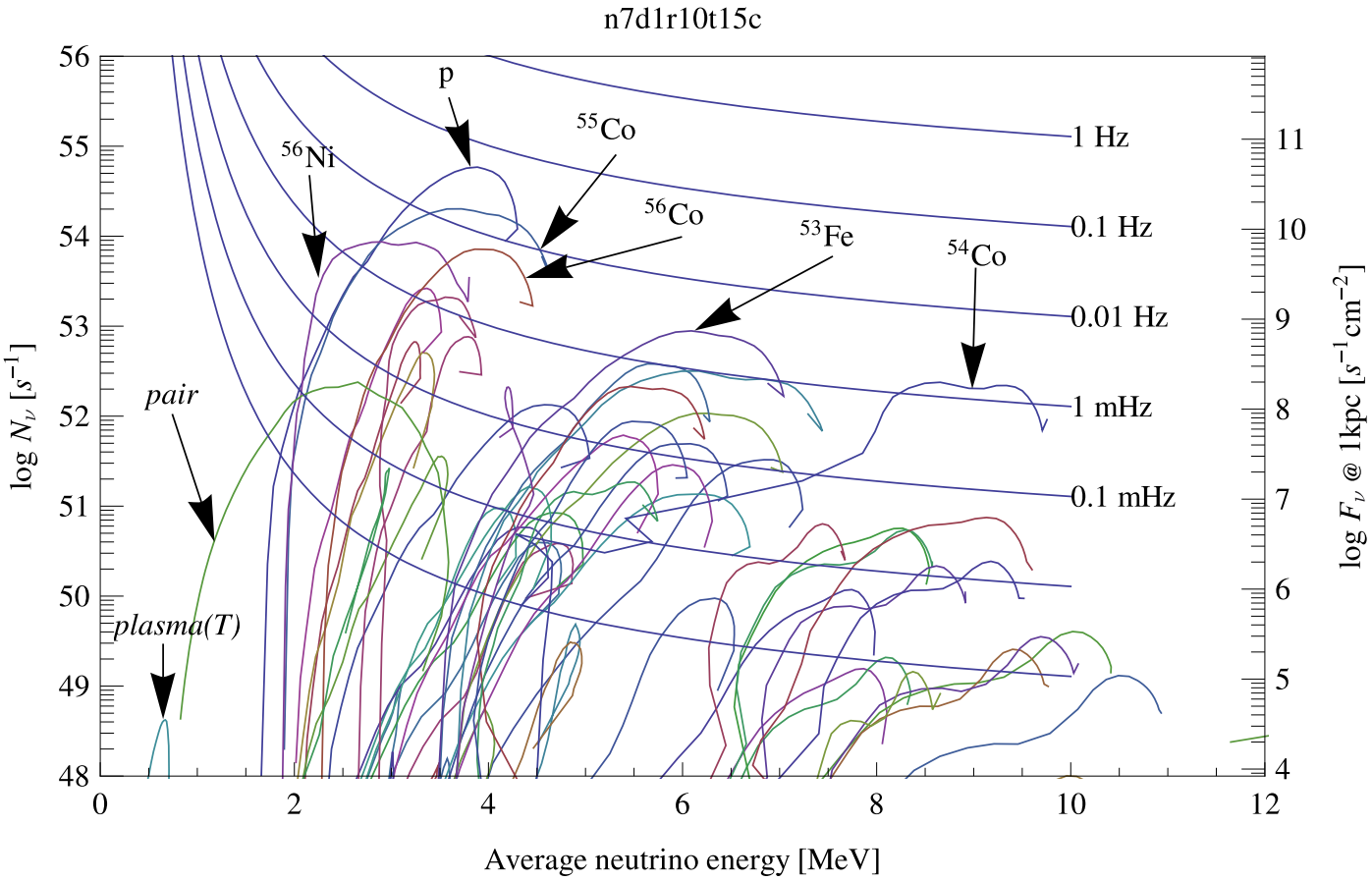

Fig. 6. Neutrino-HR diagram for the n7d1r10t15c model. Every curve is a track on a $F_{\nu_e} - \langle\mathcal{E}_{\nu_e}\rangle$ plane produced by a single nucleus/ thermal process. Assuming a single parameter neutrino energy spectrum (Eq. (5)), we are able to immediately select the most interesting for further analysis processes and estimate the expected signal in a given neutrino detection channel. Particularly, we present detection of ν_e using elastic scattering off electrons with the threshold for detection of the electron kinetic energy of 4 MeV in a water Cherenkov detector.

parameter spectral function. In neutrino astrophysics, it is common to use the Fermi-Dirac function (Kiełczewska 1990):

$$\Phi(\mathcal{E}_\nu, t) \equiv \frac{R(t)}{\langle\mathcal{E}_\nu\rangle(t)^3} \frac{a\,\mathcal{E}_\nu^2}{1 + \mathrm{e}^{b\,\mathcal{E}_\nu/\langle\mathcal{E}_\nu\rangle}} \quad a \approx 17.3574,\ b \approx 3.15137, \tag{5}$$

where $R(t)$ is the integrated particle emission rate and $\langle\mathcal{E}_\nu\rangle(t)$ the average neutrino energy dependent only on time, and a and b normalize the spectrum.

For the assumed supernova distance of 1 kpc, the results for a pure deflagration model and a Super-Kamiokande class detector (H_2O target with the Cherenkov light detector with a threshold of 4 MeV) are shown in Fig. 6. In particular, we conclude from the results shown in Fig. 6:

(1) the most important neutrino-producing nuclei for Super-Kamiokande-like detector events terms are free protons and ^{55}Co; the expected event rate is in 1 kt of H_2O up to 0.1/s: because an explosion takes ≈1 s in the Super-Kamiokande we expect up to 0.1/s/kt × 32kt × 2 nuclei ≈ 6 events from 1 kpc;
(2) secondary sources of detectable signal are: ^{56}Ni, ^{56}Co, ^{53}Fe and ^{54}Co with mean energies of ≈3 MeV, ≈4 MeV, ≈6 MeV, and ≈9 MeV, respectively;
(3) numerous other nuclei as well as thermal processes produce either a weak or an undetectable signal.

Note that in Fig. 6 the evolution proceeds along curves from high-energy to low-energy neutrinos (i.e. from right to left). This is in contrast to core-collapse supernova neutrinos.

The results of similar analyses for antineutrinos from the delayed-detonation model, Y12, are shown in Fig. 7. We consider the inverse beta decay ($\bar\nu_e + p \rightarrow n + e^+$) as the detection channel, and a Gd-loaded water Cherenkov detector proposed by Beacom & Vagins (2004) or a liquid scintillator detector, e.g. KamLAND (Eguchi et al. 2003). We note that here the detection method is simply the inverse of the essential production process ($e^+ + n \rightarrow p + \bar\nu_e$). The analysis of Fig. 7 leads to the following conclusions:

(1) most important for $\bar\nu_e$ emission processes are pair-annihilation and positron capture on neutrons;
(2) weak nuclear processes from nuclei are negligible;
(3) the expected event rate is very low (~few mHz/kt@1 kpc); at least a half-megaton detector is required to observe a single event from 1 kpc.

Following the analysis of the ν_e, $\bar\nu_e$ detection in other cases, we selected five most promising SN Ia neutrino experiments:

1. IBD2: inverse beta decay $\bar\nu_e + p \rightarrow n + e^+$ utilized in a large 50 kiloton target liquid scintillator detector (e.g. LENA Autiero et al. 2007; Marrodán-Undagoitia et al. 2006; Oberauer et al. 2005) or Gd-loaded water detector (Beacom & Vagins 2004) with 1.8 MeV threshold;

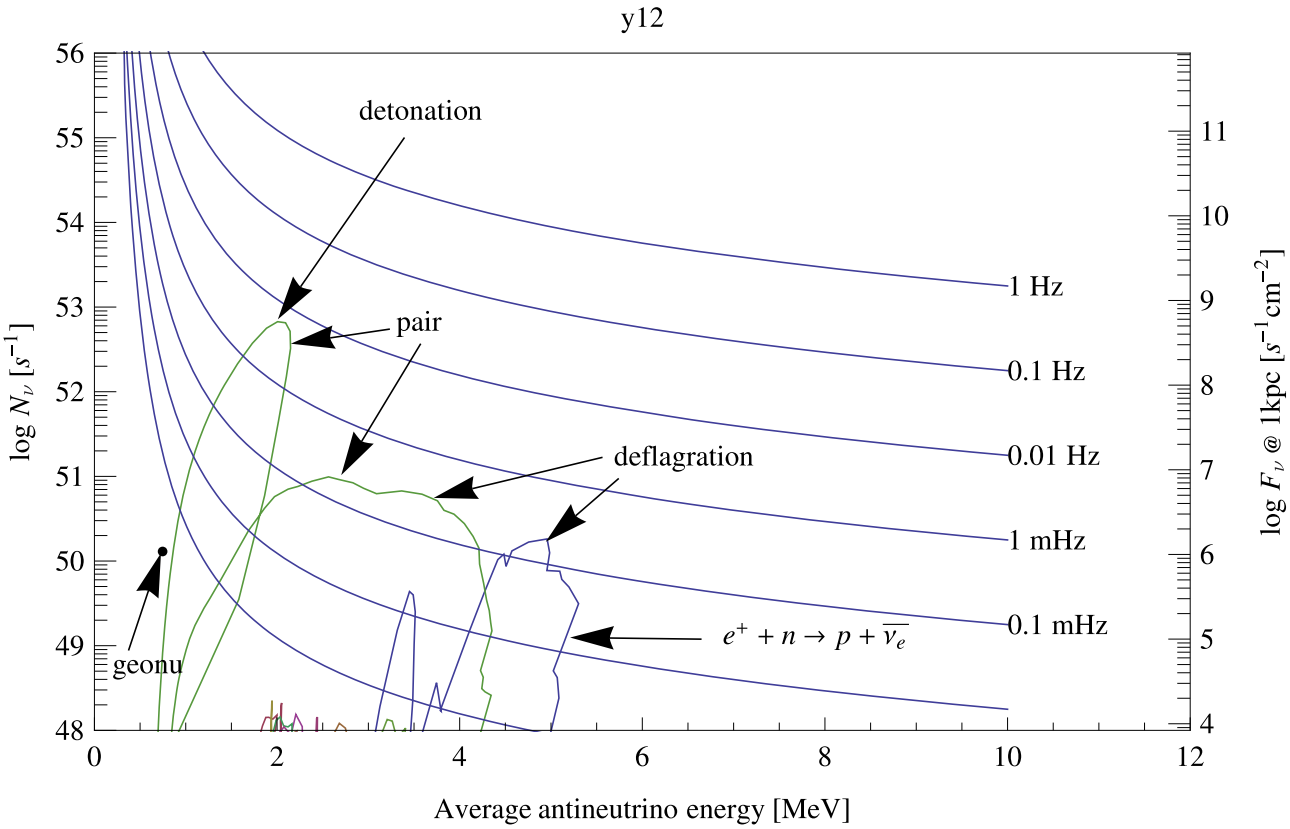

Fig. 7. Antineutrino-HR diagram for Y12 model. Similar to Fig. 6, but now we consider a detection of $\bar{\nu}_e$ via inverse beta decay in $GdCl_3$-loaded H_2O with a threshold of 2 MeV.

Table 2. Expected number of events triggered in the select proposed neutrino detectors by a thermonuclear supernova located at a distance of 1 kpc.

Detector	n7d1r10t15c Deflagration 0–2.5 s	Deflagration 0–2 s	Y12 Detonation 3.5–4.5 s	Total 0–7 s	Proposals	Status
ES4 (0.5 Mt)	19	3.2	0.1	3.3	Hyper-Kamiokande, Memphys	under construction
LAr (100 kt)	21.4 + 1.5	3.8+0.24	0.08+0.005	3.9+0.25	Glacier	under construction
IBD2 (50 kt)	0.2	0.01	0.06	0.07	Gadzooks!, LENA	proposed
ES0 (50 kt)	14	2.7	0.26	2.9	LENA	proposed
PES (50 kt)	60	11.1	0.8	12.0	LENA	proposed
COH (1000 kg)	0.03	0.005	0.0003	0.006	–	planned

2. ES0: elastic scattering off electrons $\nu_e + e^- \to \nu_e + e^-$ in a large 50 kt liquid scintillator (LENA) assuming ≈0.2 MeV threshold;
3. ES4: elastic scattering off electrons $\nu_e + e^- \to \nu_e + e^-$ in the extremely large water Cherenkov detector Memphys (Autiero et al. 2007; Rubbia 2009), Titan-D (Suzuki 2001, 2008; Kistler et al. 2008), LBNE W.C. (Scholberg 2010) etc. assuming a standard 4.0 MeV detection threshold for recoil electrons;
4. LAr: neutrino absorption in 100 kt of liquid argon (see e.g. Rubbia 2009, GLACIER proposal) detected using coincidence of electrons and delayed gammas ($\nu_e + {}^{40}Ar \to {}^{40}K^* + e^-$, Raghavan 1986) and elastic scattering off electrons (E_{th} = 5 MeV);
5. PES: elastic scattering off protons in an advanced extremely low-background liquid scintillator detector like Borexino (Alimonti et al. 2009);
6. COS: coherent elastic scattering off high A nuclei (e.g. ^{72}Ge) in a detector with a threshold on the order of 100 eV.

While scenarios IBD2, ES0, ES4, and LAr use a proven technology (Fulgione 2010), proton elastic scattering (PES) and neutrino-nucleus coherent scattering (COH) have never been used in practice for low ν energy. However, from theoretical analysis and preliminary experimental results we expect to observe significant progress in the development of neutrino detectors. Besides possible gains from the development of advanced detection methods, larger target masses are required for successful detection of SN Ia neutrinos in the foreseeable future.

Table 2 shows the expected number of neutrino events for prospective neutrino experiments. For a delayed-detonation, we separated the contributions from the initial deflagration and the following delayed detonation. For weak neutrinos and antineutrinos, the total number of expected events is simply the sum of events produced in individual explosion stages. For thermal neutrinos, there is also a minor contribution from the neutrinos emitted during the period that separates the two explosion stages and during the final expansion stage. Clearly, the largest yield comes from the ν_e emission from electron captures during

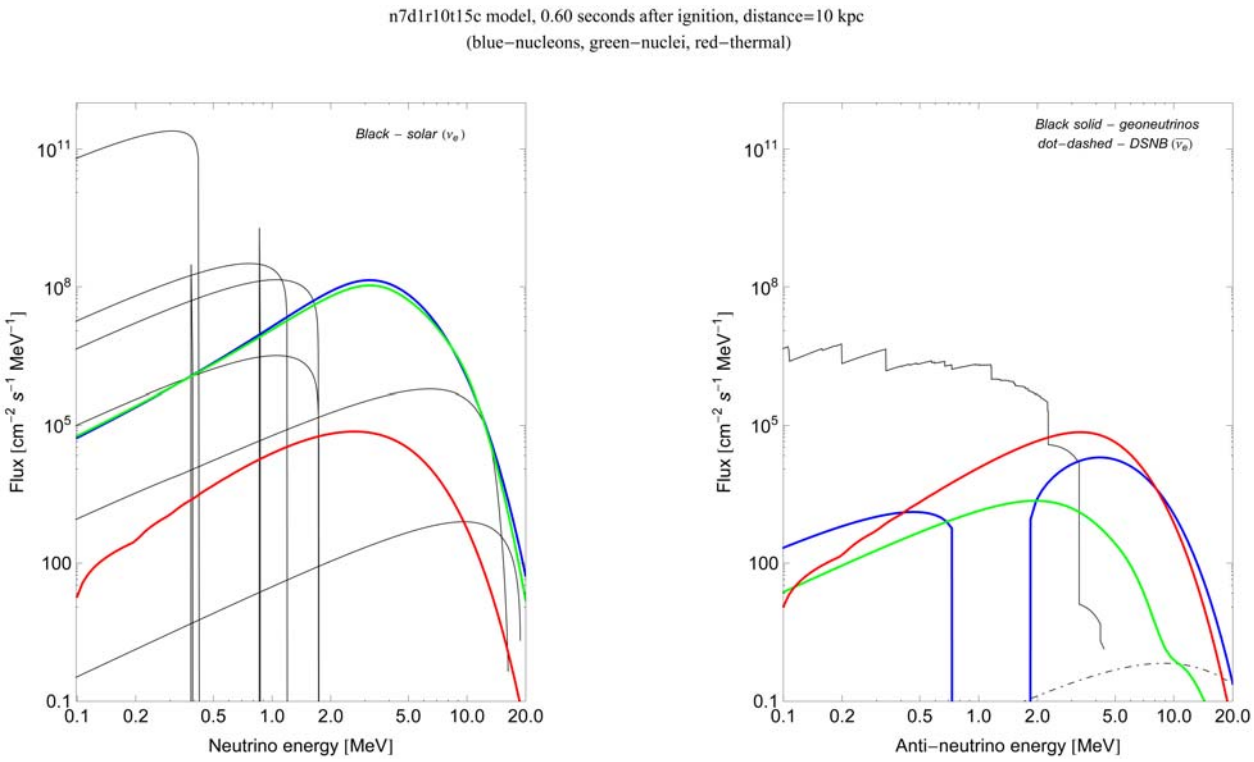

Fig. 8. The ν_e (*left*) and $\bar{\nu}_e$ (*right*) model spectra of a pure deflagration supernova near the maximum of the neutrino emission and other recently studied sources. The supernova emission level is for an event located at a distance $d = 10$ kpc. References for the data used: solar neutrinos, Bahcall et al. (2005); geoneutrinos at Kamioka, Japan, Enomoto (2005, 2006); DSNB, Lien et al. (2010).

the deflagration stage. This is expected because the neutrino luminosity is dominated by these neutrinos and reaches 1.1×10^{49} erg/s for delayed-detonation and 6.4×10^{49} for pure deflagration. Finally, the time delay between the two emission maxima of a delayed-detonation SN and their relative length will be very important aspects of the data analysis.

3.1.1. Neutrino background and signal-to-noise ratio

Additional comments on the expected background signals are due. For a ν_e emission and supernova at larger (>10 kpc) distance, we face a problem of the background emission from ^{8}B, ^{7}Be and CNO solar neutrinos (left panel in Fig. 8). Here a directional detection could be a solution, but no practical method of this kind exists. Electron antineutrino emission will be blended with the geoneutrinos (Fig. 8, right) and the terrestrial nuclear power plants. The geoneutrino flux varies slightly across the continental crust and is much lower on the ocean floor (Learned et al. 2006; Araki et al. 2005; BOREXINO Collaboration et al. 2010). Flux from human-made sources strongly depends on the location of the detector and varies in time (Lasserre & Sobel 2005). Other sources of neutrinos, e.g. from cosmological core-collapse supernovae[8] (flux $\ll 10$ cm^{-2} s^{-1}, Lien et al. 2010; Totani & Sato 1995; dot-dashed curve in the right panel of Fig. 8) are far below the expected signal from a galactic SN Ia. Relic neutrino flux is on the order of $56\,c \simeq 1 \times 10^{12}$ cm^{-2} s^{-1}, but the energy is very small in this case ($\sim 10^{-4}$ eV).

From Fig. 8 it is clear that the neutrinos from a galactic SN Ia could be detected, especially for the pure deflagration event. Neutrino observations of such a supernova are mainly a technological challenge (requires a very large detector mass, new detection techniques, low-energy threshold, etc.) and, similar to SN 1987A, a matter of chance. Cappellaro et al. (1997) estimated 4 ± 1 type Ia supernovae per millennium for Galaxy. An Earth-centered ball with the radius of 10 kpc (1 kpc) contains ≈50% (≈0.5%) of stars (Bahcall & Soneira 1980), and the corresponding SN Ia explosion probability within a period of 10 years is therefore ≈0.02 ($\approx 2 \times 10^{-4}$).

4. Conclusions

We have obtained and analyzed neutrino light curves and neutrino spectra for two models of the most popular type Ia supernova explosion scenarios: a pure deflagration and a delayed detonation. We discussed the role of physical conditions in producing neutrinos in these types of explosions. In particular, the neutrino emission studies allow us to directly probe the density, temperature, and composition of the neutrino-emitting matter. This motivates the development of neutrino experiments for exploring stellar evolution physics beyond core-collapse supernova and solar applications.

Because of their cosmological importance and because their exact origins remain unknown, thermonuclear supernovae are a class of exciting future targets of the neutrino astronomy. The upcoming challenge is a detection of the SN Ia neutrinos. Several recently proposed neutrino experiments will offer a sensitivity that will allow detecting a thermonuclear event at kpc distances. More importantly, we find the that *the next generation of neutrino detectors will be able to unambiguously identify the mechanism responsible for the explosion*. In particular, SN Ia

[8] Those supernovae are a source of the diffuse supernova neutrino background (Horiuchi et al. 2009). The fact that the sky is relatively dark in $\bar{\nu}_e$, compared to individual sources is the neutrino version of the Olbers paradox.

supernova electron neutrinos probe the thermonuclear deflagration stage, while the electron antineutrinos probe the detonation phase. Because the electron neutrinos stem almost exclusively from electron captures associated with the thermonuclear flame, they offer a means to study both nuclear and combustion physics under extreme conditions. On the other hand, the delayed electron antineutrino signal provides direct evidence for thermonuclear detonation. Finally, the muon neutrinos are exclusively produced in thermal processes and could potentially be used to extract weak nuclear signals.

Given a relatively low neutrino luminosity of SN Ia events that are caused by delayed detonations, their characteristic double-peaked neutrino light curves can be used to reduce the false-alarm rate and serve as an early warning system for this type of events. A pure deflagration SN Ia produces only a single neutrino emission maximum with a somewhat faster rise time compared to a delayed detonation. The predicted number of observed neutrino events is, however, higher for deflagrations thanks to both a higher neutrino luminosity and slightly higher energies of the emitted neutrinos. For a 0.5 Mt classical water Cherenkov detector (LBNE WC, long baseline neutrino experiment Scholberg 2010; Memphys, Autiero et al. 2007; Rubbia 2009), we predict the recording about 20 elastic scattering events above 4 MeV per second for a SN Ia event located at a distance of 1 kiloparsec. Still larger detectors (e.g. Titan-D Suzuki 2001, 2008; Kistler et al. 2008) almost certainly guarantee positive detection of a galactic SN Ia. However, this holds true only for a pure deflagration; *the predicted neutrino fluxes for a delayed detonation are about five times lower which makes these events much harder to detect*. We also found that the neutrino emission is very similar to two-dimensional axisymmetric and spherically symmetric pure deflagration models (i.e. W7 by Nomoto et al. 1984). This leads us to believe that *the neutrino observations will not help to distinguish between specific scenarios of pure deflagrations* (e.g. ignition occurring at a single point or at multiple points).

The majority of neutrino experiments considered here (detectors IBD2, ES0, and PES in Table 2) use large amounts of a liquid scintillator. This type of experiments might be the most viable and successful in detecting type Ia supernovae, especially if a proton elastic scattering (PES) method is used (Beacom et al. 2002). One example of such a device is the Borexino detector (Alimonti et al. 2009). Although it is perhaps too small for detecting a thermonuclear supernova at a kpc distance, Borexino will be an essential testbed for the proposed and much larger LENA (Autiero et al. 2007; Marrodán-Undagoitia et al. 2006; Oberauer et al. 2005) and other similar experiments (Maricic & the Hanohano collaboration 2010). We also note that neutrinos can be detected through neutrino-nucleus elastic scattering (Drukier & Stodolsky 1984; Giomataris et al. 2008; Collar 2010; Barbeau et al. 2003). However, a practical application of this technique to SN Ia may not be possible because of the prohibitively large required mass of the detector.

We conclude that a significant progress in terms of neutrino detection methods is needed for the neutrinos to become a practical tool for studying type Ia supernovae. However, a detection of a thermonuclear event at a distance of few kiloparsecs will be within the reach of the planned neutrino observatories and will offer a perfect chance to identify the mechanism that drives the explosion.

Acknowledgements. We thank Thomas Janka for encouragement and helpful advice, and an anonymous referee for comments that helped improving the initial version of this paper. T.P. was supported through the DOE grant DE-FG52-03NA000064. This research used resources of the National Energy Research Scientific Computing Center, which is supported by the Office of Science of the US Department of Energy under Contract No. DE-AC02-05CH11231, and NASA's Astrophysics Data System.

References

Ahmad, Q. R., Allen, R. C., Andersen, T. C., et al. 2001, Phys. Rev. Lett., 87, 071301
Alekseev, E. N., Alekseeva, L. N., Volchenko, V. I., & Krivosheina, I. V. 1987, JETP Lett., 45, 589
Alimonti, G., Arpesella, C., Back, H., et al. 2009, Nuclear Instruments and Methods in Physics Research Section A: Accelerators, Spectrometers, Detectors and Associated Equipment, 600, 568
Ando, S., Beacom, J. F., & Yüksel, H. 2005, Phys. Rev. Lett., 95, 171101
Araki, T., Enomoto, S., Furuno, K., et al. 2005, Nature, 436, 499
Arcones, A., Martínez-Pinedo, G., Roberts, L. F., & Woosley, S. E. 2010, A&A, 522, A25
Arnett, D. 1996, Supernovae and Nucleosynthesis (Princeton: Princeton University Press)
Arnett, W. D., Bahcall, J. N., Kirshner, R. P., & Woosley, S. E. 1989, ARA&A, 27, 629
Arpesella, C., Back, H. O., Balata, M., et al. 2008, Phys. Rev. Lett., 101, 091302
Aufderheide, M. B., Fushiki, I., Fuller, G. M., & Weaver, T. A. 1994a, ApJ, 424, 257
Aufderheide, M. B., Fushiki, I., Woosley, S. E., & Hartmann, D. H. 1994b, ApJS, 91, 389
Autiero, D., Äystö, J., Badertscher, A., et al. 2007, J. Cosmol. Astro-Part. Phys., 11, 11
Badenes, C., Hughes, J. P., Bravo, E., & Langer, N. 2007, ApJ, 662, 472
Bahcall, J. N. 1989, Neutrino Astrophysics (Cambridge: Cambridge University Press)
Bahcall, J. N., & Soneira, R. M. 1980, ApJS, 44, 73
Bahcall, J. N., Serenelli, A. M., & Basu, S. 2005, ApJ, 621, L85
Barbeau, P. S., Collar, J. I., Miyamoto, J., & Shipsey, J. 2003, IEEE Trans. Nucl. Sci., 50, 1285
Beacom, J. F., & Vagins, M. R. 2004, Phys. Rev. Lett., 93, 171101
Beacom, J. F., Farr, W. M., & Vogel, P. 2002, Phys. Rev. D, 66, 033001
BOREXINO Collaboration, Arpesella, C., Bellini, G., et al. 2008, Phys. Lett. B, 658, 101
BOREXINO Collaboration, Bellini, G., Benziger, J., et al. 2010, Phys. Lett. B, 687, 299
Bowden, N. S. 2008, J. Phys. Conf. Ser., 136, 022008
Braaten, E. 1991, Phys. Rev. Lett., 66, 1655
Braaten, E., & Segel, D. 1993, Phys. Rev. D, 48, 1478
Bruenn, S. W. 1985, ApJS, 58, 771
Burrows, A. 1984, ApJ, 283, 848
Burrows, A. 1990, Ann. Rev. Nucl. Part. Sci., 40, 181
Burrows, A., & Thompson, T. A. 2002, Neutrino-Matter Interaction Rates in Supernovae: The Essential Microphysics of Core Collapse, astro-ph/0211404
Cappellaro, E., Turatto, M., Tsvetkov, D. Y., et al. 1997, A&A, 322, 431
Caurier, E., Langanke, K., Martínez-Pinedo, G., & Nowacki, F. 1999, Nuclear Physics A, 653, 439
Clayton, D. D. 1984, Principles of Stellar Evolution and Nucleosynthesis (Chicago: The University of Chicago Press)
Cleveland, B. T., Daily, T., Davis, R., Jr., et al. 1998, ApJ, 496, 505
Clifford, F. E., & Tayler, R. F. 1965a, MNRAS, 129, 104
Clifford, F. E., & Tayler, R. J. 1965b, MmRAS, 69, 21
Collar, J. I. 2010, Collar Group, Kavli Institute for Cosmological Physics, http://collargroup.uchicago.edu/
Drukier, A., & Stodolsky, L. 1984, Phys. Rev. D, 30, 2295
Dutta, S. I., Ratković, S., & Prakash, M. 2004, Phys. Rev. D, 69, 023005
Dye, S. E. 2006, Neutrino Geophysics: Proceedings of Neutrino Sciences 2005 (Springer Verlag)
Eguchi, K., Enomoto, S., Furuno, K., et al. 2003, Phys. Rev. Lett., 90, 021802
Ellis, R. S., Sullivan, M., Nugent, P. E., et al. 2008, ApJ, 674, 51
Enomoto, S. 2005, Ph.D. Thesis, Tohoku University
Enomoto, S. 2006, Earth Moon and Planets, 99, 131
Esposito, S., Mangano, G., Miele, G., Picardi, I., & Pisanti, O. 2003, Nuc. Phys. B, 658, 217
Fickett, W., & Davis, C. 1979, Detonation (Berkeley: University of California Press)
Fogli, G. L., Lisi, E., Mirizzi, A., & Montanino, D. 2005a, J. Cosmol. Astro-Part. Phys., 4, 2
Fogli, G. L., Lisi, E., Mirizzi, A., & Montanino, D. 2005b, J. Cosmol. Astro-Part. Phys., 4, 2
Fukuda, S., Fukuda, Y., Ishitsuka, M., et al. 2001, Phys. Rev. Lett., 86, 5651
Fulgione, W. 2010, J. Phys. Conf. Ser., 203, 012077

Fuller, G. M., Fowler, W. A., & Newman, M. J. 1980, ApJS, 42, 447
Fuller, G. M., Fowler, W. A., & Newman, M. J. 1982a, ApJ, 252, 715
Fuller, G. M., Fowler, W. A., & Newman, M. J. 1982b, ApJS, 48, 279
Fuller, G. M., Fowler, W. A., & Newman, M. J. 1985, ApJ, 293, 1
Galeotti, P., Aglietta, M., Badino, G., et al. 1987, Helv. Phys. Acta, 60, 619
Gilfanov, M., & Bogdán, Á. 2010, Nature, 463, 924
Giomataris, I., Irastorza, I., Savvidis, I., et al. 2008, J. Instrum., 3, P09007
Guillian, E. H. 2006, Earth, Moon and Planets, 99, 309
Hachisu, I., Eriguchi, Y., & Nomaoto, K. 1986, ApJ, 308, 161
Hampel, W., Handt, J., Heusser, G., et al. 1999, Phys. Lett. B, 447, 127
Han, Z. 1998, MNRAS, 296, 1019
Han, Z., & Podsiadlowski, P. 2004, MNRAS, 350, 1301
Hirata, K., Kajita, T., Koshiba, M., Nakahata, M., & Oyama, Y. 1987, Phys. Rev. Lett., 58, 1490
Höflich, P., & Stein, J. 2002, ApJ, 568, 779
Horiuchi, S., Beacom, J. F., & Dwek, E. 2009, Phys. Rev. D, 79, 083013
Hoyle, F., & Fowler, W. A. 1960, ApJ, 132, 565
Iben, Jr., I., & Tutukov, A. V. 1984, ApJS, 54, 335
Immler, S., Weiler, K., & McCray, R. 2007, in Supernova 1987A: 20 Years After: Supernovae and Gamma-Ray Bursters, ed. S. Immler, K. Weiler, & R. McCray, Am. Inst. Phys. Conf. Ser., 937
Isern, J., Bravo, E., Canal, R., & Labay, J. 1993, in Nuclei in the Cosmos 2, ed. F. Kaeppeler, & K. Wisshak, 569
Itoh, N., Mutoh, H., Hikita, A., & Kohyama, Y. 1992, ApJ, 395, 622
Itoh, N., Hayashi, H., Nishikawa, A., & Kohyama, Y. 1996a, ApJS, 102, 411
Itoh, N., Nishikawa, A., & Kohyama, Y. 1996b, ApJ, 470, 1015
Iwamoto, K., & Kunugise, T. 2006, in Origin of Matter and Evolution of Galaxies, ed. S. Kubono, W. Aoki, T. Kajino, T. Motobayashi, & K. Nomoto (New York: AIP), Am. Inst. Phys. Conf. Ser., 847, 406
Iwamoto, K., Brachwitz, F., Nomoto, K., et al. 1999, ApJS, 125, 439
Juodagalvis, A., Langanke, K., Hix, W. R., Martínez-Pinedo, G., & Sampaio, J. M. 2010, Nuc. Phys. A, 848, 454
Kantor, E. M., & Gusakov, M. E. 2007, MNRAS, 381, 1702
Keil, M. T., Raffelt, G. G., & Janka, H.-T. 2003, ApJ, 590, 971
Kessler, R., Becker, A. C., Cinabro, D., et al. 2009, ApJS, 185, 32
Khokhlov, A. M. 1989, MNRAS, 239, 785
Khokhlov, A. M. 1991, A&A, 245, 114
Khokhlov, A. M. 1995, ApJ, 449, 695
Kiełczewska, D. 1990, Phys. Rev. D, 41, 2967
Kistler, M. D., Yuksel, H., Ando, S., Beacom, J. F., & Suzuki, Y. 2008, [arXiv:0810.1959]
Kohyama, Y., Itoh, N., Obama, A., & Hayashi, H. 1994, ApJ, 431, 761
Kuhlen, M., Woosley, S. E., & Glatzmaier, G. A. 2006, ApJ, 640, 407
Kunugise, T., & Iwamoto, K. 2007, Publications of the Astronomical Society of Japan, 59, L57
Kutschera, M., Odrzywołek, A., & Misiaszek, M. 2009, Acta Physica Polonica B, 40, 3063
Langanke, K., & Martínez-Pinedo, G. 2000, Nuc. Phys. A, 673, 481
Langanke, K., Martínez-Pinedo, G., & Sampaio, J. M. 2001, Phys. Rev. C, 64, 055801
Lasserre, T., & Sobel, H. W. 2005, C. R. Phys., 6, 749
Learned, J. G. 2004, White paper on Gigaton Array, www.phys.hawaii.edu/~jgl/post/gigaton_array.eps
Learned, J. G. 2005, Nuc. Phys. B – Proc. Suppl., 143, 152
Learned, J. G., Dye, S. T., & Pakvasa, S. 2006, Earth Moon and Planets, 99, 1
Leonard, D. C. 2009, Seeking Core-Collapse Supernova Progenitors in Pre-Explosion Images [arXiv:0908.1812v1]
Lhuillier, D. 2009, Nuc. Phys. B – Proc. Suppl., 188, 112, Proceedings of the Neutrino Oscillation Workshop
Lien, A., Fields, B. D., & Beacom, J. F. 2010, Phys. Rev. D, 81, 083001
Maricic, J., & the Hanohano collaboration. 2010, J. Phys. Conf. Ser., 203, 012137
Marrodán-Undagoitia, T., von Feilitzsch, F., Goeger-Neff, M., et al. 2006, Progress in Particle and Nuclear Physics, 57, 283, International Workshop of Nuclear Physics 27th course – Neutrinos in Cosmology, in Astro, Particle and Nuclear Physics
Meng, X., & Yang, W. 2010, ApJ, 710, 1310
Misiaszek, M., Odrzywolek, A., & Kutschera, M. 2006, Phys. Rev. D, 74, 043006
Munakata, H., Kohyama, Y., & Itoh, N. 1985, ApJ, 296, 197
Nabi, J., & Klapdor-Kleingrothaus, H. V. 1999, Atomic Data and Nuclear Data Tables, 71, 149
Nabi, J.-U., & Sajjad, M. 2008, Phys. Rev. C, 77, 055802
Nakahata, M. 2007, Super-Kamiokande, http://sn1987a-20th.physics.uci.edu/0830-Nakahata.eps
Nakahata, M., & Sobel, H. 2007, Twenty Years after SN1987A, What did we learn, what will the next Supernova teach us?, http://sn1987a-20th.physics.uci.edu/
Nomoto, K., Sugimoto, D., & Neo, S. 1976, Ap&SS, 39, L37
Nomoto, K., Thielemann, F.-K., & Yokoi, K. 1984, ApJ, 286, 644
Nomoto, K., Iwamoto, K., Tsujimoto, T., & Hashimoto, M. 1993, in Frontiers of Neutrino Astrophysics, ed. Y. Suzuki, & K. Nakamura (Tokyo: Universal Academy Press), 235
Nomoto, K., Iwamoto, K., Nakasato, N., et al. 1997, Nuc. Phys. A, 621, 467
Oberauer, L., von Feilitzsch, F., & Potzel, W. 2005, Nuc. Phys. B – Proc. Suppl., 138, 108, Proceedings of the Eighth International Workshop on Topics in Astroparticle and Undeground Physics
Oda, T., Hino, M., Muto, K., Takahara, M., & Sato, K. 1994, Atomic Data and Nuclear Data Tables, 56, 231
Odrzywolek, A. 2005–2010, PSNS code http://th-www.if.uj.edu.pl/psns/
Odrzywołek, A. 2007, Eur. Phys. J. C, 52, 425
Odrzywolek, A. 2007, Silicon burning neutrinos, http://sn1987a-20th.physics.uci.edu/1630-Odrzywolek.eps
Odrzywolek, A. 2009, Phys. Rev. C, 80, 045801
Pakmor, R., Kromer, M., Röpke, F. K., et al. 2010, Nature, 463, 61
Phillips, M. M. 2005, in Supernovae as Cosmological Lighthouses, ed. M. Turatto, S. Benetti, L. Zampieri, & W. Shea, ASP Conf. Ser., 342, 1604, 211
Piro, A. L. 2008, ApJ, 679, 616
Piro, A. L., & Bildsten, L. 2008, ApJ, 673, 1009
Plewa, T. 2007, ApJ, 657, 942
Podsiadlowski, P. 2010, Astron. Nachr., 331, 218
Podsiadlowski, P., Mazzali, P., Lesaffre, P., Han, Z., & Förster, F. 2008, New Astron. Rev., 52, 381
Pons, J. A., Steiner, A. W., Prakash, M., & Lattimer, J. M. 2001, Phys. Rev. Lett., 86, 5223
Raghavan, R. S. 1986, Phys. Rev. D, 34, 2088
Raskin, C., Scannapieco, E., Rhoads, J., & Della Valle, M. 2009, ApJ, 707, 74
Riess, A. G., Filippenko, A. V., Challis, P., et al. 1998, AJ, 116, 1009
Riess, A. G., Macri, L., Casertano, S., et al. 2009, ApJ, 699, 539
Rubbia, A. 2009, J. Phys. Conf. Ser., 171, 012020
Ruiter, A. J., Belczynski, K., & Fryer, C. 2009, ApJ, 699, 2026
Ruiz-Lapuente, P., Comeron, F., Méndez, J., et al. 2004, Nature, 431, 1069
Saio, H., & Nomoto, K. 1985, A&A, 150, L21
Sandage, A., & Tammann, G. A. 1993, ApJ, 415, 1
Scannapieco, E., & Bildsten, L. 2005, ApJ, 629, L85
Schawinski, K. 2009, MNRAS, 397, 717
Schinder, P. J., Schramm, D. N., Wiita, P. J., Margolis, S. H., & Tubbs, D. L. 1987, ApJ, 313, 531
Scholberg, K. 2010, J. Phys. Conf. Ser., 203, 012079
Seitenzahl, I. R., Townsley, D. M., Peng, F., & Truran, J. W. 2009, Atomic Data and Nuclear Data Tables, 95, 96
Smartt, S. J. 2009, ARA&A, 47, 63
Smirnov, A. 2009, Workshop Towards Neutrino Technologies, http://cdsagenda5.ictp.trieste.it/full_display.php?ida=a08170
Suzuki, Y. 2001, [arXiv:0110005]
Suzuki, Y. 2008, J. Phys. Conf. Ser., 136, 022057
Thielemann, F.-K. 1984, Adv. Space Res., 4, 67
Timmes, F. X., Brown, E. F., & Truran, J. W. 2003, ApJ, 590, L83
Totani, T., & Sato, K. 1995, Astrop. Phys., 3, 367
Van Der Velde, J. C., Haines, Todd, Bratton, C. B., et al. 1988, Nucl. Instrum. Meth. A, 264, 28
Wang, B., Li, X., & Han, Z. 2010, MNRAS, 401, 2729
Webbink, R. F. 1984, ApJ, 277, 355
Whelan, J., & Iben, Jr., I. 1973, ApJ, 186, 1007
Wood-Vasey, W. M., Miknaitis, G., Stubbs, C. W., et al. 2007, ApJ, 666, 694
Woosley, S. E., & Weaver, T. A. 1994, in Supernovae, ed. S. A. Bludman, R. Mochkovitch, & J. Zinn-Justin, 63, given at Les Houches Summer School, Session 54: Supernovae, Les Houches, France, 31 Jul.–1 Sep. 1990
Yakovlev, D. G., Kaminker, A. D., Gnedin, O. Y., & Haensel, P. 2001, Phys. Rep., 354, 1
Yoon, S., & Langer, N. 2003, A&A, 412, L53
Yoon, S., Podsiadlowski, P., & Rosswog, S. 2007, MNRAS, 380, 933
Zingale, M., Almgren, A. S., Bell, J. B., Nonaka, A., & Woosley, S. E. 2009, ApJ, 704, 196

Pages 13 to 15 are available in the electronic edition of the journal at http://www.aanda.org

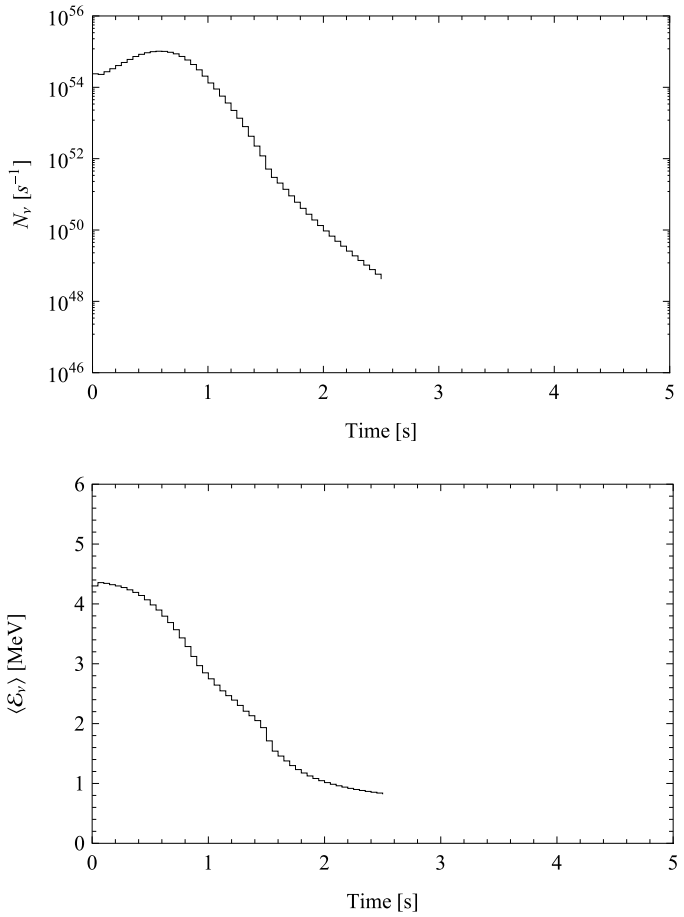

Fig. 9. Model neutrino (ν_e) particle emission in the deflagration model n7d1r10t15c (*top*). Average neutrino energy (*bottom*).

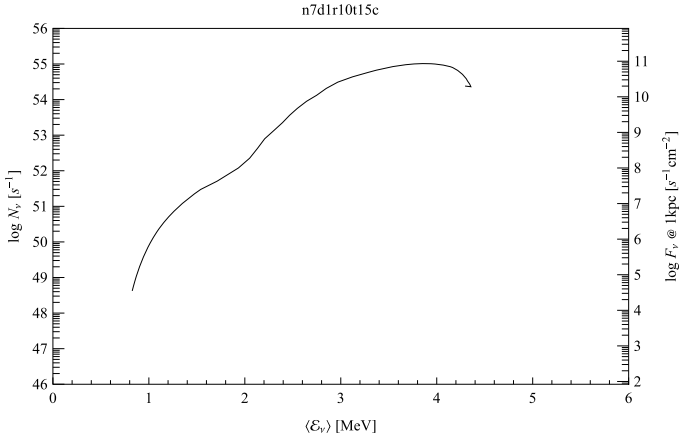

Fig. 10. Total ν_e-HR diagram for the deflagration model n7d1r10t15c.

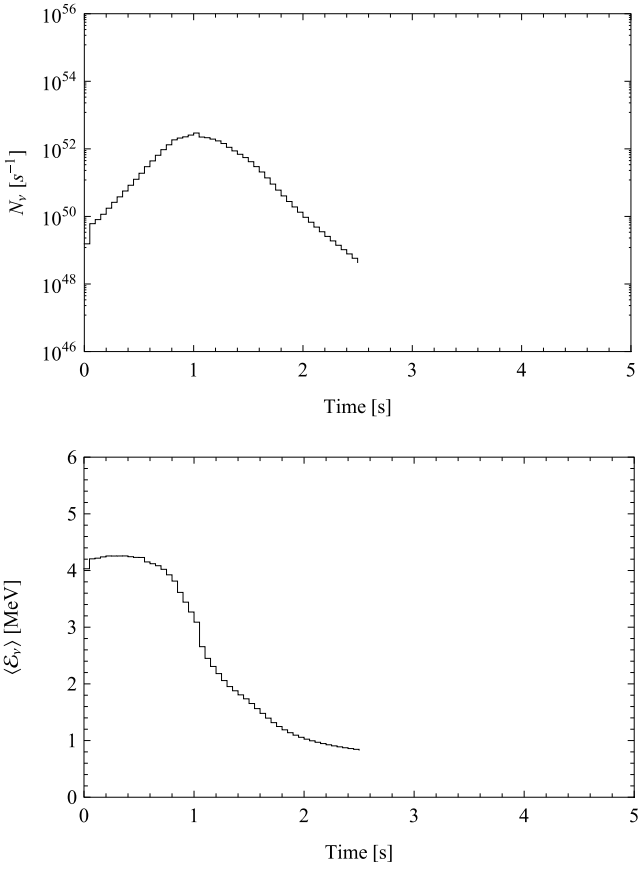

Fig. 11. Model antineutrino ($\bar{\nu}_e$) particle emission in the deflagration model n7d1r10t15c (*top*). Average antineutrino energy (*bottom*).

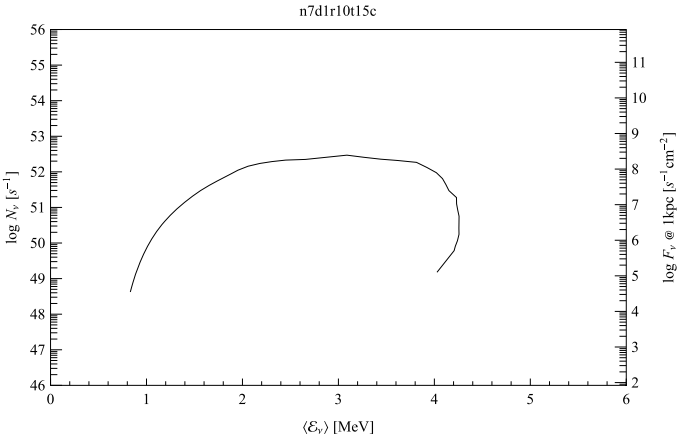

Fig. 12. Total $\bar{\nu}_e$-HR diagram for the deflagration model n7d1r10t15c.

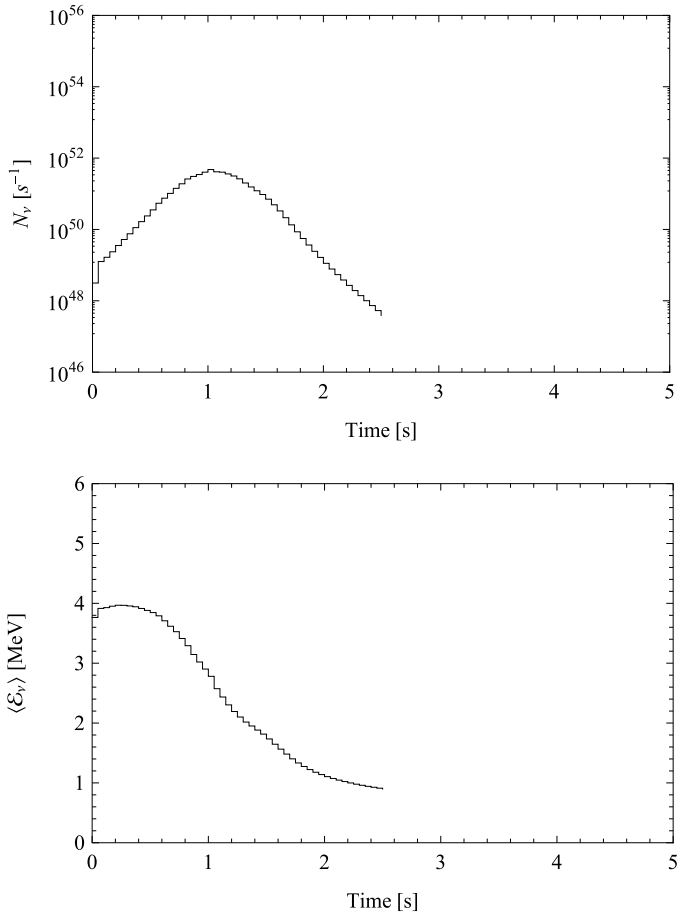

Fig. 13. Model muon/tau neutrino (ν_μ) particle emission in the deflagration model n7d1r10t15c (*top*). Average neutrino energy (*bottom*).

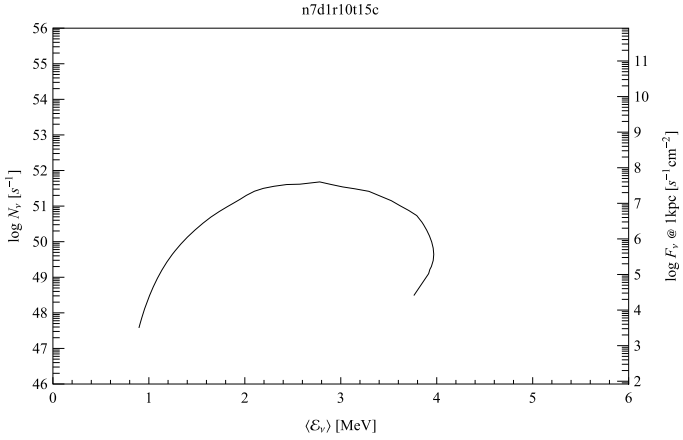

Fig. 14. Total ν_μ-HR diagram for the deflagration model n7d1r10t15c.

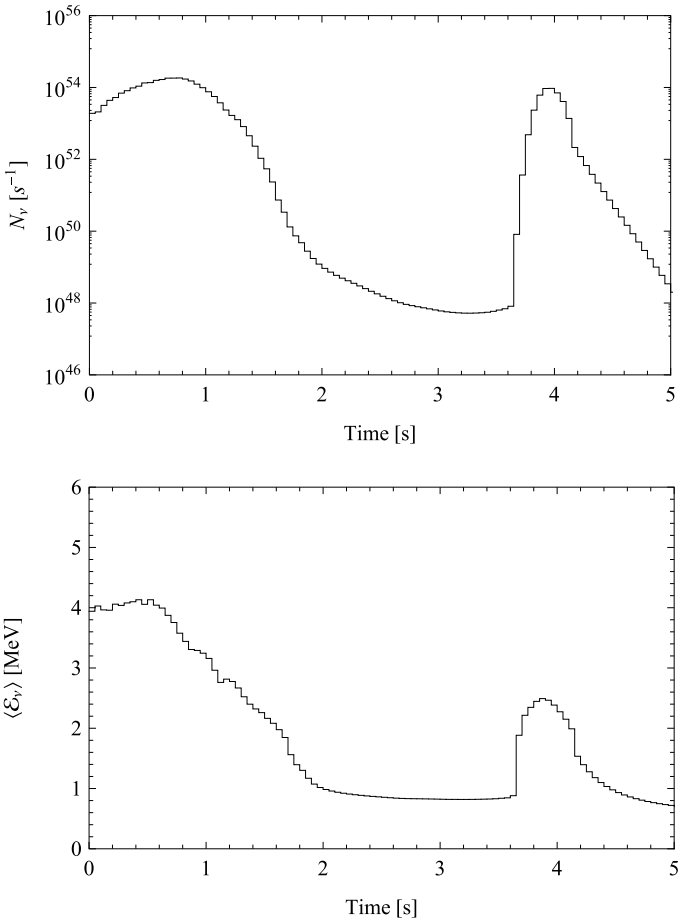

Fig. 15. Model neutrino (ν_e) particle emission in the delayed detonation model Y12 (*top*). Average neutrino energy (*bottom*).

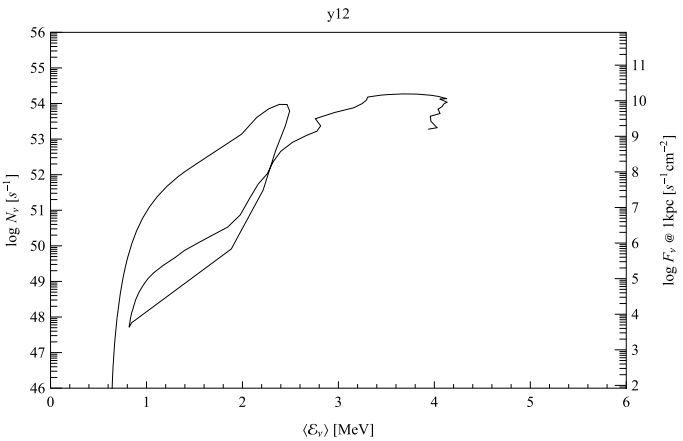

Fig. 16. Total ν_e-HR diagram for the delayed detonation model Y12.

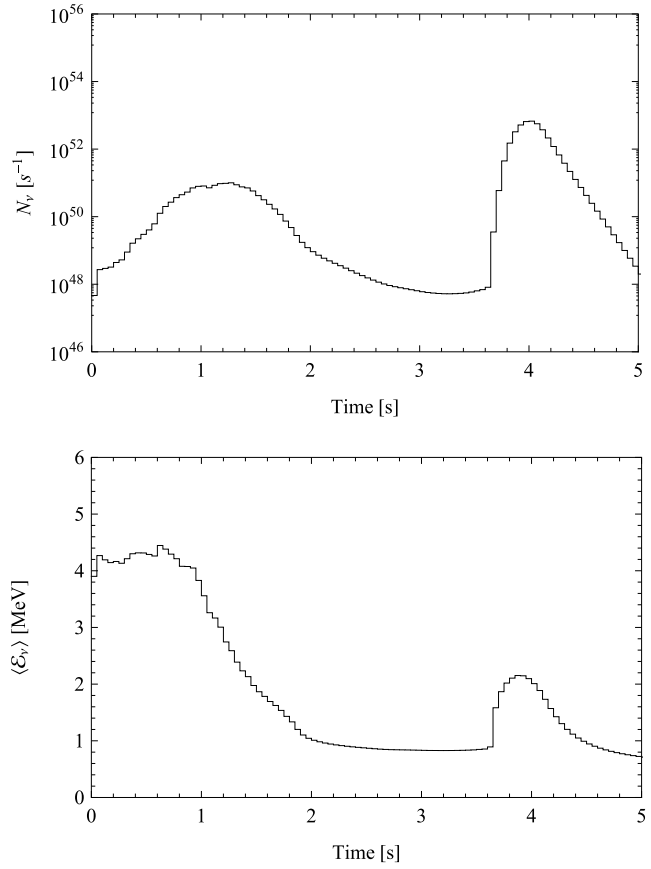

Fig. 17. Model antineutrino ($\bar{\nu}_e$) particle emission in the delayed detonation model Y12 (*top*). Average antineutrino energy (*bottom*).

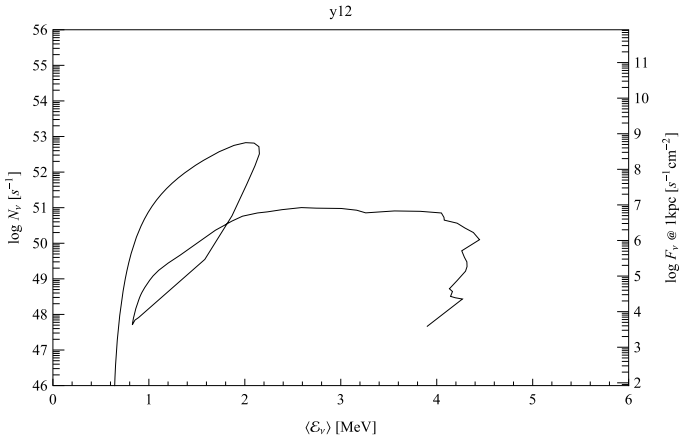

Fig. 18. Total $\bar{\nu}_e$-HR diagram for the delayed detonation model Y12.

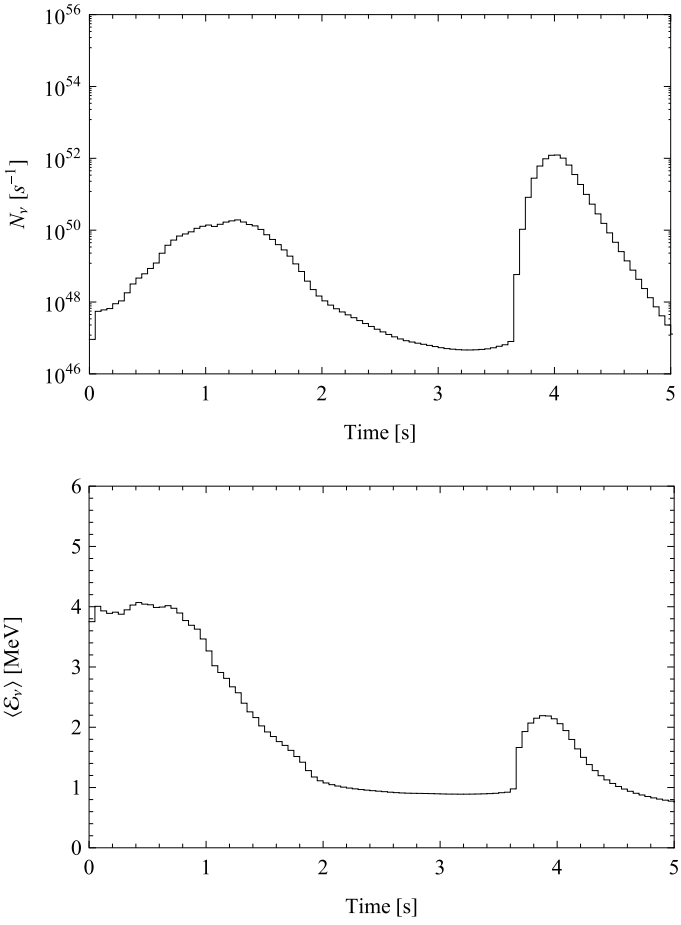

Fig. 19. Model muon/tau neutrino (ν_μ) particle emission in the delayed detonation model Y12 (*top*). Average neutrino energy (*bottom*).

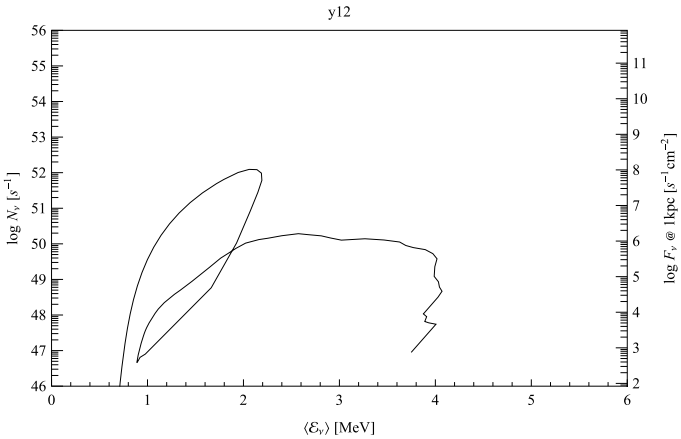

Fig. 20. Total ν_μ-HR diagram for the delayed detonation model Y12.

PHYSICAL REVIEW C **80**, 045801 (2009)

Nuclear statistical equilibrium neutrino spectrum

Andrzej Odrzywolek*
M. Smoluchowski Institute of Physics, Jagiellonian University, Reymonta 4, PL-30-059 Krakow, Poland
(Received 16 March 2009; revised manuscript received 17 June 2009; published 9 October 2009)

The spectral emission of neutrinos from a plasma in nuclear statistical equilibrium (NSE) is investigated. Particular attention is paid to the possible emission of high-energy (>10 MeV) neutrinos or antineutrinos. A newly developed numerical approach for describing the abundances of nuclei in NSE is presented. Neutrino emission spectra, resulting from general Fuller-Fowler-Newman conditions, are analyzed. Regions of T-ρ-Y_e space favoring detectability are selected. The importance of critical Y_e values with zero net rate of neutronization ($\dot{Y}_e$) is discussed. Results are provided for the processing of matter under conditions typical for thermonuclear and core-collapse supernovae, presupernova stars, and neutron star mergers.

DOI: 10.1103/PhysRevC.80.045801 PACS number(s): 95.30.−k, 23.40.−s, 26.50.+x, 26.60.−c

I. INTRODUCTION

Neutrino cooling is of paramount importance in modern astrophysics [1–3]. It governs late stages of stellar evolution, especially massive stars (>8–10 $M_\odot$) [4,5], red giant cores [6], white dwarfs [7], core-collapse supernovae [8–13], and (proto-)neutron stars [14]. Neutrino emission is important in mergers involving neutron stars [15–19], the dense accretion disks of γ-ray burst (GRB) models [20–22], type Ia supernovae [23], and x-ray flashes [24].

Usually, neutrinos carry away energy, and only the total neutrino emissivity, i.e., amount of energy carried out by neutrinos, is of interest. The neutronization induced by the net ν_e-$\bar{\nu}_e$ flux is crucial for understanding of the nucleosynthesis. Therefore, previous research on nuclear statistical equilibrium (NSE) neutrino emission [25] focused on (i) ν_e-$\bar{\nu}_e$ particle emission rates and (ii) total $\nu_e + \bar{\nu}_e$ energy carried out by the neutrinos. We extend this analysis to cover spectral/flavor properties of the NSE neutrino flux.

In known research a detailed treatment of the neutrino emission is done for core-collapse simulations [26,27]. However, it is frequently neglected for other astrophysical objects (e.g., Ia supernovae). Nowadays more interest is dedicated toward spectral properties of the neutrino flux. The neutrino energy is important for core-collapse supernovae, for the neutrino-induced nucleosynthesis (ν-process, [28–30]), neutrino oscillations, and the detection of neutrinos in terrestrial experiments. The last area is poorly explored. The neutrino spectrum for neutrino cooling processes is rarely treated in rigorous way. The typical procedure is to use some more or less justified analytic forms for the neutrino energy spectrum. There are parameters that are found from known neutrino emissivity and the average neutrino energy. In this article we continue our former investigation [31,32] to find spectral properties for important neutrino emission processes. We proceed now to processes involving weak nuclear β transitions.

Neutrino cooling processes can be separated into two classes. There are (i) thermal processes, including e^-e^+ pair annihilation, massive in-medium photon and plasmon decay, and neutrino photoproduction, and (ii) weak nuclear processes (i.e., $\beta^\pm$ decays and $\epsilon^\pm$ captures). We point out that for all thermal processes (pair, plasma, photoproduction, bremsstrahlung, neutrino de-excitation of the nuclei) the neutronization rate vanishes, i.e., the change of the proton/neutron ratio is due exclusively to weak nuclear processes. Class (i) produces all flavors while (ii) only ν_e and $\bar{\nu}_e$. However, neutrino oscillations can mix flavors. Information on thermal and weak components might be destroyed. It happens somewhere between emission and interaction/detection.

We assume that matter is transparent to neutrinos. Therefore, weak nuclear processes often tend to dominate neutrino emission of hot and very dense plasma. In particular, electron captures by both protons and heavy nuclei are progressively more intense. With growing density, the Fermi energy $E_F \simeq \mu_e$ can become larger than the capture threshold (Q value) for increasing number of nuclear species. High temperature additionally enhances emission. Many of the nuclei remain in the thermally excited states. Matrix elements for these weak transitions are often large. For temperatures above ∼0.5 MeV, a significant fraction of equilibrium positrons builds up. This causes a strong $\bar{\nu}_e$ flux due to e^+ captures, particularly on free neutrons.

In contrast to thermal processes, determined entirely (including energy spectrum) by the local thermodynamic properties of matter (e.g., temperature kT and electron chemical potential μ_e), weak nuclear processes depend also on abundances of nuclei. This renders the task of calculating neutrino spectrum difficult to achieve. This is especially true for evolutionary advanced objects.[1] All that we can say for rapidly evolving object, is that the neutrino spectrum emitted from plasma is of the form:

$$\phi(\mathcal{E}_\nu) = \sum_k X_k(t)\psi_k(\mathcal{E}_\nu, kT, \mu_e)\,\frac{\rho}{m_p A_k}. \qquad (1)$$

Here ψ_k represent (assumed known from theory or experiment) spectral shape of single-nuclei neutrino emission and $X_k(t)$

*URL: http://www.ribes.if.uj.edu.pl/; odrzywolek@th.if.uj.edu.pl

[1]This situation is, however, very difficult to describe using statistical methods. A variety of astrophysical objects and processes make it closer to complex systems rather than gases.

the set of usually unknown and rapidly varying abundances. Tracking of the required required number of a few hundred abundances is possible at most, to our knowledge, in simplest one-dimensional models.

Fortunately, if the temperature becomes high enough, nuclei begin to "melt" due to photodisintegrations. Nuclei rearrange due to strong interactions into the most probable state favored by the thermodynamics [33]. This is the NSE approximation [34]. The time scale required to achieve NSE is temperature dependent [35]. It can be approximated as [36]:

$$\tau_{\rm NSE} \sim \rho^{0.2} e^{179.7/T_9 - 40.5} \tag{2}$$

where ρ is the density in g/cm^3, $T_9 = T/10^9$ K, and T is the temperature in K. Equation (2) provides one of the most important constraints limiting the use of the NSE approach. We assume implicitly in Eq. (2) that $Y_e = 0.5$ [35]. Therefore, in a plasma with the value of Y_e that is far from 0.5 caution is required. Both under- and overestimate are possible. The time scale is of the order of the age of the universe, $\tau_{\rm NSE} \sim 10^9$ years, for $kT = 0.2$ MeV and $\tau_{\rm NSE} \sim 10^{-9}$ s for $kT = 1$ MeV. In the core of a typical presupernova star with $\rho = 10^9$ g/cm^3 and $kT = 0.32$ MeV we have $\tau_{\rm NSE} \simeq 2$ days. A typical duration of the Si burning stages depends on stellar mass and varies from few hours to 3 weeks. During the thermonuclear explosion of type Ia supernova in the flame region temperatures grow up to $kT = 0.4 \ldots 0.6$ MeV, the time scale $\tau_{\rm NSE} \simeq 5$ ms, and the explosion time is of the order of 1 s.

The weak transmutation rate between protons and neutrons is denoted by $\dot{Y}_e$,

$$\dot{Y}_e \equiv \frac{dY_e(t)}{dt} = \lambda_{\nu_e} - \lambda_{\bar{\nu}_e}, \tag{3}$$

where

$$\lambda_\nu = \sum_k \lambda_\nu^{(k)} \frac{X_k}{A_k}, \quad \lambda_\nu^{(k)} = \int_0^\infty \psi_k(\mathcal{E}_\nu)\, d\mathcal{E}_\nu.$$

If the hydrodynamic time scale is longer than $\tau_{\rm NSE}$ and $\dot{Y}_e$ change slowly,[2] then we can safely assume a quasistatic evolution in the three-parameter space. Usually[3] these parameters are temperature kT, the density ρ, and the electron fraction Y_e. For the given triad (kT, ρ, Y_e) we are able to determine abundances of all nuclei. This approximation is widely used in "iron" cores of presupernova stars, supernovae, nuclear networks, thermonuclear flames, and nucleosynthesis studies. Under NSE conditions the neutrino emission does not differ much from thermal processes (especially if $\dot{Y}_e = 0$), and no prior knowledge of abundances is required. This allows, e.g., for postprocessing of models with a known history of temperature, density, and electron fraction. If $Y_e(t)$ is not known we still can use the NSE approximation assuming some value, e.g., $Y_e = 0.5$, for symmetric nuclear matter. The composition (and therefore neutrino emission) is extremely sensitive to small changes in Y_e in the most interesting range of $Y_e = 0.35 \ldots 0.55$ and relatively low temperatures of $kT < 0.5$ MeV. One method to overcome this problem is to use the so-called tracer particles built into simulation to remember the thermodynamic history of matter. In the next step one then finds the history of Y_e. Another application of the NSE neutrino emission, described in Ref. [25], is the subgrid-scale model of nuclear flame energetics in thermonuclear supernovae.

This article is organized as follows: in Sec. II we discuss spectra of individual nuclei under conditions of high temperature and density. We use solar ^{7}Be neutrinos as an example. In Sec. III we use NSE and get neutrino emissivities and energy spectra, using Fuller-Fowler-Newman (FFN) [37–40] weak rates. Final section comprises concluding remarks and a programme for future theoretical neutrino astronomy (calculations of the neutrino spectra and so on).

For details related to the implementation of NSE the reader is directed to the accompanying article that has been submitted to *Atomic Data and Nuclear Data Tables* [41].

II. NEUTRINO SPECTRUM FROM β PROCESSES IN THERMAL BATH

Bahcall [42,43] laid fundamental theoretical foundations in the context of the solar neutrino spectrum. Later work is an upgrade of the results of Bahcall concerning the number of nuclei involved, better nuclear data, and so on. With the notable exception of the Sun [44] and geoneutrinos [45], a rigorous treatment of the neutrino spectra from individual nuclei is usually ignored in astroparticle physics. Core-collapse simulations use parameterized approach (cf. e.g. Refs. [27,46]). Unfortunately, in the case of multipeaked neutrino spectrum this approach simply does not work, cf. Fig. 1 and related comments in Ref. [46]. The antineutrino spectrum is computed only for free neutrons in applications known to the author.

The spectrum of neutrinos emitted from single nuclei in astrophysical plasma depends strongly on the temperature and the chemical potential of electrons (and positrons if

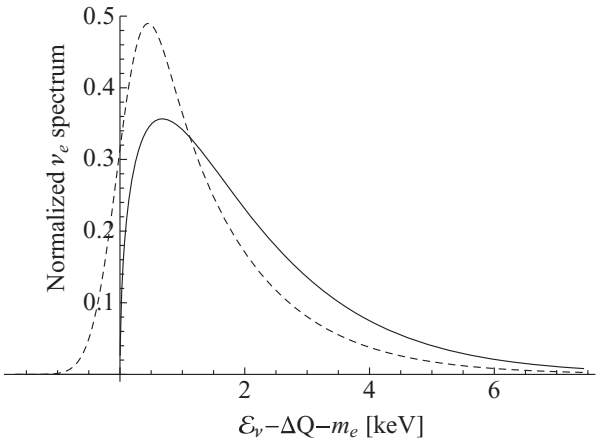

FIG. 1. The normalized neutrino spectrum for solar ^{7}Be electron capture neutrino line, computed according to Eq. (4) (solid line) and the state-of-art result computed by Bahcall ([47], Eq. (46)) is shown by dashed line.

[2]Slow in the sense of Eq. (3), not actual weak rates λ_ν, $\lambda_{\bar{\nu}_e}$, which may be very high.

[3]As noted by Ref. [25], relativistically invariant triad T-n_B-Y_e, where n_B is conserved baryon number density may be used if the general relativity formulation is required.

$kT \sim m_e = 0.511$ MeV or larger). The temperature is large in typical evolutionary advanced astrophysical objects (presupernova or supernova, for example). We will study neutrino spectrum in this regime. On the contrary, for the solar interior, $kT = 1.35 \times 10^{-3}$, $\mu_e = 0$, and this makes little change with respect to laboratory experiments.

Let us begin with typical example of the continuum electron capture process:

$$^7\mathrm{Be} + e^- \rightarrow {}^7\mathrm{Li} + \nu_e$$

We make assumptions concerning the infinite nucleus mass and we neglect various correction factors (screening, Coulomb factor). The $\epsilon^{\pm}$ capture rate is proportional to the constant matrix element multiplied by the so-called phase space factor Φ:

$$\Phi_c = \frac{\mathcal{E}_\nu^2(\mathcal{E}_\nu - \Delta Q)\sqrt{(\mathcal{E}_\nu - \Delta Q)^2 - {m_e}^2}}{1 + \exp\left[(\mathcal{E}_\nu - \Delta Q - \mu)/kT\right]}\Theta(\mathcal{E}_\nu - \Delta Q - m_e), \tag{4}$$

where $\mathcal{E}_\nu$ denotes the neutrino energy for e^- capture and $\mathcal{E}_\nu$ is the antineutrino energy for e^+ capture. ΔQ is the energy difference between initial and final states (both can be excited) and m_e is the electron rest mass. The chemical potential μ_e of the electron includes m_e and therefore for positrons $\mu_{e^+} = -\mu_{e^-} \equiv -\mu$; kT is the temperature of the electron gas.

It is worth noting that by expressing factor (4) by the neutrino (antineutrino) energy rather than electron (positron) energy, we have just one formula, because both signs of $\Delta Q + m_e$ are covered and $\mathcal{E}_\nu > 0$.

The neutrino spectrum from $\beta^{\pm}$ decay is proportional to

$$\Phi_d = \frac{\mathcal{E}_\nu^2(\Delta Q - \mathcal{E}_\nu)\sqrt{(\mathcal{E}_\nu - \Delta Q)^2 - {m_e}^2}}{1 + \exp\left(\mathcal{E}_\nu - \Delta Q + \mu\right)/kT}\Theta(\Delta Q - m_e - \mathcal{E}_\nu). \tag{5}$$

Figure 1 compares neutrino spectrum given by formula (4) with the more elaborated result of Ref. [47] for solar neutrinos. Results are in good qualitative agreement. In both cases shown in Fig. 1 the neutrino spectrum is simply a line of negligible (Fig. 2, upper left) width. The horizontal axis in Fig. 1 is the difference between the Q value (including m_e) and the neutrino energy, in keV. This is because for solar conditions the Q value for ^{7}Be capture is by many orders of magnitude larger than the

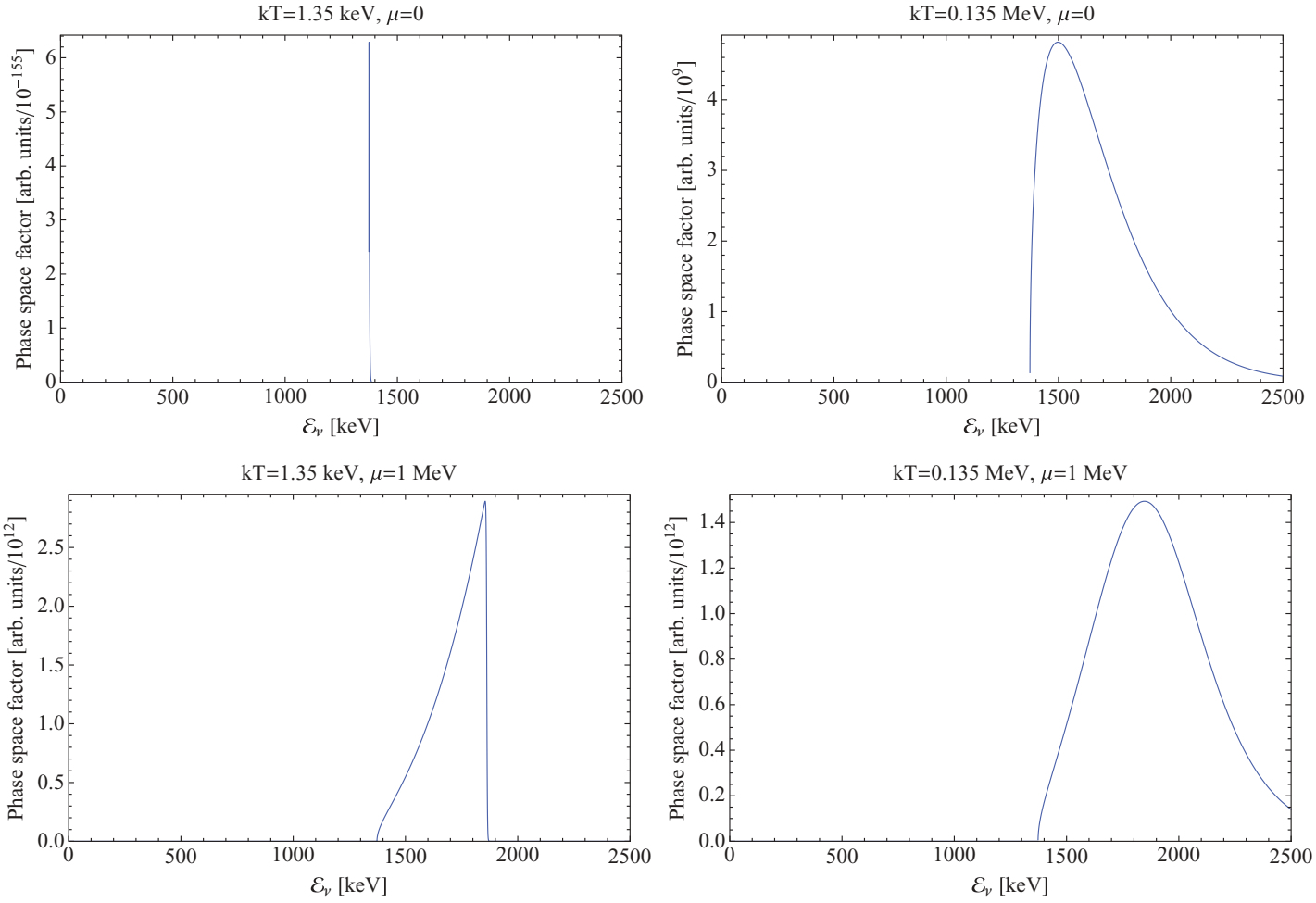

FIG. 2. (Color online) The influence of the degeneracy (large μ) and high temperatures (large kT) on the electron capture neutrino spectrum. (Upper left) Solar neutrinos (in laboratory conditions). (Lower left) Cold degenerate electron gas. The upper-right figure refers to high temperature and the lower-right figure includes both degeneracy and high temperature.

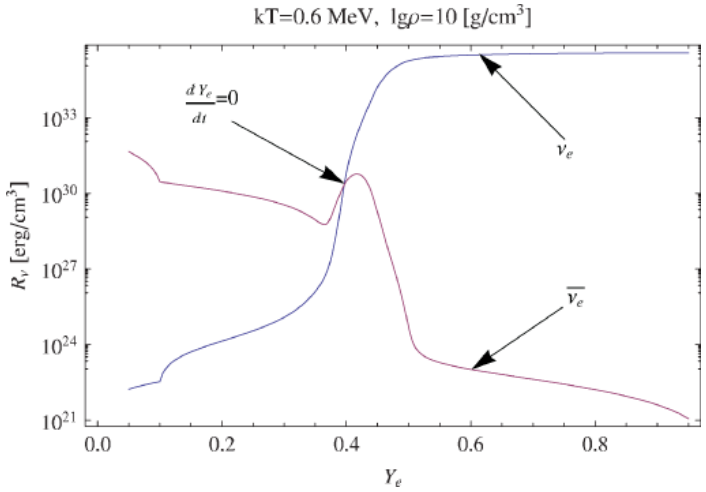

FIG. 3. (Color online) Neutrino and antineutrino emissivities as functions of Y_e. Critical Y_e, defined as $\dot{Y}_e = 0$, is seen at the crossing point of the neutrino and the antineutrino particle emission rates.

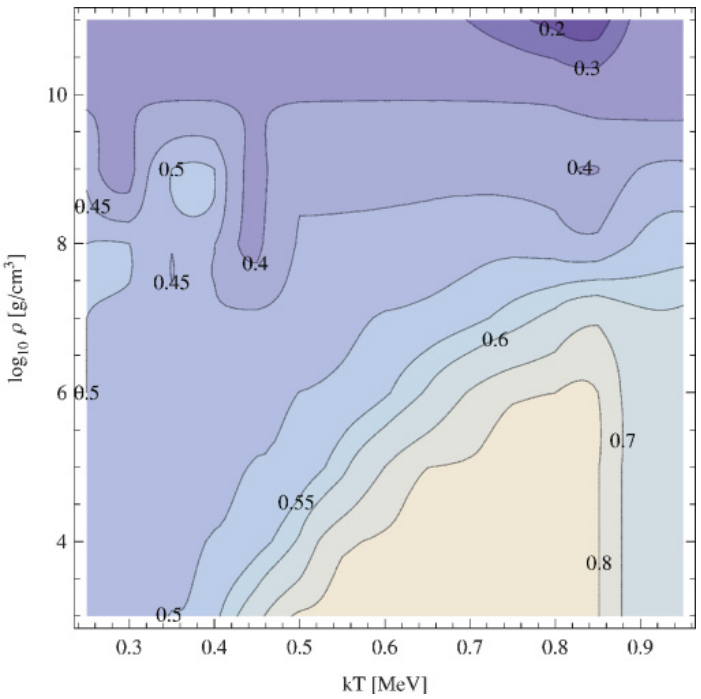

FIG. 4. (Color online) Critical Y_e (see Fig. 3 for explanation) for a range of considered temperatures and densities.

temperature and the chemical potential of the electron gas. If we put ^{7}Be into a plasma where kT or μ is comparable to the Q value, both capture rate and neutrino spectrum change dramatically, cf. Fig 2. In general, spectrum shape is a result of the competition between the Fermi-Dirac distribution and the unit step function Θ in Eq. (4). While e^- kinetic energy always adds to the neutrino energy, for low temperatures it is negligible compared to $\Delta Q + m_e$. If the temperature becomes non-negligible compared to Q values, say, $kT > 0.1$ MeV, the thermal broadening due to kinetic energy of electrons becomes important and the capture rate is enhanced, cf. Fig. 2, upper-right panel. For some of the laboratory stable nuclei the electron (positron) capture might be possible for high-energy electrons (positrons) from the thermal distribution tail.

The increase of density results in large μ_e, and that leads to a more visible effect. This is because most of the electrons, not just a small fraction from the tail, have large energies. The neutrino spectrum (Fig. 2, lower-left) has a very characteristic shape in this case, with sharp edge on the high $\mathcal{E}_\nu$ end. With the increasing μ_e progressively more nuclei become unstable to the electron capture with the continuously growing capture rate. The lower-right panel in Fig. 1 shows the effects of large kT and μ.

Anyway, possibly the most striking feature of Fig. 2 is not the shape of the spectrum but the dramatic scale change on the vertical axis. Weak rates are extremely sensitive to both kT and μ, mainly due to phase-space factors [Eqs. (4) and (5)].

To get a combined NSE spectrum we have to sum up all terms [Eqs. (4) and (5)] for all relevant pairs of excited states, multiply them by the partition function and matrix elements, and then substitute into Eq. (1) with X_k obtained from NSE [41]. A typical behavior of the NSE ν_e and $\bar{\nu}_e$ emissivities [37–39,48–50] as a function of Y_e is presented in Fig. 3. As Y_e decrease, electron neutrino flux (produced mainly in electron captures on protons and by heavy nuclei) also tends to decrease. However, a decrease in Y_e causes an increase in the flux of $\bar{\nu}_e$'s. Usually antineutrino emissivity peaks due to β decays of heavy nuclei and rise due to the positron capture on neutrons and by neutron decay, cf. Fig. 3. For almost all pairs (kT,ρ) we can find the value of Y_e (Fig. 4) where the flux of ν_e is equal to the flux of $\bar{\nu}_e$. These threshold values are particularly interesting for the neutrino astronomy, because they might lead to the strong neutrino and antineutrino emission without further neutronization, in agreement with constraints from nucleosynthesis. The increase of the $\bar{\nu}_e$ flux (with decreasing Y_e) stops neutronization a little bit earlier than the derived from, e.g., the expansion of matter and the related decrease in rates alone. The neutronization can also stop if Y_e becomes too low and positron captures/β^- decays start to dominate. Surprisingly, these critical Y_e values [defined as Y_e for which $\lambda_{\nu_e} = \lambda_{\bar{\nu}_e}$, Fig. 3 and Eq. (3)] vary in a broad range (Fig. 4), reaching values close to $Y_e = 0.875$ [primoidal big bang nucleosynthesis (BBN) mixture of hydrogen and helium] for low densities and $kT = 0.5 \ldots 0.8$. However, for highest densities ($\rho > 10^{11}$ g/cm^3) and temperatures, $kT \simeq 0.8$ MeV, an equilibrium sets at $Y_e = 0.2 \ldots 0.3$. It is important to note that due to the low accuracy of the weak rates derived from FFN tables and the variability of the NSE state with Y_e, Fig. 4 provides only a very approximate outlook of critical values. The critical value[4] is also very important for NSE time scales, as "stalled" Y_e provide additional time without breaking assumption on the quasistatic Y_e evolution.

The competition between ν_e and $\bar{\nu}_e$ emission (Fig. 4) is usually described in terms of the balance between electron captures (mainly on protons) and β^- decays of the heavy nuclei [51]. However, for Y_e outside range of 0.35..0.45 the most important process leading to the $\bar{\nu}_e$ emission is the positron capture by neutrons.

[4]The state with $\dot{Y}_e = 0$ is frequently refereed to as *kinetic* β *equilibrium.*

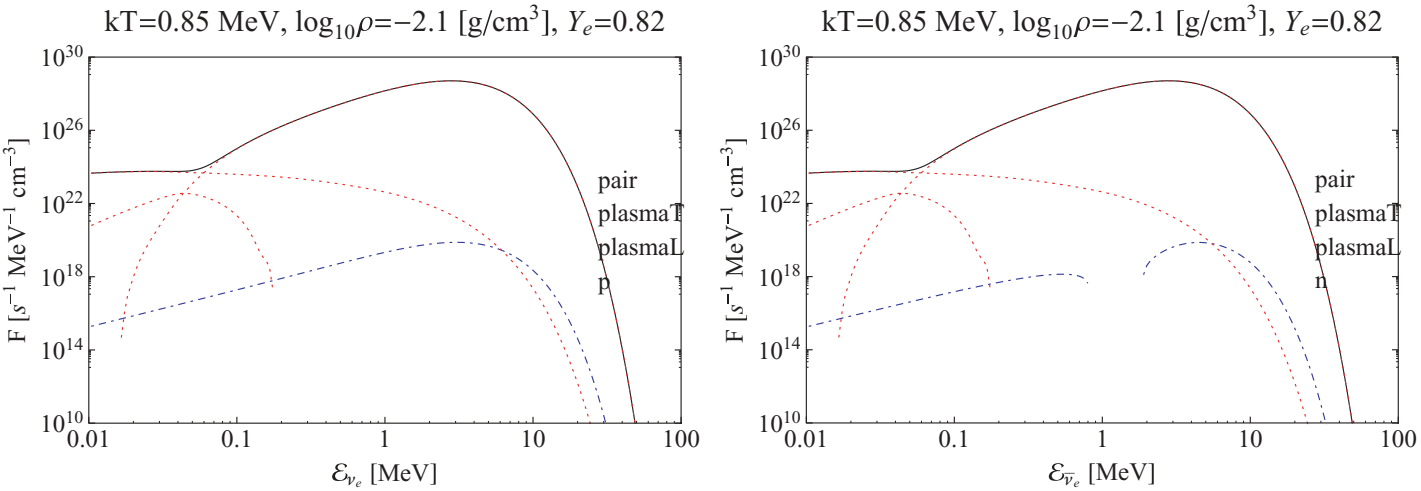

FIG. 5. (Color online) Neutrino (left) and antineutrino (right) spectra emitted per unit volume under conditions typical for the big bang nucleosynthesis era.

III. SPECTRA UNDER ASTROPHYSICAL CONDITIONS OF INTEREST

We are able to compute approximate neutrino/antineutrino spectra for a wide range of astrophysical phenomena if the NSE time scale is short compared to dynamic and weak time scales. Main limitation of our method is the neutrino trapping. The core-collapse supernovae and related phenomena, e.g., long γ-ray bursts, are examples of objects where neutrino trapping is essential. We can use our method for the initial infall stage of the collapse only. As long as we are in the free streaming regime this is the method of choice. We can produce much more detailed and accurate neutrino spectra (than hydrodynamic simulations itself) via postprocessing. The latter is trivial to parallelize and allows us to achieve greater accuracy. Our method can be applied to cosmological-like [1] neutrinos (Fig. 5), the center of the presupernova [4] star (Fig. 6), and typical conditions during type Ia thermonuclear explosions (Figs. 7 and 8). Other examples, less interesting because there are many known results [8,12,13,52–78], are provided for the merger of NS (Fig. 9) and the core-collapse SN (Fig. 11). The spectrum might be calculated for exotic conditions which are not related to any recently considered model as well, cf. Fig. 10. Examples are listed in Table I.

An illustrative example is provided using cosmological weak freezout values as input. Following Ref. [1] we used $T_9 \simeq 9.9$, $\rho = 0.008$ g/cm^3, and $Y_e = 0.82$. The neutrino and antineutrino spectra in Fig. 5 are produced mainly from a pair-annihilation process, whereby the spectra are almost purely thermal. This is not surprising, because a thermal spectrum is what is expected for big bang neutrinos. Thus, our method is working qualitatively well even in this extremal example.

Presupernova stars are neutrino sources of particular interest [82]. The neutrino spectrum has been obtained using values at the center of a star during the maximum compression stage. This stage is achieved just prior to the shell Si ignition above the iron core, a few hours before the start of the collapse. The spectra for $kT = 0.43$ MeV, $\rho = 7 \times 10^8$ g/cm^3, and $Y_e = 0.445$ are presented in Fig. 6. The important reference for these numbers is Ref. [4]. A striking feature in Fig. 6 is the significant contribution from heavy nuclei for both ν_e and $\bar{\nu}_e$ spectra. This is particularly important for the detection of these neutrinos, as previous studies [82] were based solely on the thermal emission. For $\bar{\nu}_e$ the pair-annihilation process dominates the high-energy tail ($\mathcal{E}_{\bar{\nu}_e} > 10$ MeV), and the number of detectable inverse-β events in a standard large water Cherenkov detectors [82–84] does not change. For a

TABLE I. Examples of neutrino and antineutrino spectra.

Object	kT (MeV) (T_9)	ρ (g/cm^3)	Y_e	Figure	Refs.
BBN	0.85(9.9)	0.008	0.82	Fig. 5	[1]
Pre-SN	0.43(5.3)	7.0×10^8	0.445	Fig. 6	[4]
SN Ia DET	0.53(6.1)	7.8×10^7	0.5	Fig. 7	[79,80]
SN Ia DEF	0.52(6.0)	2.0×10^9	0.5	Fig. 8	[79,80]
NS-NS merger	1.0(11.6)	1.0×10^{10}	0.05	Fig. 9	[81]
–	0.9(11.6)	2.0×10^9	0.8	Fig. 10	–
CC SN[a]	1.0(11.6)	1.0×10^{12}	0.73	Fig. 11	[1]

[a]Note: this example pushes our method to the limits of applicability. A more realistic spectrum differs, because neutrinos are trapped and they begin to diffuse rather than escape freely.

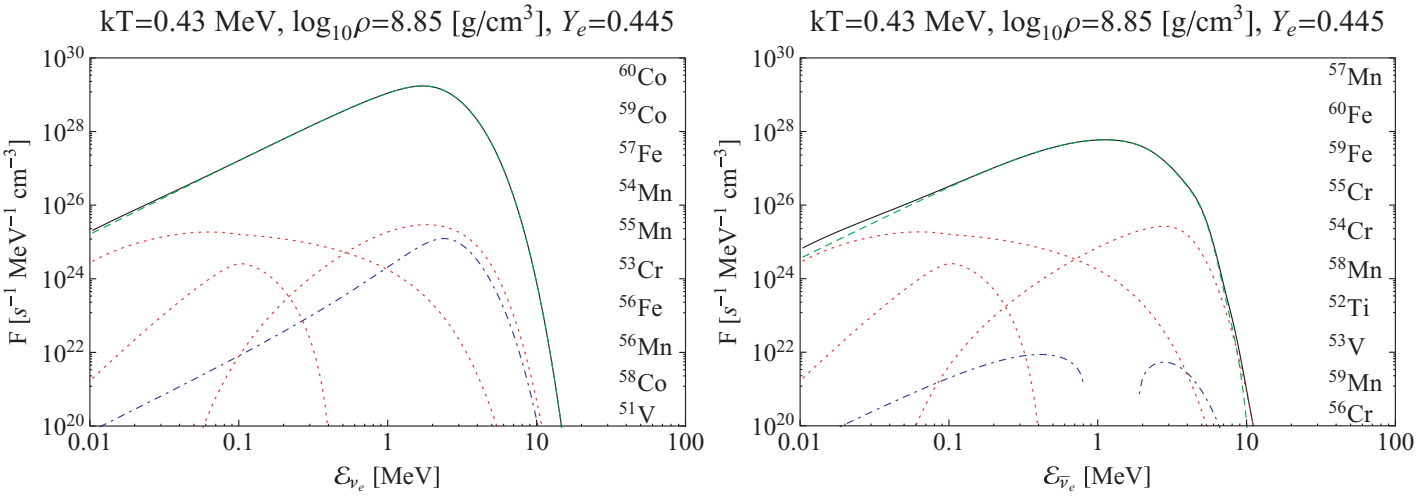

FIG. 6. (Color online) Neutrino (left) and antineutrino (right) spectra emitted per unit volume under conditions typical for a presupernova star.

different detector design, e.g., a liquid scintillator [85], the threshold might be as low as 0.2 MeV [86] and the number of events will be much larger than anticipated from thermal processes only. The situation is even more pronounced for electron neutrinos. A large number of nuclei participate in massive electron captures, leading to the flux that is two orders of magnitude larger than from a pair process even for $\mathcal{E}_{\nu_e} > 5$ MeV. Therefore, the detection of ν_e's, previously rejected from analysis due to experimental difficulties, should be reconsidered. The contribution from free nucleons can be neglected in the presupernova case.

Another very important example of application for our method is the type Ia thermonuclear supernova. Two important regimes for thermonuclear burning in type Ia supernovae are deflagration and detonation. For deflagration we use $kT = 0.53$ MeV and $\rho = 2 \times 10^9$ g/cm^3. For detonation a similar temperature of $kT = 0.52$ MeV has been used, but the density has been reduced due to pre-expansion to $\rho = 7.8 \times 10^7$ g/cm^3. $Y_e = 0.5$ was used, but it is important to point out that small neutronization is inevitable, because the ν_e flux dominates over the flux of $\bar{\nu}_e$, cf. Fig. 8. Neutrino emission is very sensitive to these small changes. Models y12 and n7d1r10t15c of Refs. [79,80] are the sources of the values used above. For a type Ia supernovae free nucleons are among the top neutrino sources; see Figs. 7 and 8. Two presented cases are related to detonation and deflagration. A lower density used for detonation stage (Fig. 7) is the result of the white dwarf pre-expansion due to the previous deflagration stage [79]. The high density in Fig. 8 is connected to the initial stage of subsonic nuclear burning in the pure deflagration model of Ref. [79]. Only three nuclei contribute significantly to the ν_e spectrum in both cases: ^{55}Co, ^{56}Ni, and protons. Relative contributions and total flux are different, however. The neutrino flux per unit volume is four orders of magnitude larger for deflagration compared to detonation. Nevertheless, the deflagration involve tiny volume of the white dwarf only, while the detonation wave usually traverses the entire star. Integrated flux might be similar, but this is model dependent. The antineutrino spectrum is dominated by thermal processes: pair annihilation during detonation and plasmon decay during deflagration. The total flux is much smaller than for neutrinos, and this imbalance causes Y_e to decrease.

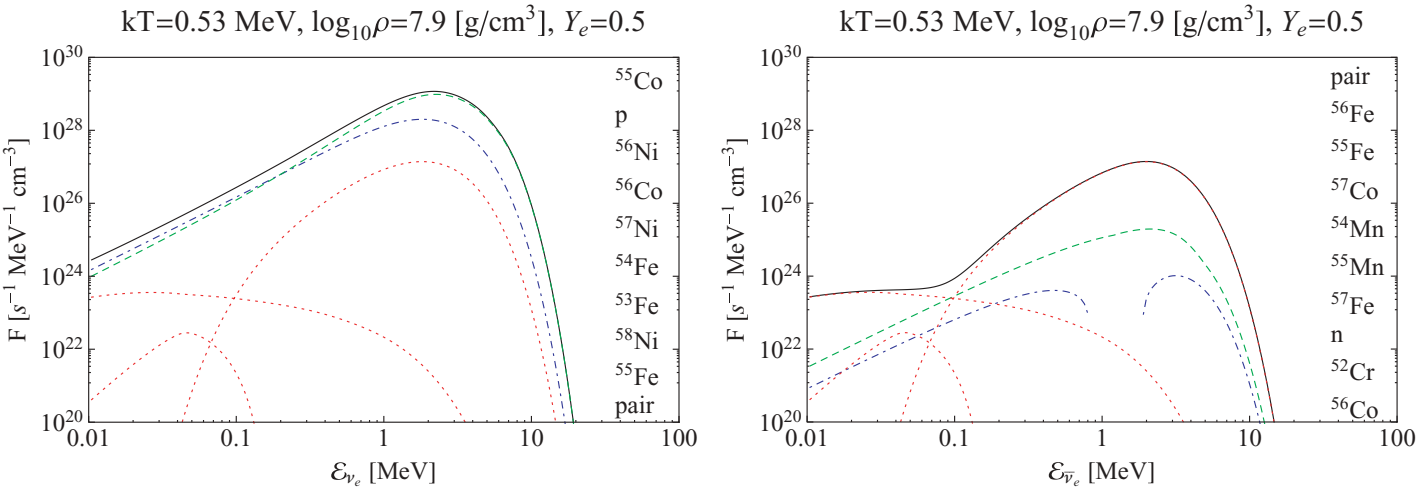

FIG. 7. (Color online) Neutrino (left) and antineutrino (right) spectrum emitted per unit volume under conditions typical for detonation stage of thermonuclear supernova in the delayed-detonation class of models.

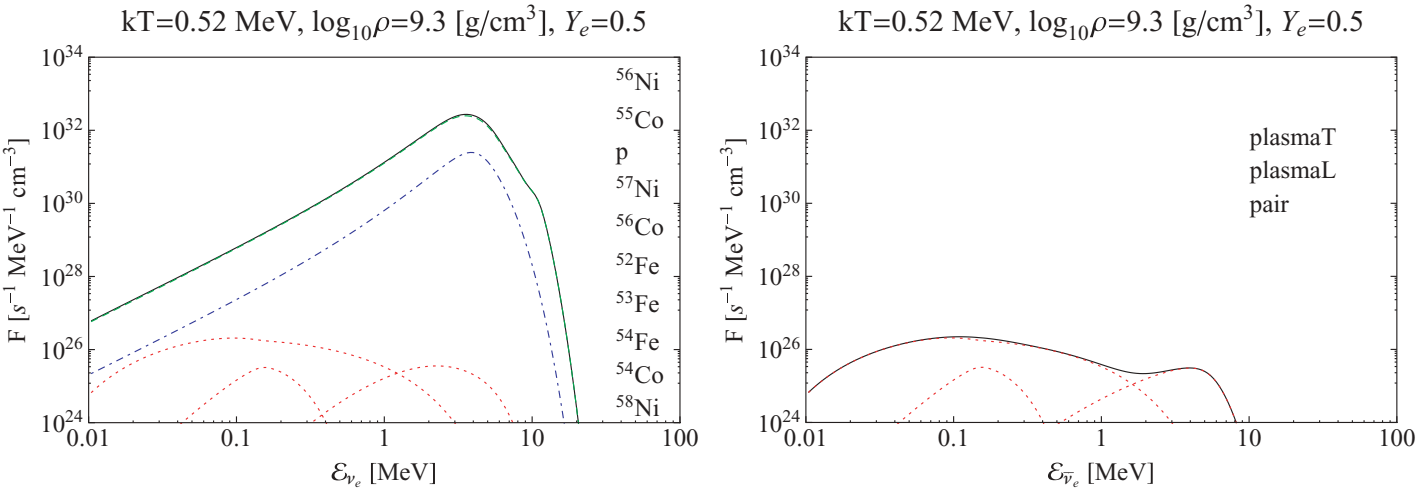

FIG. 8. (Color online) Neutrino (left) and antineutrino (right) spectrum emitted per unit volume under conditions typical for early deflagration stage of a thermonuclear supernova.

Therefore results from Figs. 7 and 8, with assumed $Y_e = 0.5$, should be taken with care. For example, the NSE abundance of ^{55}Co drops rapidly in the range $Y_e = 0.5 \ldots 0.47$. A more detailed investigation of type Ia neutrinos shows also an important contribution from free neutrons to the antineutrino spectrum above 2 MeV.

Now we study the neutrino spectrum for the accretion disk formed in NS-NS merger. Needed data are taken from Fig. 1 of Ref. [81]: temperature of $kT = 1.0$ MeV, $\rho = 10^{10}$ g/cm^3, and $Y_e = 0.05$. Similar results are expected for the neutron star–black hole mergers and other phenomena forming low Y_e, dense, high-temperature accretion disks. The neutrino spectrum (Fig. 9) is a result of pair process and electron captures on protons. The antineutrino spectrum is heavily dominated by the neutron decay and positron captures on neutrons. The gap $0.8 < \mathcal{E}_{\bar{\nu}_e} < 1.8$ MeV is filled by processes involving heavy nuclei. Moreover, antineutrino flux is much larger compared to the neutrino flux. The spectrum peaks at $\mathcal{E}_{\bar{\nu}_e} \simeq 5$ MeV provide an interesting candidate for neutrino detection using the inverse β decay.

Another example (Fig. 10), not related to a particular astrophysical phenomena, shows the importance of thermal processes and those involving free nucleons. The antineutrino spectrum, especially the high-energy end due to the positron capture, is particularly important. Spectral features of this process should be interesting for future neutrino astronomy, based on gigantic $\bar{\nu}_e$ water-based detectors [85,87–89].

The core-collapse process is poorly described using our method, but we have provided an example for the sake of the completeness. The calculated neutrino spectrum in Fig. 11 has a complex multipeak structure. This is in contrast to the results of the more sophisticated neutrino radiation transport results, which are always single peaked. This can be explained by (i) smoothing nature of the diffusive transport and (ii) too small energy resolution (to few energy bins) of the transport codes used in simulations. The high-energy neutrinos seen in Fig. 11 are in reality downscattered to much smaller energies. The same applies to antineutrinos. Additionally, ν-$\bar{\nu}$ pairs are created in the process of collisions between neutrinos and electrons and between pairs of neutrinos [90]. This leads to

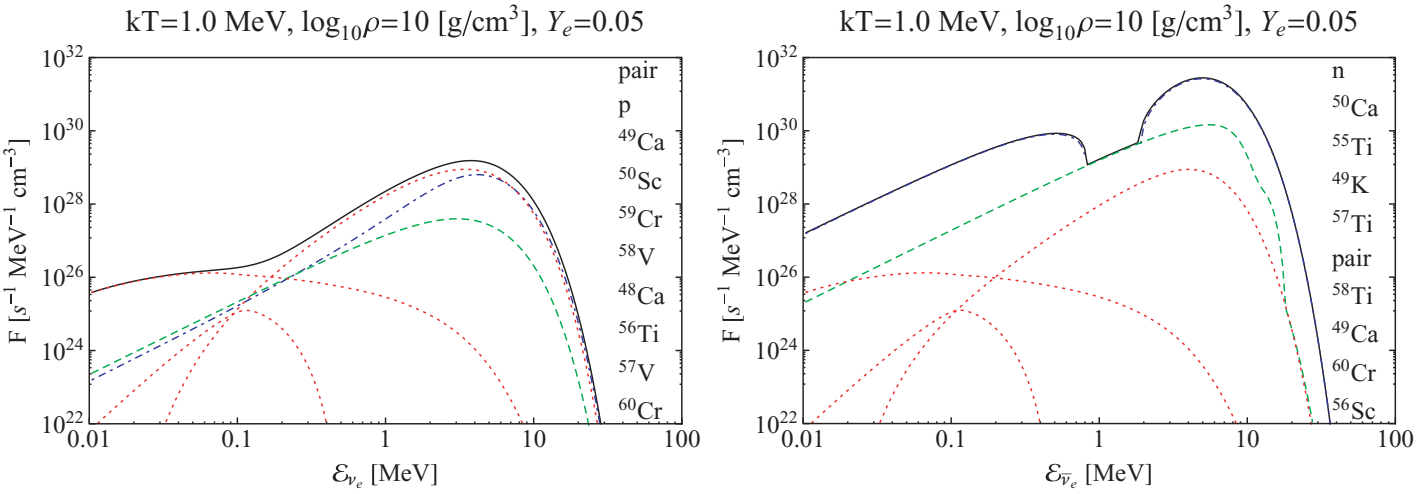

FIG. 9. (Color online) Neutrino (left) and antineutrino (right) spectrum emitted per unit volume under conditions typical for neutron star merger.

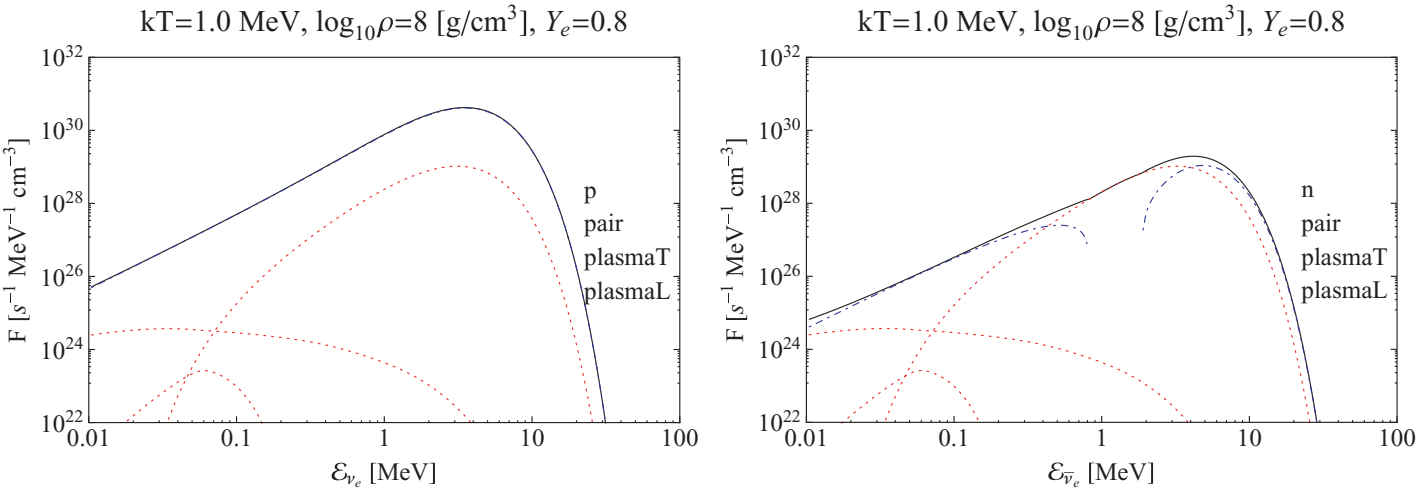

FIG. 10. (Color online) Neutrino (left) and antineutrino (right) spectrum emitted per unit volume under conditions of large Y_e and high temperature.

the energy exchange between flavors, and realistic ν_x spectra[5] are not as distinct as those from Figs. 11. Factors that block outgoing neutrinos and could shape the neutrino spectrum under such extreme conditions were omitted. Clearly, our method is not working for the core-collapse supernovae as anticipated.

IV. CONCLUSIONS

One of our important conclusions is related to typical way of publishing data on weak nuclear processes in astrophysics. This approach dates back to 1980 and was introduced in a famous article [37]. Tables published by the FFN have become standard in modern astrophysics. Upgrades [37,48,91] did not change the structure of the FFN tables. Unfortunately, an FFN grid using only 13×11 points is not enough to obtain precise results, as noted by the FFN authors [40]. While we understand the reasons to preserve this standard for 30 years, "reverse engineering" FFN-like tables to obtain spectra is impractical now, as is the complicated interpolating procedure. If one wants to calculate the spectrum precisely, without using analytical approximate formulas for individual nuclei, precalculated tables are useless. The following set of data are much more convenient:

(i) energy and spins for ground and excited states and
(ii) weak transition matrix elements between all relevant pairs of the excited states for the parent and daughter nuclei.

Alternatively, a tabulated spectrum for all T-ρY_e pairs would be a good choice, with the amount of stored data up to several megabytes. While such approach will increase the amount of published numerical data by a factor of ∼10, it would remove any ambiguity in the representation of the spectra.

[5]Muon and τ spectra are almost identical to the thermal electron flavor spectra, except for smaller integrated flux.

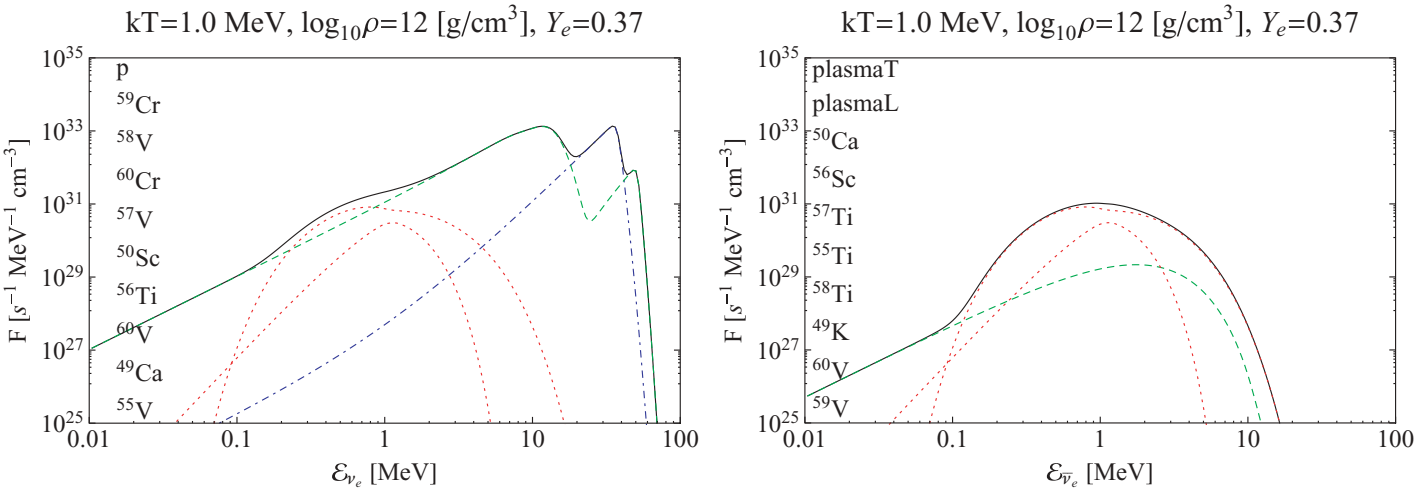

FIG. 11. (Color online) Neutrino (left) and antineutrino (right) spectra emitted per unit volume under conditions typical for the infall stage of the core collapse.

Inspection of virtually any of the figures presented here (Figs. 5–11) clearly shows the importance of both nuclear and thermal processes. The thermal emission and captures on free nucleons and nuclei should be included in consistent calculations. However, depending on the subject, all combinations of these can be found in astrophysical applications. For example, type Ia supernova simulations include NSE emission but older simulations completely neglect neutrino emission or include only electron captures [23]. Other important regimes, particularly core collapse and presupernovae, frequently neglect positron captures, particularly on neutrons. Estimates of the neutrino signal in detectors from presupernovae rely purely on thermal emission [82–84].

The ultimate goal, which is beyond scope of the article, is to know exactly (not approximately!) the neutrino spectrum from weak nuclear processes under NSE. In the past, weak rates were usually integrated and only the total neutrino flux (particles and energy) has been tabulated and presented to the public. We argue again that this is not the best approach if one wants to calculate the neutrino spectrum. Without full input used to calculate weak rates we are unable to restore information lost in the integration. Typical (FFN-like) weak interaction tables are not sufficient. Tables of the excited states, spins, and weak matrix elements for all considered nuclei will allow researchers to calculate both neutrino/antineutrino spectra and customized weak interaction rate tables.

Weak rates prepared in the FFN fashion (i.e., all published rates [37,48,91]), even those with tabulated effective $\log \langle ft \rangle$, do not facilitate estimates of the neutrino spectrum. This is not surprising, because these rates were prepared for a different purpose: neutrino energy loss and neutronization. Maximal information on the spectrum extracted from FFN-like tables can be extracted as described in the accompanying article [41]. We retabulate effective $\lg \langle ft \rangle$ values and effective $Q_{\rm eff}$ values for every grid point to get from Eq. (4) or Eq. (5) the original total rate and average neutrino energy. If the total rate is not dominated by the captures we switch from Eq. (4) to Eq. (5). This approach produces significant side effects if capture and decay rates are comparable. The neutron provides good example. Due to the non-negligible contribution of $\bar{\nu}_e$'s from the neutron decay, the average energy differs from that deduced from pure positron capture. Therefore the effective spectrum has a variable effective Q value. The realistic positron (and electron) capture spectrum always starts with energy equal to the lowest Q value. To sum up, the obvious next step in the research is to give up precalculated tables of weak rates and to re-calculate the neutrino spectrum from scratch, using nuclear data and weak matrix elements as an input.

Despite these difficulties, we obtained new results:

(i) We get interpolating procedures for NSE abundances with a number of convenient features: the ability to choose from NSE-selected nuclei the computational time scaling linearly with the number of nuclides and independent of the position in T-ρ-Y_e space for the full $Y_e = 0.05 \ldots 0.95$ range [41].

(ii) **the energy spectrum**, fluxes, mean energies, etc., of the emitted neutrinos and antineutrinos *separately* for ν_e and $\bar{\nu}_e$.

Our analysis was meant to be general, but we can identify some possible astrophysical targets for presented methods. The NSE neutrino spectrum would be a good approximation for massive stars after Si burning and thermonuclear supernovae. Related research is underway. Procedures developed here will be useful for the analysis of neutrino signals from x-ray flashes, neutron stars, merger events, accretion disks, and some types of cosmic explosions, e.g., pair-instability supernovae.

The electron antineutrino emission due to the positron capture on neutrons provides strong and relatively high-energy flux for surprisingly large volume in kT-ρ-Y_e space. Needed thermodynamic conditions, $kT > 0.6$ and $\rho > 10^7$ g/cm^3, can be met in many astrophysical objects. Megaton-scale neutrino detectors [92] will search for antineutrinos with energy $\mathcal{E}_{\bar{\nu}_e} > 1.8$ MeV. The detection of strong ν_e flux above 5 MeV produced mainly by captures on protons and heavy nuclei is standard in water Cherenkov [87–89] or liquid scintillator [85,87,93] detectors. Therefore further investigation of NSE neutrinos, particularly in the unexplored region of large $0.87 > Y_e \gg 0.55$, should give researchers some additional hints to the existence (or nonexistence) of detectable astrophysical antineutrino sources.

ACKNOWLEDGMENTS

I thank I. Seitenzahl for discussion of the NSE calculations and T. Plewa for motivation and support of this work. My colleagues, E. Malec and S. Dye, contributed significantly to this work by carefully reading the manuscript. I also thank the anonymous referee for important suggestions, making presentation of the results much more useful for the astrophysical community.

[1] D. Arnett, *Supernovae and Nucleosynthesis* (Princeton University Press, Princeton, NJ, 1996).
[2] G. S. Bisnovatyi-Kogan, *Stellar Physics: Fundamental Concepts and Stellar Equilibrium* (Springer, New York, 2001), Vol. 1.
[3] R. Kippenhahn and A. Weigert, *Stellar Structure and Evolution* (Springer-Verlag, Berlin, 1994).
[4] S. E. Woosley, A. Heger, and T. A. Weaver, Rev. Mod. Phys. **74**, 1015 (2002).
[5] P. Young, D. Arnett, C. Meakin, and C. Fryer, Astrophys. J. **629**, L101 (2005).
[6] M. Haft, G. Raffelt, and A. Weiss, Astrophys. J. **425**, 222 (1994).
[7] E. M. Kantor and M. E. Gusakov, MNRAS **381**, 1702 (2007).
[8] J. W. Murphy and A. Burrows, Astrophys. J. **688**, 1159 (2008).
[9] H. Duan, G. M. Fuller, J. Carlson, and Y.-Z. Qian, Phys. Rev. Lett. **100**, 021101 (2008).
[10] S. W. Bruenn, C. J. Dirk, A. Mezzacappa, J. C. Hayes, J. M. Blondin, W. R. Hix, and O. E. B. Messer, J. Phys. Conf. Ser. **46**, 393 (2006).
[11] K. Nakazato, K. Sumiyoshi, and S. Yamada, Astrophys. J. **666**, 1140 (2007).

[12] R. Buras, M. Rampp, H.-T. Janka, and K. Kifonidis, Astron. Astrophys. **447**, 1049 (2006).
[13] R. Buras, H.-T. Janka, M. Rampp, and K. Kifonidis, Astron. Astrophys. **457**, 281 (2006).
[14] D. G. Yakovlev, A. D. Kaminker, O. Y. Gnedin, and P. Haensel, Phys. Rep. **354**, 1 (2001).
[15] S. Rosswog, R. Speith, and G. A. Wynn, Mon. Not. R. Astron. Soc. **351**, 1121 (2004).
[16] L. Dessart, C. D. Ott, A. Burrows, S. Rosswog, and E. Livne, Astrophys. J. **690**, 1681 (2009).
[17] H.-T. Janka, T. Eberl, M. Ruffert, and C. L. Fryer, Astrophys. J. **527**, L39 (1999).
[18] M. A. Aloy, H.-T. Janka, and E. Müller, Astron. Astrophys. **436**, 273 (2005).
[19] M. Ruffert and H.-T. Janka, Astron. Astrophys. **380**, 544 (2001).
[20] D. Lazzati, R. Perna, and M. C. Begelman, Mon. Not. R. Astron. Soc. **388**, L15 (2008).
[21] D. Giannios, arXiv:0704.1659.
[22] R. Birkl, M. A. Aloy, H.-T. Janka, and E. Müller, Astron. Astrophys. **463**, 51 (2007).
[23] T. Kunugise and K. Iwamoto, Publ. Astron. Soc. Jpn. **59**, L57 (2007).
[24] S. E. Woosley, A. Heger, A. Cumming, R. D. Hoffman, J. Pruet, T. Rauscher, J. L. Fisker, H. Schatz, B. A. Brown, and M. Wiescher, Astrophys. J. Suppl. Ser. **151**, 75 (2004).
[25] I. R. Seitenzahl, D. M. Townsley, F. Peng, and J. Truran, At. Data Nucl. Data Tables **95**, 96 (2009).
[26] A. Burrows and T. A. Thompson, "Neutrino-Matter Interaction Rates in Supernovae: The Essential Microphysics of Core Collapse", in "Core Collapse of Massive Stars", edited by C. L. Fryer (Kluwer Academic Publishers, 2002), arXiv:astro-ph/0211404.
[27] S. W. Bruenn, Astrophys. J. Suppl. Ser. **58**, 771 (1985).
[28] A. Heger, E. Kolbe, W. C. Haxton, K. Langanke, G. Martínez-Pinedo, and S. E. Woosley, Phys. Lett. **B606**, 258 (2005).
[29] C. Fröhlich, G. Martínez-Pinedo, M. Liebendörfer, F.-K. Thielemann, E. Bravo, W. R. Hix, K. Langanke, and N. T. Zinner, Phys. Rev. Lett. **96**, 142502 (2006).
[30] J. Pruet, R. D. Hoffman, S. E. Woosley, H.-T. Janka, and R. Buras, Astrophys. J. **644**, 1028 (2006).
[31] M. Misiaszek, A. Odrzywolek, and M. Kutschera, Phys. Rev. D **74**, 043006 (2006).
[32] A. Odrzywolek, Eur. Phys. J. C **52**, 425 (2007).
[33] I. R. Seitenzahl, F. X. Timmes, A. Marin-Laflèche, E. Brown, G. Magkotsios, and J. Truran, Astrophys. J. **685**, L129 (2008).
[34] F. E. Clifford and R. J. Tayler, Mem. R. Astron. Soc. **69**, 21 (1965).
[35] V. S. Imshennik, S. S. Filippov, and A. M. Khokhlov, Pisma Astron. Zh. **7**, 219 (1981) [Sov. Astron. Lett. **7**, 121 (1981)].
[36] A. M. Khokhlov, Astron. Astrophys. **245**, 114 (1991).
[37] G. M. Fuller, W. A. Fowler, and M. J. Newman, Astrophys. J. Suppl. Ser. **42**, 447 (1980).
[38] G. M. Fuller, W. A. Fowler, and M. J. Newman, Astrophys. J. **252**, 715 (1982).
[39] G. M. Fuller, W. A. Fowler, and M. J. Newman, Astrophys. J. Suppl. Ser. **48**, 279 (1982).
[40] G. M. Fuller, W. A. Fowler, and M. J. Newman, Astrophys. J. **293**, 1 (1985).
[41] A. Odrzywolek, Atom. Data Nucl. Data (2009) (submitted).
[42] J. N. Bahcall, Phys. Rev. **126**, 1143 (1962).
[43] J. N. Bahcall, Phys. Rev. **128**, 1297 (1962).
[44] J. N. Bahcall, *Neutrino Astrophysics* (Cambridge University Press, Cambridge/New York, 1989), p. 584.
[45] S. Enomoto, Ph.D. thesis, Tohoku University, 2005.
[46] K. Langanke, G. Martínez-Pinedo, and J. M. Sampaio, Phys. Rev. C **64**, 055801 (2001).
[47] J. N. Bahcall, Phys. Rev. D **49**, 3923 (1994).
[48] J.-U. Nabi and K. H. V., Atom. Data Nucl. Data **88**, 237 (2004).
[49] E. Caurier, K. Langanke, G. Martínez-Pinedo, and F. Nowacki, Nucl. Phys. **A653**, 439 (1999).
[50] K. Langanke and G. Martinez-Pinedo, Nucl. Phys. **A673**, 481 (2000).
[51] M. B. Aufderheide, I. Fushiki, S. E. Woosley, and D. H. Hartmann, Astrophys. J. Suppl. Ser. **91**, 389 (1994).
[52] R. Tomàs, M. Kachelrieß, G. Raffelt, A. Dighe, H.-T. Janka, and L. Scheck, J. Cosmol. Astropart. Phys. 09 (2004) 015.
[53] H.-T. Janka and W. Hillebrandt, Astron. Astrophys. **224**, 49 (1989).
[54] J. Pruet, R. D. Hoffman, S. E. Woosley, H.-T. Janka, and R. Buras, Astrophys. J. **644**, 1028 (2006).
[55] J. Pruet, S. E. Woosley, R. Buras, H.-T. Janka, and R. D. Hoffman, Astrophys. J. **623**, 325 (2005).
[56] H.-T. Janka and E. Mueller, Astron. Astrophys. **290**, 496 (1994).
[57] H.-T. Janka, K. Langanke, A. Marek, G. Martínez-Pinedo, and B. Müller, Phys. Rep. **442**, 38 (2007).
[58] R. Buras, M. Rampp, H.-T. Janka, and K. Kifonidis, Phys. Rev. Lett. **90**, 241101 (2003).
[59] A. Mezzacappa, A. C. Calder, S. W. Bruenn, J. M. Blondin, M. W. Guidry, M. R. Strayer, and A. S. Umar, Astrophys. J. **495**, 911 (1998).
[60] L. Scheck, K. Kifonidis, H.-T. Janka, and E. Müller, Astron. Astrophys. **457**, 963 (2006).
[61] M. Liebendörfer, M. Rampp, H.-T. Janka, and A. Mezzacappa, Astrophys. J. **620**, 840 (2005).
[62] M. Rampp and H.-T. Janka, Astrophys. J. **539**, L33 (2000).
[63] C. D. Ott, H. Dimmelmeier, A. Marek, H.-T. Janka, I. Hawke, B. Zink, and E. Schnetter, Phys. Rev. Lett. **98**, 261101 (2007).
[64] M. Rampp and H.-T. Janka, Astron. Astrophys. **396**, 361 (2002).
[65] T. A. Thompson, A. Burrows, and J. E. Horvath, Phys. Rev. C **62**, 035802 (2000).
[66] A. Burrows, E. Livne, L. Dessart, C. D. Ott, and J. Murphy, Astrophys. J. **640**, 878 (2006).
[67] A. Burrows and J. M. Lattimer, Astrophys. J. **307**, 178 (1986).
[68] A. Burrows, J. Hayes, and B. A. Fryxell, Astrophys. J. **450**, 830 (1995).
[69] A. Burrows, L. Dessart, E. Livne, C. D. Ott, and J. Murphy, Astrophys. J. **664**, 416 (2007).
[70] T. A. Thompson, A. Burrows, and P. A. Pinto, Astrophys. J. **592**, 434 (2003).
[71] R. Walder, A. Burrows, C. D. Ott, E. Livne, I. Lichtenstadt, and M. Jarrah, Astrophys. J. **626**, 317 (2005).
[72] A. Burrows, Astrophys. J. **334**, 891 (1988).
[73] A. Burrows, S. Reddy, and T. A. Thompson, Nucl. Phys. **A777**, 356 (2006).
[74] A. Mezzacappa and S. W. Bruenn, Astrophys. J. **405**, 669 (1993).
[75] A. Mezzacappa, M. Liebendörfer, O. E. B. Messer, W. R. Hix, F.-K. Thielemann, and S. W. Bruenn, Phys. Rev. Lett. **86**, 1935 (2001).

[76] M. Liebendörfer, O. E. B. Messer, A. Mezzacappa, S. W. Bruenn, C. Y. Cardall, and F.-K. Thielemann, Astrophys. J. Suppl. Ser. **150**, 263 (2004).
[77] W. R. Hix, O. E. B. Messer, A. Mezzacappa, M. Liebendörfer, J. Sampaio, K. Langanke, D. J. Dean, and G. Martínez-Pinedo, Phys. Rev. Lett. **91**, 201102 (2003).
[78] K. Langanke, G. Martínez-Pinedo, J. M. Sampaio, D. J. Dean, W. R. Hix, O. E. B. Messer, A. Mezzacappa, M. Liebendörfer, H.-Th. Janka, and M. Rampp, Phys. Rev. Lett. **90**, 241102 (2003).
[79] T. Plewa, Astrophys. J. **657**, 942 (2007).
[80] D. Kasen and T. Plewa, Astrophys. J. **662**, 459 (2007).
[81] W. H. Lee, E. Ramirez-Ruiz, and D. Page, Astrophys. J. **632**, 421 (2005).
[82] A. Odrzywolek, M. Misiaszek, and M. Kutschera, Astropart. Phys. **21**, 303 (2004).
[83] A. Odrzywolek, M. Misiaszek, and M. Kutschera, Acta Phys. Pol. B **35**, 1981 (2004).
[84] A. Odrzywolek, in Twenty Years after SN1987A (2007), http://sn1987a-20th.physics.uci.edu/.
[85] S. Katsanevas, Acta Phys. Pol. B **37**, 2115 (2006).
[86] G. Alimonti *et al.* (Borexino Collaboration), Nucl. Instrum. Methods Phys. Res. A **600**, 568 (2009).
[87] M. Fechner and C. Walter (submitted to PRD), arXiv:0901.1950v1.
[88] The ISS Detector Working Group *et al.*, JINST **4**, T05001 (2009).
[89] A. de Bellefon, J. Bouchez, J. Busto, J. E. Campagne, C. Cavata, J. Dolbeau, J. Dumarchez, P. Gorodetzky, S. Katsanevas, M. Mezzetto *et al.*, Memphys: A Large Scale Water Cerenkov Detector at Fréjus, arXiv:hep-ex/0607026.
[90] R. Buras, H.-T. Janka, M. T. Keil, G. G. Raffelt, and M. Rampp, Astrophys. J. **587**, 320 (2003).
[91] K. Langanke and G. Martínez-Pinedo, Atom. Data Nucl. Data **79**, 1 (2001).
[92] M. D. Kistler, H. Yuksel, S. Ando, J. F. Beacom, and Y. Suzuki, arXiv:0810.1959.
[93] J. F. Beacom, W. M. Farr, and P. Vogel, Phys. Rev. D **66**, 033001 (2002).

Eur. Phys. J. C 52, 425–434 (2007)
DOI 10.1140/epjc/s10052-007-0378-4

THE EUROPEAN PHYSICAL JOURNAL C

Regular Article – Theoretical Physics

Plasmaneutrino spectrum

A. Odrzywołek[a]

M. Smoluchowski Institute of Physics, Jagiellonian University, Reymonta 4, 30-059 Krakow, Poland

Received: 10 April 2007 /
Published online: 11 August 2007 –

Abstract. The spectrum of the neutrinos produced in the massive photon and longitudinal plasmon decay process has been computed with four levels of approximation for the dispersion relations. Some analytical formulae in the limit cases are derived. Interesting conclusions related to previous calculations of the energy loss in stars are presented. The high energy tail of the neutrino spectrum is shown to be proportional to $\exp(-E/kT)$, where E is the neutrino energy and kT is the temperature of the plasma.

PACS. 97.90.+j; 97.60.-s; 95.55.Vj; 52.27.Ep

1 Introduction and motivation

Thermal neutrino losses from a plasma are very important for stellar astrophysics [1, 2]. Plasmon decay is one of the three main reactions. Extensive calculations for these processes were done by the group of Itoh [3–11]. Other influential articles include [12–20]. Meanwhile, our abilities to detect neutrinos has grown by many orders of magnitude, beginning with the 1.4 tonne experiment of Reines and Cowan [21] up to the biggest one existing now, the 50 kt super-Kamiokande detector [22]. Recently, the "GADZOOKS!" upgrade to Super-Kamiokande proposed by Beacom and Vagins [23] has attracted attention of both experimental and theoretical physicists. At least one new source of astrophysical antineutrinos is guaranteed with this upgrade, namely a diffuse supernova neutrino background [24–26]. Pre-supernova stars will be available to observations out to ~ 2 kps [26]. This technique is the only one extensible to the megaton scale [26]. Memphys, the Hyper-Kamiokande and UNO (for Mt-scale water Cherenkov detectors cf. e.g. [27]) proposals now seriously consider to add $GdCl_3$ to the one of the tanks with typically the three-tank design [28]. Recently, the discussion of geoneutrino detection [29] increased attention to deep underwater neutrino observatories [30] with a target mass of 5–10 Mt [26] and even larger [31]. It seems that (anti-) neutrino astronomy is on our doorstep, but numerous astrophysical sources of the ν still are not analyzed from the detection point of view.

Detection of the solar [32–40] and supernova [41–49] neutrinos was accompanied and followed by an extensive set of detailed calculations (see e.g. [50–57] and references therein as representatives of this broad subject) of the neutrino spectrum. On the contrary, very little is known about spectral neutrino emission from other astrophysical objects. Usually, some analytical representation of the spectrum is used, based on earlier experience and numerical simulations; cf. e.g. [58]. While this approach is justified for supernovae, where neutrinos are trapped, other astrophysical objects are transparent to neutrinos, and the spectrum can be computed with arbitrary precision. Our goal is to compute neutrino spectra as exact as possible and fill this gap. The plasmaneutrino process dominates dense, degenerate objects like red giant cores [59], cooling white dwarfs [60], including Ia supernova progenitors before the so-called "smoldering" phase [61]. Plasmaneutrino is important secondary cooling processes in neutron star crusts [62] and massive stars [63]. Unfortunately, thermal neutrino losses usually are calculated using methods completely erasing almost any information related to the neutrino energy $\mathcal{E}_\nu$ and the directionality as well. This information is not required to compute the total energy Q radiated as neutrinos per unit volume and time. From the experimental point of view, however, it is extremely important if a given amount of energy is radiated as e.g. numerous keV neutrinos or one 10 MeV neutrino. In the first case we are unable to detect (using available techniques) any transient neutrino source regardless of the total luminosity and proximity of the object. In the second case we can detect astrophysical neutrino sources if they are strong and not too far away using an advanced detector that is big enough.

A few of the research articles in this area attempt to estimate the average neutrino energy [16, 17, 65, 66], additionally computing the reaction rate R. Strangely, the authors of these references presented figures and formulae for Q/R instead of $\frac{1}{2}Q/R$. This gives a false picture of the real situation, as the former expression gives $\langle \mathcal{E}_\nu + \mathcal{E}_{\bar{\nu}} \rangle$. Obviously, we detect *neutrinos*, not ν–$\bar{\nu}$ pairs. Values of $\frac{1}{2}Q/R$ *do not* give the average neutrino energy, as in gen-

[a] e-mail: odrzywolek@th.if.uj.edu.pl

eral the neutrino and antineutrino spectra are different. As we will see, *only* for longitudinal plasmon decay neutrinos the energies of neutrinos and antineutrinos are equal. However, the difference in all situations where thermal neutrino losses are important is numerically small and the formula

$$\langle \mathcal{E}_\nu \rangle \simeq \frac{1}{2}\frac{Q}{R} \tag{1}$$

is still a "working" estimate.

The mean neutrino energy is useful for the purpose of a qualitative discussion of the detection prospects/methods. A quantitative discussion requires knowledge of the spectrum shape (the differential emissivity $\mathrm{d}R/\mathrm{d}\mathcal{E}_\nu$). The high energy tail is particularly important from the point of view of experimental detection. Detection of the lowest energy neutrinos is extremely challenging due to numerous background signal noise sources e.g. ^{14}C decay for $\mathcal{E}_\nu < 200\,\mathrm{keV}$ [64]. Relevant calculations for the spectrum of the medium energy neutrinos with $\langle \mathcal{E}_\nu \rangle \sim 1\,\mathrm{MeV}$ emitted from thermal processes have become available recently [65–67]. The purpose of this article is to develop accurate methods and discuss various theoretical and practical (important for detection) aspects of the spectra of neutrinos from astrophysical plasma processes. This could help experimental physicists to discuss a possible realistic approach to detect astrophysical sources of neutrinos in the future.

2 Plasmaneutrino spectrum

2.1 Properties of plasmons

Emissivity and the spectrum shape from plasmon decay is strongly affected by the dispersion relation for transverse plasmons (massive in-medium photons) and longitudinal plasmons. In contrast to transverse plasmons, with the vacuum dispersion relation $\omega(k) = k$, longitudinal plasmons exist only in the plasma. The dispersion relation by definition is a function $\omega(k)$, where $\hbar\omega$ is the energy of the (quasi-) particle and $\hbar k$ is the momentum. The issues related to particular handling of these functions are discussed clearly in the article of Braaten–Segel [15]. We will repeat here the most important features of the plasmons.

For both types, the plasmon energy for momentum $k = 0$ is equal to ω_0. The value $\omega_0 \equiv \omega(0)$ is referred to as the *plasma frequency* and can be computed from

$$\omega_0^2 = \frac{4\alpha}{\pi}\int_0^\infty \frac{p^2}{E}\left(1 - \frac{v^2}{3}\right)(f_1 + f_2)\,\mathrm{d}p\,, \tag{2}$$

where $v = p/E$ and $E = \sqrt{p^2 + m_e^2}$ ($\hbar = c = 1$ units are used), $m_e \simeq 0.511\,\mathrm{MeV}$, and the fine structure constant is $\alpha = 1/137.036$ [68]. The functions f_1 and f_2 are the Fermi–Dirac distributions for electrons and positrons, respectively:

$$f_1 = \frac{1}{\mathrm{e}^{(E-\mu)/kT} + 1}\,, \quad f_2 = \frac{1}{\mathrm{e}^{(E+\mu)/kT} + 1}\,. \tag{3}$$

The quantity μ is the chemical potential of the electron (including the rest mass). Other important parameters include the first relativistic correction ω_1,

$$\omega_1^2 = \frac{4\alpha}{\pi}\int_0^\infty \frac{p^2}{E}\left(\frac{5}{3}v^2 - v^4\right)(f_1 + f_2)\,\mathrm{d}p\,, \tag{4}$$

the maximum longitudinal plasmon momentum (energy) $k_{\max}$,

$$k_{\max}^2 \equiv \omega_{\max}^2 = \frac{4\alpha}{\pi}\int_0^\infty \frac{p^2}{E}\left(\frac{1}{v}\ln\frac{1-v}{1+v} - 1\right)(f_1 + f_2)\,\mathrm{d}p\,, \tag{5}$$

and the asymptotic transverse plasmon mass m_t,

$$m_\mathrm{t}^2 = \frac{4\alpha}{\pi}\int_0^\infty \frac{p^2}{E}(f_1 + f_2)\,\mathrm{d}p\,. \tag{6}$$

The quantity m_t is often referred to as the thermal photon mass. We also define the parameter v_*:

$$v_* = \frac{\omega_1}{\omega_0} \tag{7}$$

interpreted as the typical velocity of the electrons in the plasma [15]. The axial polarization coefficient is

$$\omega_\mathrm{A} = \frac{2\alpha}{\pi}\int_0^\infty \frac{p^2}{E^2}\left(1 - \frac{2}{3}v^2\right)(f_1 - f_2)\,\mathrm{d}p\,. \tag{8}$$

The value of ω_A is a measure of the difference between the neutrino and antineutrino spectra. The set of numerical values used to display this sample result is presented in Table 1.

The values of $\omega_0, \omega_{\max}, m_\mathrm{t}$ define a sub-area of the ω–k plane, where the dispersion relations for the photons $\omega_\mathrm{t}(k)$ and the longitudinal plasmons $\omega_\mathrm{l}(k)$ are found:

$$\max(k, \omega_0) \le \omega_\mathrm{l}(k) \le \omega_{\max}, \quad 0 \le k \le k_{\max}\,, \tag{9a}$$

$$\sqrt{k^2 + \omega_0^2} \le \omega_\mathrm{t}(k) \le \sqrt{k^2 + m_\mathrm{t}^2}, \qquad 0 \le k \le \infty\,. \tag{9b}$$

The dispersion relations are solutions to the equations [15]

$$k^2 = \Pi_\mathrm{l}\left(\omega_\mathrm{l}(k), k\right) \tag{10a}$$

$$k^2 = \omega_\mathrm{t}(k)^2 - \Pi_\mathrm{t}\left(\omega_\mathrm{t}(k), k\right)\,, \tag{10b}$$

Table 1. Plasma properties for a typical massive star during Si burning. All values are in MeV

kT	μ	ω_0	ω_1	m_t	$\omega_{\max}$	ω_A
0.32	1.33	0.074	0.070	0.086	0.133	0.002

where the longitudinal and transverse polarization functions are given as integrals:

$$\Pi_{\rm l} = \frac{4\alpha}{\pi}\int\limits_0^\infty \frac{p^2}{E}\left(\frac{\omega_{\rm l}}{vk}\ln\frac{\omega_{\rm l}+vk}{\omega_{\rm l}-vk} - 1 - \frac{\omega_{\rm l}^2-k^2}{\omega_{\rm l}^2-v^2k^2}\right) \times (f_1+f_2)\,{\rm d}p\,, \tag{11a}$$

$$\Pi_{\rm t} = \frac{4\alpha}{\pi}\int\limits_0^\infty \frac{p^2}{E}\left(\frac{\omega_{\rm t}^2}{k^2} - \frac{\omega_{\rm t}^2-k^2}{k^2}\frac{\omega_{\rm t}}{2vk}\ln\frac{\omega_{\rm t}+vk}{\omega_{\rm t}-vk}\right) \times (f_1+f_2)\,{\rm d}p\,. \tag{11b}$$

A typical example of the exact plasmon dispersion relations is presented in Fig. 1 (see the dash-dotted curve). As solving (10a) and (10b) with (11) is computationally intensive, three levels of approximation for the dispersion relations are widely used:

1. zero-order analytical approximations;
2. first-order relativistic corrections;
3. the Braaten–Segel approximation.

2.1.1 Approximations for longitudinal plasmons

For longitudinal plasmons, the simplest zero-order approach used in the early calculations of Adams et al. [13] and more recently in [66] for the photoneutrino process is to put simply

$$\omega(k) = \omega_0\,, \tag{12}$$

where ω_0 is the plasma frequency (2). The maximum plasmon energy is $\omega_{\rm max} = \omega_0$ in this approximation. The zero-order approximation is valid only for the non-relativistic regime and leads to large errors of the total emissivity [12].

The first relativistic correction to (12) has been introduced by Beaudet et al. [12]. The dispersion relation $\omega_{\rm l}(k)$ is given in an implicit form:

$$\omega_{\rm l}^2 = \omega_0^2 + \frac{3}{5}\omega_{\rm l}^2\frac{k^2}{\omega_{\rm l}^2}\,, \tag{13}$$

with the maximum plasmon energy equal to

$$\omega_{\rm max}^{(1)} = \sqrt{\omega_0^2 + \frac{3}{5}\omega_1^2}\,. \tag{14}$$

This approximation, however, does not introduce a really serious improvement (see Figs. 1, 2 (left) and 4). A breaking point was the publication of the Braaten–Segel approximation [15]. Using the simple analytical equation

$$k^2 = 3\frac{\omega_0^2}{v_*^2}\left(\frac{\omega_{\rm l}}{2v_*k}\ln\frac{\omega_{\rm l}+v_*k}{\omega_{\rm l}-v_*k} - 1\right)\,, \tag{15}$$

where v_* is defined in (7), one is able to get an almost exact dispersion relation; cf. Figs. 1 and 2, left panels. The solution to (15) exists in the range $1 < k < k_{\rm max}^{\rm BS}$, where, in this approximation, the maximum longitudinal plasmon momentum is

$$\left(\omega_{\rm max}^{\rm BS}\right)^2 = \frac{3\omega_0^2}{2v_*^2}\left(\frac{1}{2v_*}\ln\frac{1+v_*}{1-v_*} - 1\right)\,, \tag{16}$$

which gives a value slightly different from the exact value (Fig. 2, left), but it is required for consistency of the approximation.

2.1.2 Approximations for transverse plasmons

For photons in vacuum the dispersion relation is $\omega_{\rm t} = k$. The zero-order approximation for in-medium photons is

$$\omega_{\rm t}^2 = \omega_0^2 + k^2, \quad k \ll \omega_0\,, \tag{17a}$$

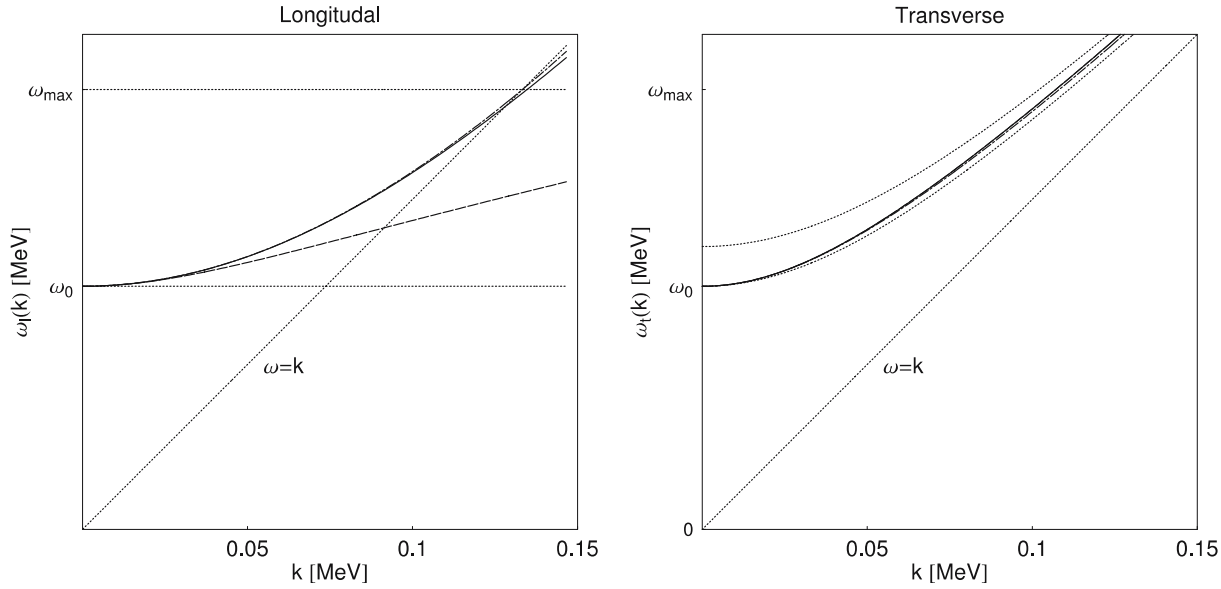

Fig. 1. Longitudinal and transverse plasmon dispersion relation $\omega_{\rm l,t}(k)$ for the plasma parameters from Table 1. The exact result (*dot-dashed*) is very close to the Braaten–Segel approximation (*solid*). Zero-order (*dotted*) and first-order (*dashed*) approximations are very poor, especially for the londitudinal mode (*left*)

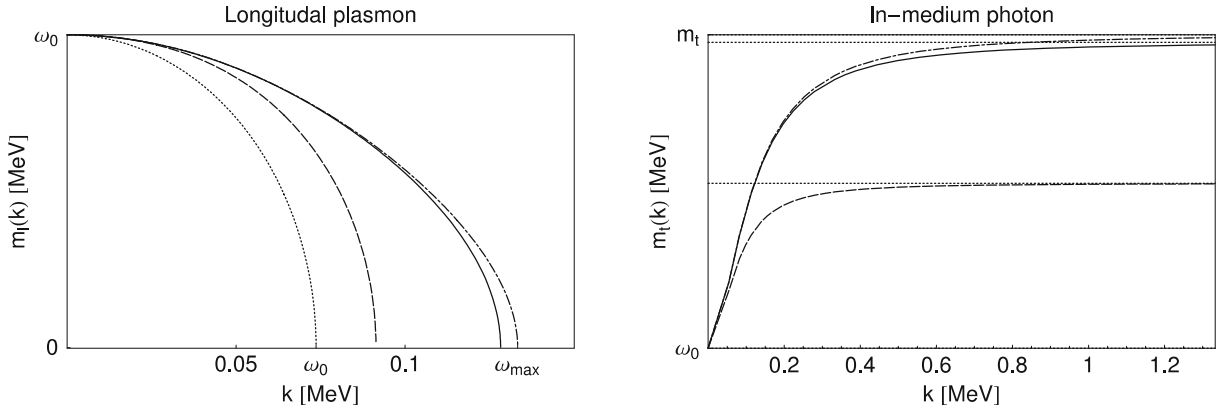

Fig. 2. Longitudinal and transverse plasmon mass. *Dotted lines* on the *right panel* show the asymptotic transverse mass. *Line dashing* is the same as in Fig. 1

valid for small k, and

$$\omega_{\mathrm{t}}^2 = m_{\mathrm{t}}^2 + k^2, \quad k \gg \omega_0\,, \tag{17b}$$

valid for very large k. Formulae (17a) and (17b) provide lower and upper limits for a realistic $\omega_{\mathrm{t}}(k)$, respectively (cf. Fig. 1, right panel, dotted curve). First-order relativistic corrections lead to the formula

$$\omega_{\mathrm{t}}^2 = \omega_0^2 + k^2 + \frac{1}{5}\omega_1^2\frac{k^2}{\omega_{\mathrm{t}}^2}\,, \tag{18}$$

with the asymptotic photon mass

$$m_{\mathrm{t}}^{(1)} = \sqrt{\omega_0^2 + \omega_1^2/5}\,. \tag{19}$$

Finally, the Braaten–Segel approximation leads to

$$\omega_{\mathrm{t}}^2 = k^2 + \omega_0^2\frac{3\omega_{\mathrm{t}}^2}{2v_*^2k^2}\left(1 - \frac{\omega_{\mathrm{t}}^2 - v_*^2k^2}{2\omega_{\mathrm{t}}v_*k}\ln\frac{\omega_{\mathrm{t}} + v_*k}{\omega_{\mathrm{t}} - v_*k}\right). \tag{20}$$

The asymptotic photon mass $m_{\mathrm{t}}^{\mathrm{BS}}$ derived from (20) is

$$\left(m_{\mathrm{t}}^{\mathrm{BS}}\right)^2 = \frac{3\omega_0^2}{2v_*^2}\left(1 - \frac{1-v_*^2}{2v_*}\ln\frac{1+v_*}{1-v_*}\right). \tag{21}$$

This is slightly smaller (left panel of Fig. 2, dashed curve) than the exact value (solid line).

All four relations are presented in Fig. 1. Differences are clearly visible, but they are much less pronounced for transverse than for longitudinal plasmons. Inspection of Fig. 2 reveals, however, that in the large momentum regime the asymptotic behavior is correct only for the exact integral relations (10b) and may be easily reproduced using (17b) with m_{t} from (6).

Let us recapitulate the main conclusions. The Braaten–Segel approximation provides a reasonable approximation, as the nonlinear equations (15) and (20) are easily solved using e.g. the bisection method. The zero- and first-order approximations (12), (17a) and (17b) with the limit values (9) provide the starting points and ranges. The approximation has been tested by [69] and is considered as the best one available [20]. Errors for the part of the kT–μ plane where the plasmaneutrino process *is not dominant* may be as large as 5% [69]. At present, these inaccuracies are irrelevant for any practical application, and the Braaten–Segel approximation is recommended for all purposes.

2.2 Plasmon decay rate

In the standard model of the electroweak interactions, massive in-medium photons and longitudinal plasmons may decay into neutrino–antineutrino pairs:

$$\gamma^* \to \nu_x + \bar{\nu}_x. \tag{22}$$

In the first-order calculations two Feynman diagrams (see Fig. 3) contribute to the decay rate [15, 65].

For the decay of the longitudinal plasmon the squared matrix element is

$$M_{\mathrm{l}}^2 = \frac{G_{\mathrm{F}}^2C_{\mathrm{V}}^2}{\pi\alpha}\left(\omega_{\mathrm{l}}^2 - k^2\right)^2\left[\frac{2K\cdot Q_1 K\cdot Q_2}{K^2} + \frac{2\mathbf{k}\cdot\mathbf{q}_1\mathbf{k}\cdot\mathbf{q}_2}{k^2} - Q_1\cdot Q_2\right], \tag{23a}$$

where $K = (\omega, \mathbf{k})$ is the four-momentum of the plasmon. $Q_1 = (\mathcal{E}_1, \mathbf{q}_1)$ and $Q_2 = (\mathcal{E}_2, \mathbf{q}_2)$ are the four-momentum of the neutrino and antineutrino, respectively.

The squared matrix element for decay of the massive photon is

$$M_{\mathrm{t}}^2 = \frac{G_{\mathrm{F}}^2}{\pi\alpha}\left[\left(C_{\mathrm{V}}^2\Pi_{\mathrm{t}}^2 + C_{\mathrm{A}}^2\Pi_{\mathrm{A}}^2\right)\left(\mathcal{E}_1\mathcal{E}_2 - \frac{\mathbf{k}\cdot\mathbf{q}_1\mathbf{k}\cdot\mathbf{q}_2}{k^2}\right) + 2C_{\mathrm{V}}C_{\mathrm{A}}\Pi_{\mathrm{t}}\Pi_{\mathrm{A}}\frac{\mathcal{E}_1\mathbf{k}\cdot\mathbf{q}_2 - \mathcal{E}_2\mathbf{k}\cdot\mathbf{q}_1}{k}\right], \tag{23b}$$

where Π_{t} is defined in (11b) and the axial polarization function Π_{A} reads

$$\Pi_{\mathrm{A}} = \frac{2\alpha}{\pi}\frac{\omega_{\mathrm{t}}^2 - k^2}{k}\int_0^\infty \frac{p^2}{E^2}\left(\frac{\omega_{\mathrm{t}}}{2vk}\ln\frac{\omega_{\mathrm{t}} + vk}{\omega_{\mathrm{t}} - vk} - \frac{\omega_{\mathrm{t}}^2 - k^2}{\omega_{\mathrm{t}}^2 - v^2k^2}\right) \times (f_1 - f_2)\,\mathrm{d}p\,. \tag{24}$$

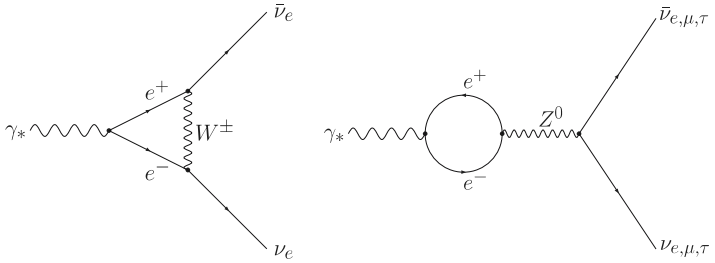

Fig. 3. Feynman diagrams for plasmon decay

The Fermi constant is $G_\mathrm{F}/(\hbar c)^3 = 1.16637(1)\ 10^{-5}\,\mathrm{GeV}^{-2}$ [68] and, in the standard model of the electroweak interactions, the vector and axial coupling constants are

$$C_\mathrm{V}^e = \frac{1}{2} + 2\sin^2\theta_\mathrm{W}\,, \quad C_\mathrm{A}^e = \frac{1}{2} \tag{25}$$

$$C_\mathrm{V}^{\mu,\tau} = -\frac{1}{2} + 2\sin^2\theta_\mathrm{W}\,, \quad C_\mathrm{A}^{\mu,\tau} = -\frac{1}{2} \tag{26}$$

for electron and μ,τ neutrinos, respectively. The Weinberg angle is $\sin^2\theta_\mathrm{W} = 0.23122(15)$ [68].

Terms containing C_A (the so-called axial contribution) in (23b) are frequently treated separately [65] or removed at all [3]. In calculations concentrated on the total emissivity this is justified as antisymmetric terms multiplied by $C_\mathrm{V}C_\mathrm{A}$ do not contribute at all and terms $C_\mathrm{A}^2 \times \ldots$ are suppressed relative to the term beginning with $C_\mathrm{V}^2 \times \ldots$ by four orders of magnitude [3]. However, if one attempts to compute the neutrino energy spectrum all three terms should be added, as the mixed V–A "channel" alone leads to a negative emission probability for some neutrino energy range (Fig. 6), which is physically unacceptable. These terms remain numerically small but *only* for electron neutrinos. For μ and τ neutrino spectra the *axial* part contributes at $\sim 1\%$ level due to the very small value $C_\mathrm{V}^{\mu,\tau} = -0.0376$, while still $C_\mathrm{A} = -0.5$. The 'mixed' term leads to significant differences between the $\nu_{\mu,\tau}$ and $\bar{\nu}_{\mu,\tau}$ spectra; cf. Fig. 6. Relative contributions of the three transverse "channels" for electron and μ,τ are presented in Table 2.

In general, all the terms in the squared matrix element (23b) should be added. We have only *two* different spectra: the longitudinal and the transverse one.

The particle production rate from plasma in thermal equilibrium is

$$R_i = \frac{g_i}{(2\pi)^5} \times \int Z_i f_{\gamma^*} \delta^4(K - Q_1 - Q_2) M_i^2 \frac{\mathrm{d}^3\mathbf{k}}{2\omega_i} \frac{\mathrm{d}^3\mathbf{q}_1}{2\mathcal{E}_1} \frac{\mathrm{d}^3\mathbf{q}_2}{2\mathcal{E}_2}\,, \tag{27}$$

where $i = \mathrm{l}$ for the longitudinal mode and $i = \mathrm{t}$ for the transverse mode. The Bose–Einstein distribution for plasmons f_{γ^*} is

$$f_{\gamma^*} = \frac{1}{\mathrm{e}^{\omega_{\mathrm{t,l}}/kT} - 1}\,, \tag{28}$$

Table 2. Relative weight of the M_t^2, see (23b), terms for e and μ,τ neutrinos

Flavor	Vector $\frac{C_\mathrm{V}^2\omega_0^4}{(C_V\omega_0^2+C_\mathrm{A}\omega_\mathrm{A})^2}$	Axial $\frac{C_\mathrm{A}^2\omega_\mathrm{A}^2}{(C_V\omega_0^2+C_\mathrm{A}\omega_\mathrm{A})^2}$	Mixed $\frac{2C_VC_\mathrm{A}\omega_0^2\omega_\mathrm{A}}{(C_V\omega_0^2+C_\mathrm{A}\omega_\mathrm{A})^2}$
electron	0.74	0.02	0.24
mu/tau	0.07	0.39	0.54

and the residue factors $Z_{\mathrm{t,l}}$ are expressed by the polarization functions $\Pi_{\mathrm{t,l}}$ of (11b) and (11a):

$$Z_\mathrm{t}^{-1} = 1 - \frac{\partial\Pi_\mathrm{t}}{\partial\omega^2} \tag{29}$$

$$Z_\mathrm{l}^{-1} = -\frac{\omega_\mathrm{l}^2}{k^2}\frac{\partial\Pi_\mathrm{l}}{\omega^2}. \tag{30}$$

For massive photons $g_\mathrm{t} = 2$ and for the longitudinal plasmon $g_\mathrm{l} = 1$.

The differential rates[1] were derived for the first time in [65]. Here, we present the result in the form valid for both types of plasmons, ready for calculations using any available form of dispersion relation:

$$\frac{\mathrm{d}^2R_i}{\mathrm{d}\mathcal{E}_1\,\mathrm{d}\mathcal{E}_2} = \frac{g_i}{\pi^4} Z_i M_i^2 f_{\gamma^*} J_i \mathcal{S}\,, \tag{31}$$

where $i = \mathrm{l}$ or $i = \mathrm{t}$. The product $\mathcal{S}$ of the unit step functions Θ in (31) restrict the result to the kinematically allowed area:

$$\mathcal{S} = \Theta(4\mathcal{E}_1\mathcal{E}_2 - m_i^2)\Theta(\mathcal{E}_1 + \mathcal{E}_2 - \omega_0)\Theta(\omega_\mathrm{max} - \mathcal{E}_1 - \mathcal{E}_2)\,. \tag{32}$$

The four-momenta in the squared matrix element are

$$\begin{aligned}
Q_1 &= (\mathcal{E}_1, 0, 0, \mathcal{E}_1)\,,\\
Q_1 &= (\mathcal{E}_2, \mathcal{E}_2\sin\theta, 0, \mathcal{E}_2\cos\theta)\,,\\
K &= (\mathcal{E}_1 + \mathcal{E}_2, \mathcal{E}_2\sin\theta, 0, \mathcal{E}_1 + \mathcal{E}_2\cos\theta)\,,\\
m_i^2 &= KK = (\mathcal{E}_1 + \mathcal{E}_2)^2 - k'^2\,,\\
\cos\theta &= \frac{k'^2 - \mathcal{E}_1^2 - \mathcal{E}_2^2}{2\mathcal{E}_1\mathcal{E}_2}\,,\\
k' &= \omega_{\mathrm{l,t}}^{-1}(\mathcal{E}_1 + \mathcal{E}_2)\,,\\
\omega_i &= \mathcal{E}_1 + \mathcal{E}_2\,,
\end{aligned}$$

where ω_i^{-1} denotes the function *inverse* to the dispersion relation. The Jacobian J_i arising from the Dirac delta integration in (27) is

$$J_i^{-1} = \frac{\mathcal{E}_1\mathcal{E}_2}{k'}\left.\frac{\partial\omega_i}{\partial k}\right|_{k=k'}. \tag{33}$$

[1] The double differential rate $\mathrm{d}^2R_i/\,\mathrm{d}\mathcal{E}\,\mathrm{d}\cos\theta$ has an identical form as (31), but now four-momenta cannot be given explicitly, unless a simple analytical approximation for $\omega_i(k)$ is used. Analytical approximations for the spectrum shape are derived this way.

The residue factors Z_i are given in (30) and (29). The maximum energy $\omega_{\max}$ in (32) for longitudinal plasmons must be in agreement with the particular approximation used for $\omega_{\mathrm{l}}(k)$: ω_0, (14) or (16) for the zero-order equation (12), and first-order, (13) or the Braaten–Segel equation (15), respectively. For transverse plasmons $\omega_{\max} \to \infty$, and the last Θ function in (32) has no effect and may be omitted.

2.3 Longitudinal neutrino spectrum

2.3.1 Analytical approximation

We begin with a general remark on the spectrum. Note that (31) is symmetric for a longitudinal mode under the change $\mathcal{E}_{1,2} \to \mathcal{E}_{2,1}$, because (23a) is symmetric with respect to the exchange $Q_{1,2} \to Q_{2,1}$. The resulting energy spectrum is thus identical for neutrinos and antineutrinos. This is not true for transverse plasmons with the axial contribution included; cf. Sect. 2.4.

Using the zero-order dispersion relation for longitudinal plasmons, (12), we are able to express the spectrum by elementary functions. The longitudinal residue factor Z_{t} is now

$$Z_{\mathrm{l}}^0 = 1\,, \tag{34}$$

and the Jacobian J_{l} resulting from the integration of the Dirac delta function is

$$J_{\mathrm{l}}^0 = 1\,. \tag{35}$$

Now, the differential rate $\mathrm{d}^2R/\,\mathrm{d}\mathcal{E}\,\mathrm{d}\cos\theta$ (cf. (31) and footnote 1) becomes much simpler, and the integral over $\mathrm{d}\cos\theta$ can be evaluated analytically. Finally, we get the longitudinal spectrum,

$$\frac{\mathrm{d}R}{\mathrm{d}\mathcal{E}} \equiv \lambda(\mathcal{E}) = \frac{{G_{\mathrm{F}}}^2 {C_{\mathrm{V}}}^2 {\omega_0}^7}{1260\pi^4\alpha\hbar^3c^9} \frac{f(\mathcal{E}/\omega_0)}{\mathrm{e}^{\omega_0/kT}-1}\,, \tag{36}$$

where the normalized spectrum is

$$f(x) = \frac{105}{32}\left[4x(x-1)(8x^4-16x^3+2x^2+6x-3) + 3(1-2x)^2\ln(1-2x)^2\right]. \tag{37}$$

Let us note that f is undefined at $x = 1/2$; we use the limit

$$\lim_{x\to 1/2} f(x) = 105/32$$

instead. The function $f(x)$ is symmetric with respect to the point $x = 1/2$, where f has a maximum value (see Fig. 4, dotted line).

In this limit, correct for a non-relativistic, non-degenerate plasma, the average neutrino and antineutrino energy is $\langle\mathcal{E}\rangle = \omega_0/2$, and the maximum ν energy is ω_0.

Inspection of Fig. 4 reveals little difference between the analytical result (36) and the result obtained with first-order relativistic corrections to the dispersion relation (13).

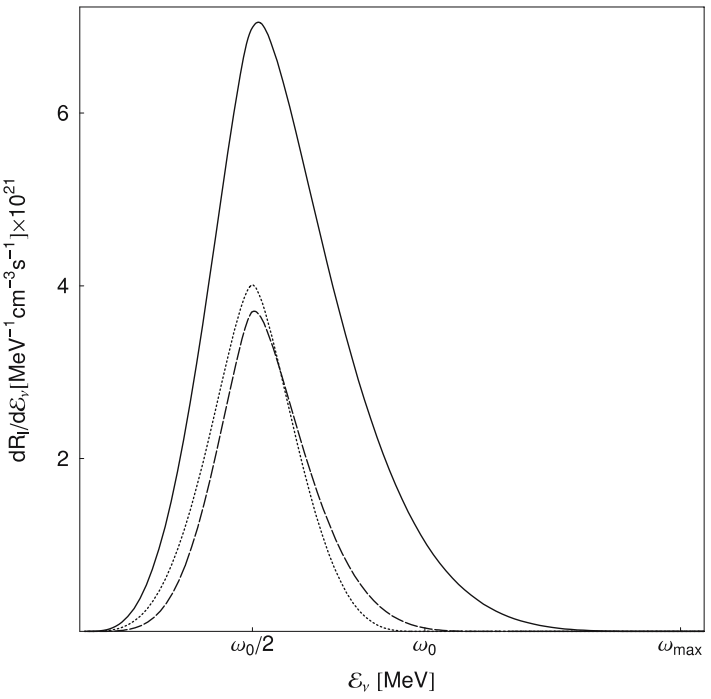

Fig. 4. Approximate longitudinal plasmon analytical neutrino spectrum, see (36), (*dotted*), with first-order correction used by BPS [12] (*dashed*), and spectrum computed using the dispersion relation [15] (*solid*). Plasma properties are according to Table 1

2.3.2 Numerical results

The simple formula (36) significantly underestimates the flux and the maximum neutrino energy, equal to $\omega_{\max}$ rather than ω_0. Therefore, we have used the Braaten–Segel approximation for the longitudinal plasmon dispersion relation.

To derive the spectrum we will use the form of the differential rate (31) provided by [65]. In the Braaten–Segel approximation we have

$$Z_{\mathrm{l}}^{\mathrm{BS}} = \frac{\omega_{\mathrm{l}}^2}{\omega_{\mathrm{l}}^2-k^2}\frac{2(\omega_{\mathrm{l}}^2-v_*^2k^2)}{3\omega_0^2-\omega_{\mathrm{l}}^2+v_*^2k^2}\,,$$
$$J_{\mathrm{l}}^{\mathrm{BS}} = \left|\frac{k^2}{\mathcal{E}_1\mathcal{E}_2}\frac{1-\beta_{\mathrm{l}}}{\omega_{\mathrm{l}}\beta_{\mathrm{l}}}\right|,$$
$$\beta_{\mathrm{l}}^{\mathrm{BS}} = \frac{3\omega_0^2}{2v_*^3}\left(\frac{3\omega_{\mathrm{l}}}{2k^3}\ln\frac{\omega_{\mathrm{l}}+v_*k}{\omega_{\mathrm{l}}-v_*k} - \frac{\omega_{\mathrm{l}}^2v_*}{k^2(\omega_{\mathrm{l}}^2-v_*^2k^2)} - \frac{2v_*}{k^2}\right).$$

The spectrum is computed as an integral of (31) over $\mathrm{d}\mathcal{E}_2$. An example is presented in Fig. 4. Integration of the function in Fig. 4 over the neutrino energy gives a result well in agreement with both (30) from [15] and (54) from [65].

2.4 Transverse plasmon decay spectrum

2.4.1 Analytical approximation

The derivation of the massive in-medium photon decay spectrum closely follows the previous subsection. Semi-analytical formula can be derived for the dispersion rela-

tions (17). For the dispersion relation (17b) the transverse residue factor $Z_{\rm t}$ is

$$Z_{\rm t}^0 = 1\,, \tag{38}$$

the polarization function $\Pi_{\rm t}$ is equal to

$$\Pi_{\rm t}^0 = m_{\rm t}^2\,, \tag{39}$$

and the Jacobian resulting from integration of the Dirac delta function $J_{\rm t}$ is

$$J_{\rm t}^0 = \frac{\mathcal{E}_1+\mathcal{E}_2}{\mathcal{E}_1\mathcal{E}_2}\,. \tag{40}$$

The approximate spectrum, neglecting differences between neutrinos and antineutrinos, is given by the following integral:

$$\lambda(\mathcal{E}) = \frac{G_{\rm F}^2 C_{\rm V}^2}{64\pi^4\alpha}\frac{m_{\rm t}^7}{\hbar^3 c^9}\int\limits_{-1}^{1}\frac{P(\cos\theta,\mathcal{E}/m_{\rm t})\,{\rm d}\cos\theta}{\exp\left[(\mathcal{E}+\frac{m_{\rm t}^2}{2\mathcal{E}(1-\cos\theta)})/kT\right]-1}\,, \tag{41}$$

where the rational function $P(ct,x)$ is

$$P(ct,x) = \frac{1+2(ct-1)^2(2x^2-1)x^2}{x(ct-1)^2[1-2ct(ct-1)x^2+2(ct-1)^2)x^4]}\,. \tag{42}$$

The result presented in Fig. 7 shows that the spectrum (41) obtained with the dispersion relation (17b) agrees well in both the low and high neutrino energy part with the spectrum obtained from the Braaten–Segel approximation for the dispersion relations. The dispersion relation (17a) produces a much larger error, and the spectrum *nowhere* agrees with the correct result. This fact is not a big surprise: as was pointed out by Braaten [16] the dispersion relation is crucial. Therefore, all previous results, including the seminal BPS work [12], could easily be improved just by the trivial replacement $\omega_0 \to m_{\rm t}$. Moreover, the closely related photoneutrino process also has been computed [3, 12, 14, 17] with the simplified dispersion relation (17a) with ω_0. One exception is the work of Esposito et al. [70]. It remains unclear, however, which result is better, as accurate dispersion relations have never been used within a photoneutrino process context. For a plasmaneutrino, (17b) is a much better approximation than (17a), especially if one puts $m_{\rm t}$ from the exact formula (6). The high energy tail of the spectrum also will be exact in this case.

As formula (41) agrees perfectly with the tail of the spectrum, we may use it to derive a very useful analytical expression. Leaving only leading terms of the rational function (42),

$$P(ct,x) \sim x^{-1}(1-ct)^{-2}\,,$$

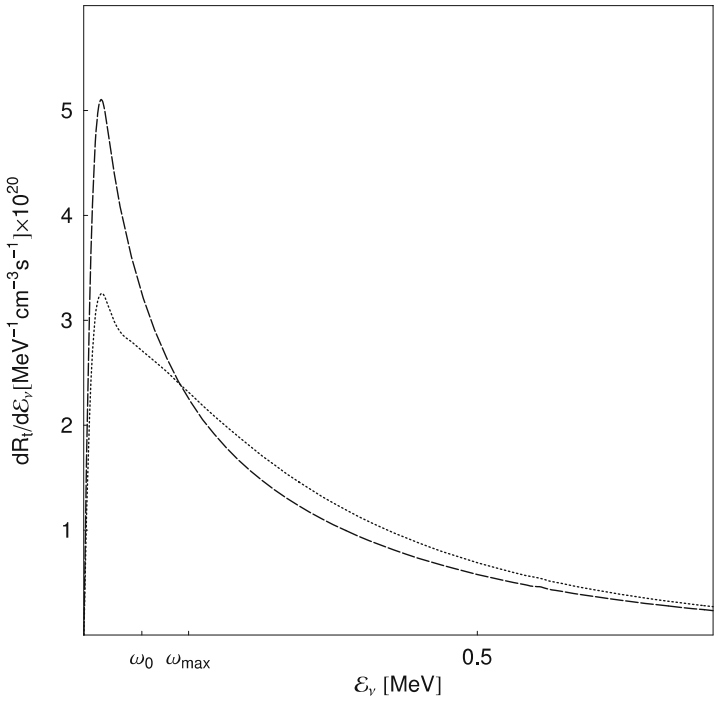

Fig. 6. Spectrum of the muon neutrinos (*dotted*) and antineutrinos (*dashed*) from transverse plasmon decay. Contributions to the spectra from the so-called mixed "vector–axial channel" produces significant differences. For electron flavor, the contribution from the "mixed channel" leads to unimportant differences. For both flavors, the contribution from the "axial channel" remains relatively small: 10^{-4} for ν_e and 10^{-2} for ν_μ. The overall contribution to the total emissivity from the μ,τ flavors is suppressed relative to electron flavor by a factor $(C_{\rm V}^{\mu,\tau}/C_{\rm V}^{e})^2 \simeq 3.3\times10^{-3}$

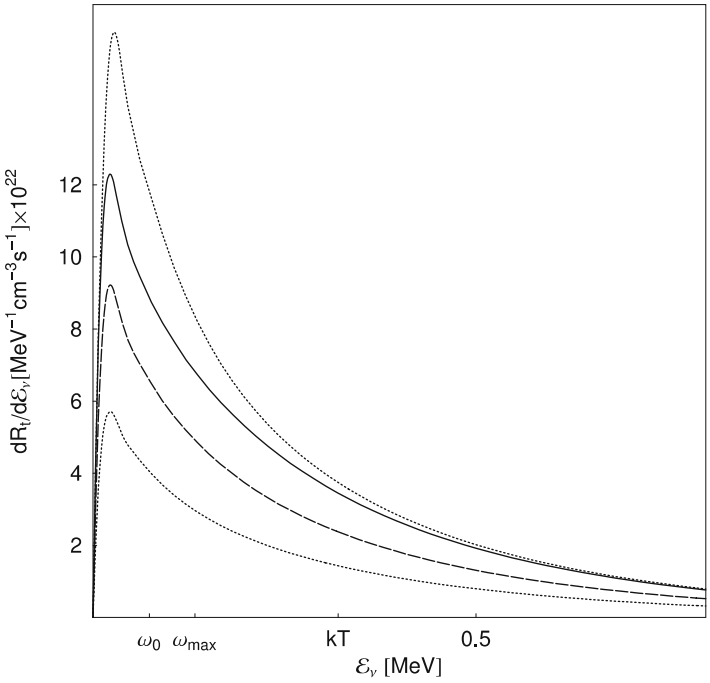

Fig. 5. Transverse plasmaneutrino spectrum computed from the approximation [15] (*solid*) with upper and lower limits, (17b) and (17a), for the dispersion relation (*dotted*). The first-order relativistic correction leads to the spectrum shown as *dashed line*. Plasma parameters are as in Fig. 3

one is able to compute the integral (41) analytically:

$$\lambda(\mathcal{E}) \simeq \frac{G_{\rm F}^2 C_{\rm V}^2}{64\pi^4\alpha}\frac{m_{\rm t}^6}{\hbar^3 c^9}\left[\kappa - \frac{2}{a}\ln\left(\mathrm{e}^{a\kappa/2}-1\right)\right], \qquad (43)$$

where $\kappa = 2x + (2x)^{-1}$, $x = \mathcal{E}/m_{\rm t}$ and $a = m_{\rm t}/kT$. Interestingly, the spectrum (43) is invariant under the transformation

$$\mathcal{E}'\mathcal{E} = m_{\rm t}^2/4\,,$$

and all results obtained for the high energy tail of the spectrum immediately may be transformed for the low energy approximation. The asymptotic behavior of (43) for $\mathcal{E} \gg kT$ is of main interest:

$$\lambda(\mathcal{E}_\nu) = AkTm_{\rm t}^6 \exp\left(-\frac{\mathcal{E}_\nu}{kT}\right), \qquad (44)$$

where for electron neutrinos

$$A = \frac{G_{\rm F}^2 C_{\rm V}^2}{8\pi^4\alpha}\frac{1}{\hbar^4 c^9} = 2.115\times 10^{30}\,\mathrm{MeV}^{-8}\mathrm{cm}^{-3}\mathrm{s}^{-1}$$

and $m_{\rm t}$ and kT are in MeV. For the μ,τ neutrinos just replace A with $A(C_{\rm V}^{\mu,\tau}/C_{\rm V}^{e})^2$.

Formula (44) gives also quite reasonable estimates of the total emissivity $Q_{\rm t}$ and the mean neutrino energies $\langle\mathcal{E}_\nu\rangle$:

$$Q_{\rm t} = AkT^3 m_{\rm t}^6 \qquad (45a)$$

$$\langle\mathcal{E}_\nu\rangle = kT\,. \qquad (45b)$$

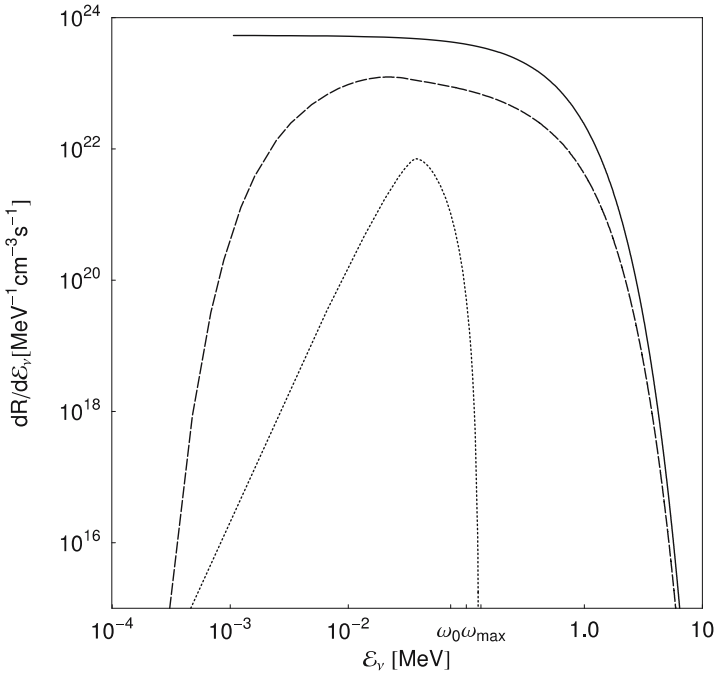

Fig. 7. Typical spectra from the plasma process. *Dotted line* is a longitudinal and *dashed* transverse spectrum. Only the $\sim\exp(-\mathcal{E}_\nu/kT)$ tail of the transverse spectrum (*solid line*) contributes to a (possibly) detectable signal. Plasma properties are according to Table 1

For comparison, we mention that Braaten–Segel [15] derived the exact formulae in the high temperature limit $kT \gg \omega_0$:

$$Q_{\rm t}^{\rm BS} = \frac{G_{\rm F}^2 C_{\rm V}^2 \zeta(3)}{12\pi^4\alpha} kT^3 m_{\rm t}^6 = 0.8AkT^3 m_{\rm t}^6\,, \qquad (46a)$$

$$\langle\mathcal{E}_\nu^{\rm BS}\rangle = \frac{6\zeta(3)}{\pi^2}kT = 0.73kT\,. \qquad (46b)$$

The formulae above agree with $\sim 25\%$ error in the leading coefficients.

2.4.2 Numerical results

The calculation of the spectrum in the framework of the Braaten–Segel approximation requires a residue factor, the polarization function [15] (transverse and axial) and the Jacobian [65]:

$$Z_{\rm t}^{\rm BS} = \frac{2\omega_{\rm t}^2\left(\omega_{\rm t}^2 - v_*^2k^2\right)}{3\omega_0^2\omega_{\rm t}^2 + \left(\omega_{\rm t}^2+k^2\right)\left(\omega_{\rm t}^2 - v_*^2k^2\right) - 2\omega_{\rm t}^2\left(\omega_{\rm t}^2-k^2\right)}\,, \qquad (47)$$

$$\Pi_{\rm t}^{\rm BS} = \frac{3\omega_0^2}{2v_*^2}\left(\frac{\omega_{\rm t}^2}{k^2} - \frac{\omega_{\rm t}^2 - v_*^2k^2}{k^2}\frac{\omega_{\rm t}}{2v_*k}\ln\frac{\omega_{\rm t}+v_*k}{\omega_{\rm t}-v_*k}\right), \qquad (48)$$

$$\Pi_{\rm A}^{\rm BS} = \omega_{\rm A}k\frac{\omega_{\rm t}^2-k^2}{\omega_{\rm t}^2 - v_*^2k^2}\frac{3\omega_0^2 - 2(\omega_{\rm t}^2-k^2)}{\omega_0^2}\,, \qquad (49)$$

$$J_{\rm t}^{\rm BS} = \frac{\mathcal{E}_1+\mathcal{E}_2}{\mathcal{E}_1\mathcal{E}_2}\left|\frac{1-\beta_{\rm t}^{\rm BS}}{1-\frac{\omega_{\rm t}^2}{k^2}\beta_{\rm t}^{\rm BS}}\right|\,, \qquad (50)$$

$$\beta_{\rm t}^{\rm BS} = \frac{9\omega_0^2}{4v_*^2k^2}\left[1+\frac{1}{6}\left(\frac{v_*k}{\omega_{\rm t}} - \frac{3\omega_{\rm t}}{v_*k}\right)\ln\frac{\omega_{\rm t}+v_*k}{\omega_{\rm t}-v_*k}\right]. \qquad (51)$$

As an example, a spectrum computed as an integral of (31) over $\mathrm{d}\mathcal{E}_2$ is shown in Fig. 5.

3 Summary

The main new results presented in the article are analytical formulae for the neutrino spectra (36) and (41) and the exact analytical formula (44) for the high energy tail of the transverse spectrum. The latter is of main interest from the point of view of detection of astrophysical sources; recently available detection techniques are unable to detect keV plasmaneutrinos emitted with typical energies $\langle\mathcal{E}_\nu\rangle \sim \omega_0/2$ (Figs. 4 and 6), where ω_0 is the plasma frequency (2). The tail behavior of the transverse spectrum quickly "decouples" from the ω_0 dominated maximum area and becomes dominated by the temperature-dependent term $\exp(-\mathcal{E}_\nu/kT)$. Calculation of the events in the detector is then straightforward, as the detector threshold in the realistic experiment will be above maximum area. This approach is much more reliable than the typical practice, where an average neutrino energy is used as a parameter in an arbitrary analytical formula.

Analytical formulae for the spectrum are shown to be a poor approximation of the realistic situation, especially for longitudinal plasmons (see Fig. 4). This is in the agreement with general remarks on the dispersion relations presented by Braaten [16]. On the contrary, the Braaten and Segel [15] approximation is shown to be a very good approach not only for the total emissivities, but also for the spectrum. An exception is the tail of the massive photon decay neutrino spectrum: the Braaten and Segel [15] formulae lead one to underestimate the thermal photon mass, while (44) gives an exact result. The numerical difference between m_{t} from (6) and (21) is however small [15]. Calculating of the emissivities by the spectrum integration seems a much longer route compared to typical methods, but we are given much more insight into details of the process. For example, we obtain exact formulae for the tail for free this way. An interesting surprise revealed in the course of our calculations is the importance of the high-momentum behavior of the massive photon. While mathematically identical to the simplest approach used in the early calculations, (17b) gives a much better approximation for the total emissivity than (17a).

Acknowledgements. This work was supported by a grant of the Polish Ministry of Education and Science (former Ministry of Scientific Research and Information Technology, now Ministry of Science and Higher Education), No. 1 P03D 005 28.

References

1. D. Arnett, Supernovae and Nucleosynthesis (Princeton University Press, Princeton, 1996)
2. G.S. Bisnovatyi-Kogan, Stellar Physics. Vol. 1: Fundamental Concepts and Stellar Equilibrium (Springer, Berlin, 2001)
3. H. Munakata, Y. Kohyama, N. Itoh, Astrophys. J. **296**, 197 (1985)
4. H. Munakata, Y. Kohyama, N. Itoh, Astrophys. J. **304**, 580 (1986)
5. Y. Kohyama, N. Itoh, H. Munakata, Astrophys. J. **310**, 815 (1986)
6. N. Itoh, T. Adachi, M. Nakagawa, Y. Kohyama, H. Munakata, Astrophys. J. **339**, 354 (1989)
7. N. Itoh, T. Adachi, M. Nakagawa, Y. Kohyama, H. Munakata, Astrophys. J. **360**, 741 (1990)
8. N. Itoh, H. Mutoh, A. Hikita, Y. Kohyama, Astrophys. J. **395**, 622 (1992)
9. Y. Kohyama, N. Itoh, A. Obama, H. Mutoh, Astrophys. J. **415**, 267 (1993)
10. Y. Kohyama, N. Itoh, A. Obama, H. Hayashi, Astrophys. J. **431**, 761 (1994)
11. N. Itoh, H. Hayashi, A. Nishikawa, Y. Kohyama, Astrophys. J. **102**, 411 (1996)
12. G. Beaudet, V. Petrosian, E.E. Salpeter, Astrophys. J. **150**, 979 (1967)
13. J.B. Adams, M.A. Ruderman, C.H. Woo, Phys. Rev. **129**, 1383 (1963)
14. D.A. Dicus, Phys. Rev. D **6**, 941 (1972)
15. E. Braaten, D. Segel, Phys. Rev. D **48**, 1478 (1993)
16. E. Braaten, Phys. Rev. Lett. **66**, 1655 (1991)
17. P.J. Schinder, D.N. Schramm, P.J. Wiita, S.H. Margolis, D.L. Tubbs, Astrophys. J. **313**, 531 (1987)
18. S.I. Blinnikov, M.A. Rudzskij, Astron. Zh. **66**, 730 (1989)
19. S.I. Blinnikov, M.A. Rudzskii, Sov. Astron. **33**, 377 (1989)
20. M. Haft, G. Raffelt, A. Weiss, Astrophys. J. **425**, 222 (1994)
21. F. Reines, C.L. Cowan, Phys. Rev. **113**, 273 (1959)
22. http://www-sk.icrr.u-tokyo.ac.jp/sk/index-e.html
23. J.F. Beacom, M.R. Vagins, Phys. Rev. Lett. **93**, 171 101 (2004)
24. J.F. Beacom, L.E. Strigari, Phys. Rev. C **73**, 035 807 (2006)
25. M. Wurm et. al., Phys. Rev. D **75**, 023 007 (2007)
26. http://sn1987a-20th.physics.uci.edu/
27. G.L. Fogli, E. Lisi, A. Mirizzi, D. Montanino, JCAP **0504**, 002 (2005)
28. http://neutrino.phys.washington.edu/nnn06/
29. J.G. Learned, S.T. Dye, S. Pakvasa, Neutrino Geophysics Conference Introduction, Earth, Moon, and Planets **99**, 1 (2006)
30. http://www.phys.hawaii.edu/ sdye/hano.html
31. J.G. Learned, White paper on Gigaton Array, www.phys.hawaii.edu/∼jgl/post/gigaton_array.pdf
32. R. Davis Jr., Phys. Rev. Lett. **12**, 303 (1964)
33. J.N. Bahcall, R. Davis Jr., Science **191**, 264 (1976)
34. GALLEX-Collaboration, P. Anselmann et al., Phys. Lett. B **357**, 237 (1995)
35. W. Hampel et al., Phys. Lett. B **388**, 384 (1996)
36. N. Bahcall, B.T. Cleveland, R. Davis et al., Phys. Rev. Lett. **40**, 1351 (1978)
37. SNO Collaboration, Q.R. Ahmad, Phys. Rev. Lett. **87**, 071 301 (2001)
38. S. Hirata et al., Phys. Rev. Lett. **65**, 1297 (1990)
39. S. Hirata et al., Phys. Rev. Lett. **66**, 9 (1991)
40. S. Hirata et al., Phys. Rev. D **44**, 2241 (1991)
41. K.S. Hirata et al., Phys. Rev. D **38**, 448 (1988)
42. K.S. Hirata et al., Phys. Rev. Lett. **58**, 1490 (1987)
43. IMB, R.M. Bionta et al., Phys. Rev. Lett. **58**, 1494 (1987)
44. P. Galeotti et al., Helv. Phys. Acta **60**, 619 (1987)
45. E.N. Alekseev, L.N. Alekseeva, V.I. Volchenko, I.V. Krivosheina, JETP Lett. **45**, 589 (1987)
46. E.N. Alekseev, L.N. Alekseeva, V.I. Volchenko, I.V. Krivosheina, Pisma. Zh. Eksp. Teor. Fiz. **45**, 461 (1987)
47. A.E. Chudakov, Y.S. Elensky, S.P. Mikheev, JETP Lett. **46**, 373 (1987)
48. A.E. Chudakov, Y.S. Elensky, S.P. Mikheev, Pisma. Zh. Eksp. Teor. Fiz. **46**, 297 (1987)
49. E.N. Alekseev, L.N. Alekseeva, I.V. Krivosheina, V.I. Volchenko, Phys. Lett. B **205**, 209 (1988)
50. J.N. Bahcall, M.H. Pinsonneault, Rev. Mod. Phys. **64**, 885 (1992)
51. J.N. Bahcall, R.N. Ulrich, Rev. Mod. Phys. **60**, 297 (1988)
52. S. Turck-Chieze, I. Lopes, Astrophys. J. **408**, 347 (1993)
53. H.-Th. Janka, K. Langanke, A. Marek, G. Martinez-Pinedo, B. Muller, Theory of core-collapse supernovae, Physics Reports, Vol. 442, Issues 1–6, The Hans Bethe Centennial Volume 1906–2006, April 2007, p. 38–74
54. A. Burrows, Nature **403**, 727 (2000)

55. J. Blondin, A. Mezzacappa, Nature **445**, 58 (2007)
56. K. Kotake, S. Yamada, K. Sato, Phys. Rev. D **68**, 044 023 (2003)
57. H.A. Bethe, Rev. Mod. Phys. **62**, 801 (1990)
58. J.A. Pons, A.W. Steiner, M. Prakash, J.M. Lattimer, Phys. Rev. Lett. **86**, 5223 (2001)
59. G. Raffelt, A. Weiss, Astron. Astrophys. **264**, 536 (1992)
60. L.G. Althaus, E. Garcia-Berro, J. Isern, A.H. Corsico, Astron. Astrophys. **441**, 689 (2005)
61. W. Hillebrandt, J.C. Niemeyer, Ann. Rev. Astron. Astrophys. **38**, 191 (2000)
62. D.G. Yakovlev, A.D. Kaminker, O.Y. Gnedin, P. Haensel, Phys. Rep. **354**, 1 (2001)
63. S.E. Woosley, A. Heger, T.A. Weaver, RMP **74**, 1015 (2002)
64. BOREXINO Collaboration, S. Schönert et al., physics/0408032 [Nucl. Instrum. Method. A (to be published)]
65. S. Ratković, S.I. Dutta, M. Prakash, Phys. Rev. D **67**, 123 002 (2003)
66. S.I. Dutta, S. Ratković, M. Prakash, Phys. Rev. D **69**, 023 005 (2004)
67. M. Misiaszek, A. Odrzywoltek, M. Kutschera, Phys. Rev. D **74**, 043 006 (2006)
68. W.M. Yao, C. Amsler, D. Asner, R. Barnett, J. Beringer, P. Burchat, C. Carone, C. Caso, O. Dahl, G. D'Ambrosio et al., J. Phys. G **33**, 1 (2006) http://pdg.lbl.gov
69. N. Itoh, A. Nishikawa, Y. Kohyama, Astrophys. J. **470**, 1015 (1996)
70. S. Esposito, G. Mangano, G. Miele, I. Picardi, O. Pisanti, Nucl. Phys. B **658**, 217 (2003)

KAON CONDENSATE WITH TRAPPED NEUTRINOS AND HIGH-DENSITY SYMMETRY ENERGY BEHAVIOR

Andrzej Odrzywolek[a], Marek Kutschera[a,b]

[a]M. Smoluchowski Institute of Physics, Jagellonian University
Reymonta 4, 30-059 Kraków, Poland

[b]H. Niewodniczanski Institute of Nuclear Physics, Polish Academy of Sciences
152 Radzikowskiego, 31-342 Kraków, Poland

(Received May 24, 2008; revised version received November 3, 2008)

Effects of the neutrino trapping and symmetry energy behavior are investigated in the framework of the chiral Kaplan–Nelson model with kaon condensation. Decrease in the condensation threshold during deleptonization if found to be generic regardless uncertainties in the nucleon–kaon interactions and symmetry energy. Quantitatively however, differences are shown to be important.

PACS numbers: 97.60.Jd, 26.60.+c, 97.60.–s

1. Introduction

Neutron stars are born in core-collapse supernova explosions [1–6]. First minutes of their life is a period of rapid evolution [7]. This is protoneutron star (PNS) stage, where matter is transformed to final cold catalyzed matter [8] state: one of the greatest mysteries in astrophysics [9]. Among other matter with kaon condenstates, proposed by Kaplan and Nelson [10, 11], is very intriguing possibility. Unfortunately, existing experimental and observational data is still unable to select one, correct model [1]. Therefore, further investigation of effects present under particular assumptions on high-density matter model is in place.

Possibly, only nearby core-collapse supernova explosion will allow researchers to collect enough data, mainly in neutrino channel (*cf.* Fig. 3 in [12]), to find clear signatures of particular model. However, neutrinos are trapped in protoneutron stars. Therefore, it is required to study nuclear matter with two-parameter (baryon number n_B and lepton number Y_L) model at least.

Deleptonization in the first seconds after PNS is born causes decrease in lepton number from value typical for initial pre-supernova "Fe" matter $Y_{\rm Le} \sim 0.4$ [13] down to some numerically small value, *e.g.* $Y_{\rm Le} = 0$ in pure neutron matter model. Meanwhile neutrinos escape outer PNS region, but in central, high-density core we may assume quasistatic evolution of matter parameterized with decreasing $Y_{\rm Le}$.

We have dropped all finite temperature effects for simplicity, however they are potentially equally important [9]. Generally, effects of decreasing temperature are smaller than decreasing lepton number and act in similar direction on critical kaon condensation density.

Article is organized as follows: Sec. 2 presents general formalism including kaon condensate, neutrino trapping and nucleon interactions with symmetry energy. Sec. 3 discusses base results without symmetry energy and with no neutrino trapping. Sec. 4 presents effects of the neutrino trapping on kaon condensate alone, and Sec. 5 combines all three components: kaon condensate, neutrino trapping and various symmetry energy models.

2. Model with kaon condensate

Energy density for matter with kaon condensate is given by:

$$\begin{aligned}&\varepsilon(n_n,\, n_p,\, \theta,\, \mu_e,\, \mu_{\nu_e},\, \mu_K,\, \mu_\mu,\, \mu_{\nu_\mu})\\ &= \varepsilon_{F_n} + \varepsilon_{F_p} + \varepsilon_{F_e} + \varepsilon_{F_{\nu_e}} + \varepsilon_{F_\mu} + \varepsilon_{F_{\nu_\mu}} + \varepsilon_{\rm int} + \varepsilon_{\rm kaon}\,,\end{aligned} \tag{1}$$

where variables on the left hand are: $n_n,\ n_p$ — neutron and proton density, θ — amplitude of the kaon condensate, μ_i — chemical potentials. Right-hand has been decomposed into: $\varepsilon_{\rm F_i}$ — Fermi sea energies, $\varepsilon_{\rm Kaon}$ — kaon–nucleon interaction and $\varepsilon_{\rm int}$ — nucleon interaction including symmetry energy.

Nucleon part can be rewritten as:

$$\varepsilon(u,\, x) = \tfrac{3}{5}\, E_{\rm F}^0\, n_0\, u^{5/3} + u\, n_0\, (1-2\,x)^2\, {\rm S}(u)\,, \tag{2}$$

where $E_{\rm F}^0 = 36.885\,{\rm MeV}$. Standard parameterization ($n_0 = 0.16\,{\rm fm}^{-3}$) has been used:

$$n_p \;=\; x\, n_B\,, \tag{3}$$

$$n_n \;=\; (1-x)\, n_B\,, \tag{4}$$

$$n_B \;=\; u\, n_0 \tag{5}$$

and $S(u)$ is the *symmetry energy.*

Leptons contribute to the total energy:

$$\varepsilon_{F_i} = \frac{g_i\ {\mu_i}^4}{8\,\pi^2}, \tag{6}$$

where g_e=2 and $g_\nu = 1$ (see, however, footnote 2).

Generalization to other lepton families is trivial. However, we have not included μ and τ flavors, as their contribution is minimal [15, 17].

Contribution to the total energy from the kaon condensate can be computed from the Kaplan–Nelson chiral formalism [14, 15]:

$$\begin{aligned}\varepsilon_{\text{kaon}} &= \frac{\mu^2 f^2 \sin^2\theta}{2} + (\cos\theta - 1) \\ &\quad \times \left[n_B\, x\, \Sigma_{\text{Kp}} + n_B\,(1-x)\,\Sigma_{\text{Kn}} - f^2 m_K^2 \right] ,\end{aligned} \tag{7}$$

where $m_K = 493,7\,\text{MeV}$ and $f = 93\,\text{MeV}$ is kaon mass and pion decay rate, respectively. Constants Σ_{Kp} and Σ_{Kn} define kaon–proton and kaon–neutron interaction strength. Due to large uncertainties they may be replaced with single quantity Σ_{KN} placed between 168 and 520 MeV. Some authors use $a_3 m_s$ instead:

$$\Sigma_{\text{KN}} = -\frac{1}{2}\left(a_1 m_s + 2\,a_2 m_s + 4\,a_3 m_s\right), \tag{8}$$

where $a_1 m_s = -67\,\text{MeV}$, $a_2 m_s = 134\,\text{MeV}$.

Kaon density is [9]:

$$n_K = \mu_K f^2 \sin^2\theta + n_B \left(\tfrac{1}{2}\,x + \tfrac{1}{2}\right)(1 - \cos\theta). \tag{9}$$

Minimalization of the energy must include conservation of the baryon number, electric charge and lepton numbers if the neutrinos are trapped:

$$n_n + n_p = n_B\,, \tag{10a}$$
$$n_p = n_e + n_{K^-} + n_\mu\,, \tag{10b}$$
$$x_i + Y_{\nu_i} = Y_{Li}\,. \tag{10c}$$

Baryon number density is a free parameter. Charged lepton fractions are denoted as $x_i \equiv n_i/n_B$, neutrinos as Y_{ν_i}. Conservation of the electric charge is ensured using kaon chemical potential as a Lagrange multiplier:

$$\tilde{\varepsilon} = \varepsilon - \mu(n_p - n_e - n_{K^-} - n_\mu)\,. \tag{11}$$

Electroweak and strong interactions allow reactions:

$$n \longleftrightarrow p^+ + e^- + \bar{\nu}_e\,, \tag{12a}$$
$$n \longleftrightarrow p^+ + K^-\,, \tag{12b}$$
$$n \longleftrightarrow p^+ + \mu^- + \bar{\nu}_\mu\,, \tag{12c}$$

and respective chemical potentials obey:

$$\mu_n - \mu_p = \mu_e - \mu_{\nu_e}\,, \tag{13a}$$
$$\mu_n - \mu_p = \mu_\mu - \mu_{\nu_\mu}\,, \tag{13b}$$
$$\mu_n - \mu_p = \mu_K\,. \tag{13c}$$

If neutrinos escape freely, one can put simply $\mu_{\nu_i} \equiv 0$ and we have left with only one independent chemical potential equal for all negative electric charge particles.

3. Kaon condensation without neutrinos

If neutrinos escape freely (old neutron star case) we have only one driving parameter: baryon density. Minimalized energy is:

$$\varepsilon(n_n,\, n_p,\, \theta,\, \mu_e,\, \mu_K) = \varepsilon_{F_n} + \varepsilon_{F_p} + \varepsilon_{F_e} + \varepsilon_{\mathrm{kaon}}\,. \tag{14}$$

Energy is minimalized numerically solving system of equations:

$$\frac{\partial\, \tilde{\varepsilon}(x, \mu,\, \theta)}{\partial \theta} = \frac{\partial\, \tilde{\varepsilon}(x, \mu,\, \theta)}{\partial x} = \frac{\partial\, \tilde{\varepsilon}(x, \mu,\, \theta)}{\partial \mu} = 0\,. \tag{15}$$

Functions $x(u)$, $\theta(u)$, $\mu(u)$ are immediate result of calculations. Other properties, *e.g.* $n_e(u)$, $n_K(u)$ and EOS can be then easily obtained. Condensation threshold is defined as a maximum density where still $\theta(u) = 0$. Numerical results were obtained for u up to 12 for three values $\Sigma_{\mathrm{KN}} = 168,\, 344,\, 520\,\mathrm{MeV}$[1]; covering entire considered range for this parameter.

Larger Σ_{KN} (*i.e.* smaller $a_3 m_s$) gives stronger kaon–nucleon interaction and lower condensation threshold. Both amplitude of the condensate and proton fraction exhibit asymptotic behavior. This is typical if symmetry energy is constant or growing with density. Chemical potential for kaons and electrons can reach large ($\mu < 100\,\mathrm{MeV}$) negative values if Σ_{KN} is large, and muon flavor will be produced. Overall contribution from muons is however small [15, 17]. As lepton number is not conserved electron/positron fraction can be relatively high. This behavior is completely changed with neutrino trapping, as we explain in the next section.

4. Kaon condensate and neutrino trapping

If neutrinos are trapped then properties of the dense matter are numbered by the two parameters: baryon density n_B and lepton number density Y_{Le}. In principle we have three separate lepton numbers, but initially only Y_{Le} is not identically zero. Therefore, due to large muon and taon masses we may safely restrict to electron lepton number conservation alone[2].

[1] Equivalent values are: $a_3\, m_s = -134,\, -222,\, -310\,\mathrm{MeV}$.

[2] Neutrino oscillation phenomenon indicates conservation of the total lepton number only. Therefore, (10c) could be replaced with $x_e + Y_{\nu_e} + Y_{\nu_\mu} + Y_{\nu_\tau} = Y_L \equiv Y_{\mathrm{Le}}$, where we have put $Y_L \mu = Y_L \tau = 0$. As neutrinos have very small masses all three terms are identical and finally we get $x_e + 3Y_{\nu_e} = Y_{\mathrm{Le}}$. Only difference is "degeneracy factor": $g = 3$ instead of $g = 1$ in Eq. (6) for neutrinos.

Lepton number conservation can be introduced into Eq. (11) in the following manner. We rewrite (10c) using chemical potentials:

$$\mu_e{}^3 + \tfrac{1}{2}\,\mu_{\nu_e}{}^3 = 3\pi^2\, n_B\, Y_{\rm Le}\,. \tag{16}$$

Eq. (13a) minus (13c) gives:

$$\mu_K = \mu_e - \mu_{\nu_e}\,. \tag{17}$$

Eq. (17) and (16) are used to derive μ_e and μ_{ν_e} as a functions of μ_K, n_B and $Y_{\rm Le}$. Now, minimalized function is:

$$\begin{aligned}\tilde{\varepsilon}(Y_{\rm Le}, n_B, x, \theta, \mu_K) \;=\; & \varepsilon_{F_n} + \varepsilon_{F_p} + \varepsilon_{\rm kaon} + \varepsilon_{F_{\nu_e}}(\mu_K,\, Y_{\rm Le}) \\ & - \mu_K\Big[n_p - n_K - n_e(\mu_K,\, Y_{\rm Le})\Big]\,. \end{aligned} \tag{18}$$

Expression above is *explicite* very complex due to presence of the third order radicals resulting from (16).

Two parameter family of solutions is presented in Figs. 1–5. Fig. 1 illustrate lepton number conservation. Without kaons electrons are required by electric charge conservation. If condensate is present, negative charge is provided by preferred due to strong interactions kaons, and neutrinos begins to provide required lepton number amount. Proton fraction strongly depends on trapped lepton number until kaon condensation threshold. This behavior depends somewhat on $\Sigma_{\rm KN}$, *cf.* Fig. 2.

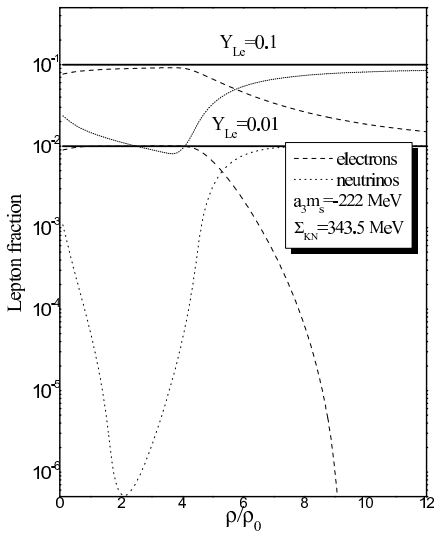

Fig. 1. Leptons fraction *versus* baryon density. Model described by Eq. (18) with no nucleon interactions.

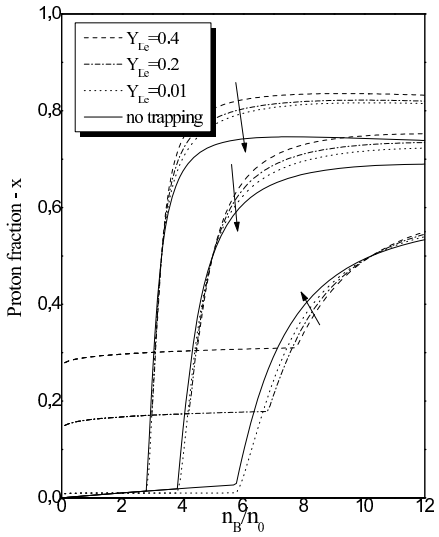

Fig. 2. Proton fraction for three values of the $\Sigma_{\rm KN}$. Arrows indicate direction of the deleptonization effects. Model as in Fig. 1.

The most important effect of deleptonization is decrease in kaon condensation threshold, *cf.* Fig. 3. Direction of the effect does not depend on $\Sigma_{\rm KN}$. Therefore, as kaons tends to "soften" EOS, deleptonization cause decrease in maximum neutron star mass. If PNS is born in stable state with large $Y_{\rm Le}$

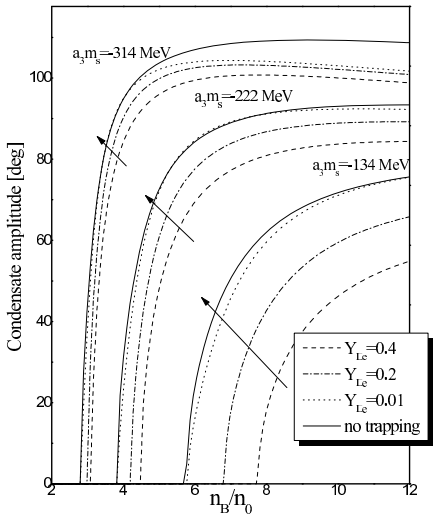

Fig. 3. Deleptonization effects on the amplitude of the kaon condensate θ. Threshold for condensation with trapped neutrinos is always higher and proportional to the lepton number density $Y_{\rm Le}$. Model as in Fig. 1.

then deleptonization may cause delayed collapse to a black hole if $Y_{\rm Le}$ reach small values long time (*i.e.* tens of seconds [5]) after core-collapse[3].

Model with $Y_{\rm Le} \to 0$ is clearly different from model without neutrino trapping (Fig. 4). Initially, for large values of $Y_{\rm Le}$ model works well, but transition to the free streaming regime requires solving transport equations rather than quasistatic evolution.

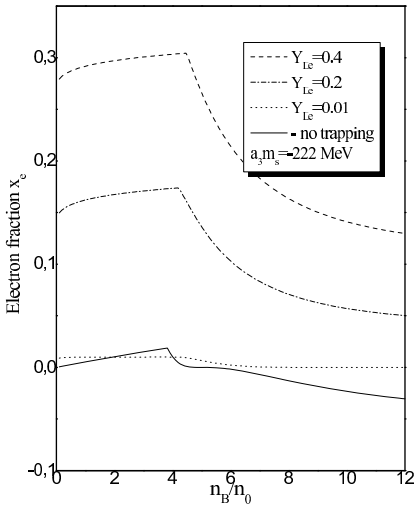

Fig. 4. Electron fraction with and without neutrino trapping. Model as in Fig. 1.

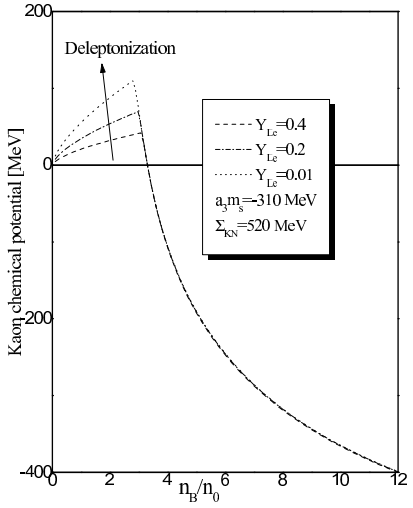

Fig. 5. Kaon chemical potential as a function of nuclear density. Model as in Fig. 1.

[3] Neutron star has not been found in the remnant of the supernova 1987A [22]. Delayed collapse is the most probable explanation.

5. Symmetry energy effects

High density energy symmetry behavior is very important for neutron stars and core-collapse supernovae (Lattimer, Yamada in [1]) but is a source of the great uncertainty [17–20]. Two qualitative behavior has been found:

- always growing (from mean field theories)
- decreasing at high densities (variational methods).

Mean field theory results can be approximated with [15]:

$$V_2 = a u\,, \qquad V_2 = a\sqrt{u}\,, \qquad V_2 = a\frac{2\,u^2}{1+u}\,, \tag{19}$$

where $a = 17\,\mathrm{MeV}$.

Minimalized energy is:

$$\begin{aligned}\tilde{\varepsilon}(Y_{\mathrm{Le}}, n_B, x, \theta, \mu_K) \;=\; & \varepsilon_{F_n} + \varepsilon_{F_p} + \varepsilon_{\mathrm{kaon}} + \varepsilon_{F_{\nu e}}(\mu_K, Y_{\mathrm{Le}}) \\ & -\mu_K\left[n_p - n_K - n_e(\mu_K, Y_{\mathrm{Le}}\right] + \varepsilon_{\mathrm{int}}\,.\end{aligned} \tag{20}$$

Fig. 6 compares mean field and variational results. In the latter, symmetry energy not only decreases, but can reach negative values and pure proton or pure neutron states are preferred.

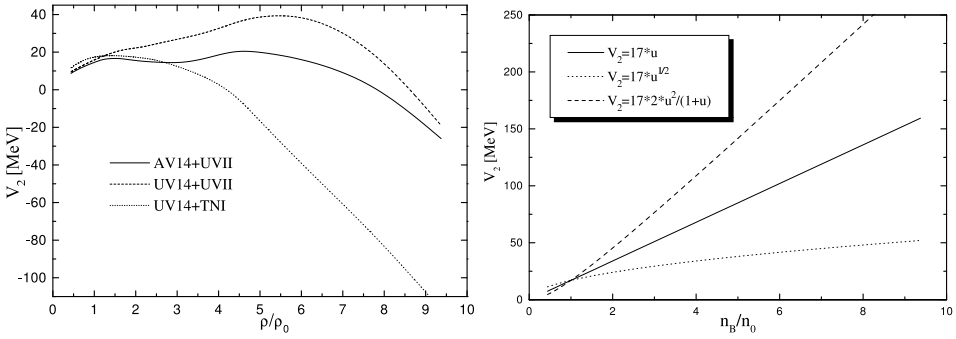

Fig. 6. Symmetry energy in variational models (left) and mean field models (right). Results are presented for UV14+UVII and linear cases (solid lines).

Symmetry energy strongly influences on matter properties both below and above condensation threshold (Figs. 7–9).

General tendency to decrease condensation threshold is however unaffected, and amplitude is still growing with density (Fig. 10).

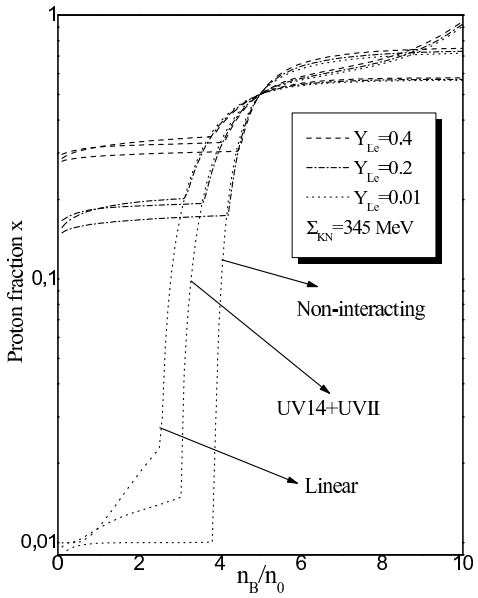

Fig. 7. Deleptonization effects on proton fraction for three symmetry energy models from Fig. 6 for $a_3 m_s = -222$ MeV. It is clear that uncertainty due to symmetry energy leads to larger effects than deleptonization itself.

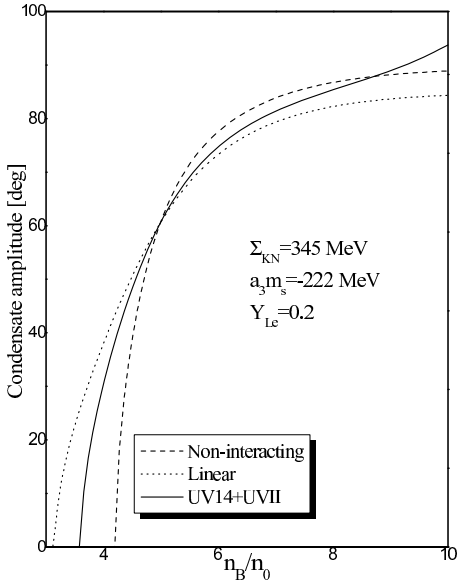

Fig. 8. Kaon condensate amplitude for $Y_{\mathrm{Le}} = 0.2$ in various symmetry energy models from Fig. 6.

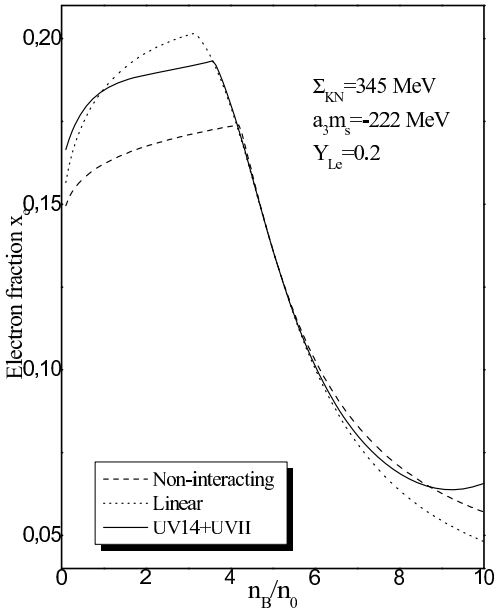

Fig. 9. The same as in Fig. 8 for the electron fraction.

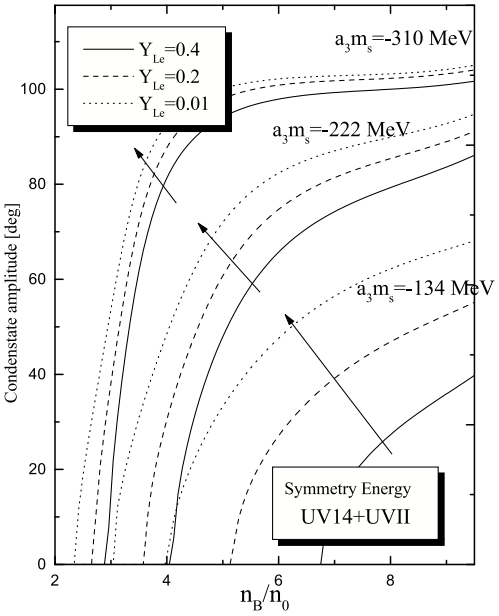

Fig. 10. Deleptonization effect on kaon condensate with symmetry energy are qualitatively similar to the case without symmetry energy, *cf.* Fig. 3.

6. Conclusions

Decrease of the kaon condensation threshold during deleptonization has been shown to be universal in the considered class of models. Main source of the uncertainty is the high density behavior of the symmetry energy and value of the kaon–nucleon interaction parameter Σ_{KN}. Decrease in the condensation threshold may cause newborn PNS to be unstable as trapped lepton number is carried away from the neutrinospheres [9].

Increasing condensate volume finally may cause collapse to a black hole and immediate disappearance of the neutrino flux (effect observable for a next Galactic supernova) as neutrino spheres are swallowed under event horizon [21].

This work was supported by grant of the Polish Ministry of Education and Science No. 1 P03D 005 28.

REFERENCES

[1] "20 years after SN1987A", 23–25 Feb 2007, Waikoloa, Hawaii `http://sn1987a-20th.physics.uci.edu/`
[2] J. Blondin, A. Mezzacappa, *Nature* **445**, 58 (2007).
[3] H.-Th. Janka *et al.*, `astro-ph/0612072`.
[4] A. Burrows *et al., Astrophys. J.* **640**, 878 (2006).
[5] A. Odrzywolek *et al., Acta Phys. Pol. B* **34**, 2791 (2003).
[6] D. Arnett, *Supernovae and Nucleosynthesis*, Princeton University Press 1996.
[7] L. Dessart *et al., Astrophys. J.* **645**, 534 (2006).
[8] N.K. Glendenning, *Compact Stars*, Springer 1997.
[9] M. Prakash *et al., Phys. Rep.* **280**, 1 (1997).
[10] D.B. Kaplan, A.E. Nelson, *Phys. Lett.* **B175**, 57 (1986).
[11] D.B. Kaplan, A.E. Nelson, *Nucl. Phys.* **A479**, 273 (1988).
[12] J. Pons *et al., Phys. Rev. Lett.* **86**, 5223 (2001).
[13] S.E. Woosley, A. Heger, T.A. Weaver, *Rev. Mod. Phys.* **74**, 1015 (2002).
[14] H. Fuji *et al., Nucl. Phys.* **A571**, 758 (1994).
[15] V. Thorsson, M. Prakash, J.M. Lattimer, *Nucl. Phys.* **A572**, 693 (1994).
[16] R.B. Wiringa, V. Fiks, A. Fabrocini, *Phys. Rev.* **C38**, 1010 (1998).
[17] S. Kubis, M. Kutschera, *Nucl. Phys.* **A720**, 189 (2003).
[18] S. Kubis, M. Kutschera, *Acta Phys. Pol. B* **30**, 2747 (1999).
[19] S. Kubis, M. Kutschera, S. Stachniewicz, *Acta Phys. Pol. B* **29**, 809 (1998).
[20] S. Kubis, M. Kutschera, *Phys. Lett.* **B399**, 191 (1997).
[21] J.F. Beacom, R.N. Boyd, A. Mezzacappa, *Phys. Rev.* **D63**, 073011 (2001).
[22] G.J.M. Graves *et al., Astrophys. J.* **629**, 944 (2005).